COMPARISONS OF ENERGY DISSIPATION IN STRUCTURAL DEVICES WITH FOUNDATION SOIL DURING SEISMIC LOADING

A Thesis
Submitted to the Graduate Faculty
of the
North Dakota State University
of Agriculture and Applied Science

By

Duraisamy Soundararajan Saravanathiiban

In Partial Fulfillment of the Requirements
for the Degree of
MASTER OF SCIENCE

Major Department:
Civil Engineering

April 2010

Fargo, North Dakota

North Dakota State University
Graduate School

Title

COMPARISONS OF ENERGY DISSIPATION IN STRUCTURAL DEVICES WITH FOUNDATION SOIL DURING SEISMIC LOADING

By

DURAISAMY SOUNDARARAJAN SARAVANATHIIBAN

The Supervisory Committee certifies that this ***disquisition*** complies with North Dakota State University's regulations and meets the accepted standards for the degree of

MASTER OF SCIENCE

ABSTRACT

Saravanathiiban, Duraisamy Soundararajan, M.S., Department of Civil Engineering, North Dakota State University, April 2010. Comparisons of Energy Dissipation in Structural Devices with Foundation Soil During Seismic Loading. Major Professor: Dr. Sivapalan Gajan.

The effectiveness of structural energy dissipation mechanisms such as passive energy dissipation devices and base isolation methods used in seismic design depends on their capacity, ductility, energy dissipation, isolation, and self-centering characteristics. Though rocking shallow foundations could also be designed to possess many of these desirable characteristics, current seismic design codes often avoid nonlinear behavior of soil and energy dissipation beneath foundations because of concerns about permanent deformations at foundation level.

This thesis compares the effectiveness of energy dissipation in foundation soil with structural energy dissipation devices during seismic loading. Numerical simulations of structures with and without energy dissipation devices were carried out to systematically study the seismic energy dissipation in structural elements and energy dissipation devices. The numerical model was validated using shaking table experimental results on model frame structures with and without energy dissipation devices. The energy dissipation in the structure, drift ratio, and the force and displacement demands on the structure are compared with energy dissipation characteristics of rocking shallow foundations as observed in centrifuge experiments, where shallow foundations were allowed to rock on dry sandy soil stratum during dynamic loading.

The comparisons of results clearly indicate that foundation (rocking) energy dissipation mechanism is as efficient as structural passive energy dissipation devices. For

the structures with energy dissipating devices, about 70% to 90% of the seismic input energy is dissipated by energy dissipating devices, while foundation rocking dissipates about 30% to 90% of the total seismic input energy in foundation soil (depending on static factor of safety). Inclusion of energy dissipating braces increases the base shear force transmitted to the structure, while normalized base shear forces transmitted to the foundation during rocking are smaller than those of the structures with energy dissipating devices because of the isolation effect of rocking foundations. If properly designed (with reliable capacity and tolerable settlements), adverse effects of foundation rocking can be minimized while taking advantage of the favorable features of foundation rocking, and hence they can be used as efficient and economical seismic energy dissipation mechanisms in buildings and bridges.

ACKNOWLEDGEMENTS

I would like to thank my major advisor and my thesis committee chair Dr. Sivapalan Gajan. His continuous invaluable guidance, encouragement, and sharing of his knowledge over the last three years has not only made this thesis possible, but has had an immeasurable influence on the person I am today.

I acknowledge the Department of Civil Engineering, North Dakota State University, for the support provided to me.

My sincere thanks to Drs. Dolce, Cardone, Giuseppe, Claudio and Ponzo for sharing their shaking table experimental data which were very valuable for this research work.

Also, I thank Dr. Gajan, Mr. Ugalde, Dr. Kutter, and Dr. Jeremic for sharing their centrifuge test results, which helped to make this research work a complete one.

I thank the other thesis committee members Dr. Dinesh Katti, Dr. Chung Han, Dr. Yail Kim, and Dr. Zhili Gao.

Finally, I would like to thank my parents and family for all of their love and support that has helped me through this challenge among many others. Their love, encouragement, and understanding have made this thesis possible.

TABLE OF CONTENTS

LIST OF TABLES

LIST OF FIGURES

CHAPTER 1. INTRODUCTION

1.1. Background

Conventional seismic design practice of structures allows inelastic deformation in especially designed locations such as beams adjacent to beam-column joints (Aiken et al., 1993). The inelastic deformation aids to dissipate energy through hysteretic behavior of those specially designed locations, so that collapse of the structure is prevented. However, excessive inelastic deformation causes considerable damage to structural member, non-structural elements, and repeated cyclic inelastic behavior will cause degradation in hysteretic behavior of specially designed locations (Aiken et al., 1993).

Alternative seismic design strategies, commonly referred to as passive control techniques, have been developed in the last 20 years (Dolce and Cardone, 2006). They are aimed at eliminating, or at least reducing, damage in structure under strong earthquakes by exploiting the constant and predetermine favorable behavior of special devices inserted into the structural system (Dolce et al., 2000). Though it increases cost of the structure, this cost is typically offset by the reduced need for stiffening and strengthening measures that would otherwise be required (FEMA, 2000). Current passive control applications mainly utilize the following two strategies: seismic base isolation and energy dissipation (Dolce and Cardone, 2006; Soong and Spencer, 2002; Dolce et al., 2000).

Passive energy dissipation (PED) systems for seismic applications have been under development for a number of years with a rapid increase in implementations starting in the mid-1990s (Symans et al., 2008). In North America, PED systems have been implemented in approximately 103 buildings and bridges, either for retrofit or for new construction (Soong and Spencer et al., 2002). The objective of PED devices is to concentrate hysteretic

behavior in specially designed and detailed regions of the structure and to avoid inelastic behavior in primary gravity load-resisting structural elements (Aiken et al., 1993). By controlling response in this way, inter-storey drifts may be reduced, thus reducing nonstructural damage, and lower accelerations and lower shear forces lead to lower demands on the primary structural system (Hanson et al., 1993). Also, by including energy dissipation systems into structure, structural members can be optimized for gravity loading and energy dissipating systems can be optimized for hysteresis energy dissipation. Currently used PED devices generally operate principles such as yielding of metals, frictional sliding, motion of a piston or plate within viscous fluid, fluid orificing, and deformation of viscoelastic solids (Dolce et al., 2005; Soong and Spencer, 2002).

However, there are some limitations in currently available PED systems. For example, the drawbacks include: (1) problems related to ageing and durability (e.g. for rubber components), (2) installation complexity, (3) replacement and geometry restoration after strong events (e.g. for metallic dampers), (4) maintenance (e.g. for viscous fluids dampers), (5) dependence of mechanical performances on temperature (e.g. for viscoelastic dampers) (Dolce, et al., 2000), and (6) long term reliability and maintenance on friction dampers (Hanson et al., 1993).

The concept of seismic isolation is quite simple and well-known (Naeim and Kelly, 1999). It decouples the building from the horizontal components of the ground motion by creating a discontinuity along the height and introducing an isolation system (Dolce et al., 2007). If the discontinuity is placed at the base of the structure, the technique is commonly referred to as base isolation (Dolce et al., 2007). In 1986, the first building in the United State was built using base isolation (Kelly, 1986). Base isolation is indented to reduce the

force transmitted to the structure by lengthening the period of the structure and dissipating some amount of energy (FEMA, 2000). Isolation system reduces drift and acceleration of the superstructure (FEMA, 2000). However, reduction of acceleration depends on the force-deflection characteristics of the isolators and may not be as significant as the reduction of drift (FEMA, 2000). The components of an isolation system can be classified as isolators and auxiliary devices (Dolce and Cardone, 2006). Isolators are bearing devices with high vertical stiffness, low lateral stiffness and/or low friction, allowing for large horizontal displacements, typically of the order of 200–400 mm (Dolce et al., 2000). On the other hand, auxiliary devices can play different functions, such as dissipating energy and/or laterally restraining the structure under service loads and/or re-centering the structure at the end of an earthquake, when such functions are not directly played by the isolators (Dolce et al., 2007). Since the auxiliary devices can make use of hysteretic properties of metals, friction, viscous fluid, and viscoelastic materials, the limitations listed under PED systems are applicable to base isolation as well. Apart from those limitations, large residual displacement at the end of earthquake in sliding isolators, inadequate control of the force transmitted to the superstructure in rubber isolators are concerns in base isolation systems (Dolce and Cardone, 2006).

Innovative techniques for controlling structural response are searching for smart materials which can introduce new possibilities in earthquake protection methods. One class of such materials is metallic alloys known as Shape Memory Alloys (SMA), which is in use for a long time in medical sciences, and electrical and mechanical engineering (Dolce and Cardone, 2001). SMA devices have been installed in the "San Francesco Basilica Superior" in Italy (Croci et al., 2000, and Lafortune at al., 2007). Properties of

SMA are strictly related to a reversible solid-to-solid phase transformation, which can be thermal-induced or stress-induced. This micromechanical phase transition process is capable of producing a high damping capacity in SMAs as compared to conventional metals (Graesser and Cozzarelli, 1991). Graesser and Cozzarelli (1991) suggested the use of Nitinol (NiTi alloy) as a material for SMA dampers. Dolce et al. (2000) also suggested Nitinol since it has better superelastic properties, lower sensitivity to temperature, higher resistance to corrosion and fatigue. Pre-tensioned SMA wires are utilized in both PED systems and seismic isolation systems. Dolce et al. (2000) concluded many basic features of SMA devices, such as great versatility (the possibility to obtain a wide range of cyclic behaviors), simplicity of the functioning mechanism (in spite of their sophisticated behavior), self-centering capability, high stiffness for small displacements, good energy dissipation capability, extraordinary fatigue resistance (no need of substitution or maintenance), long-term reliability, high durability. However, the major concern of SMA based damper devices is that they are expensive to construct (Christopoulos et al., 2008).

Another mechanism to dissipate seismic energy is foundation rocking, though it is not included in current civil engineering design codes. A huge inventory of buildings and bridges in seismically active zones in the United States are supported by shallow foundations. One of the major changes in the traditional seismic design procedures, adopted in 2000 in the design guidelines of National Earthquake Hazard Reduction Program (NEHRP), was that by allowing mobilization of the ultimate capacity and rocking behavior of shallow foundations, the ductility demands on structures can be reduced (FEMA, 1997 and 2000). Researchers in the past have emphasized the importance of incorporating the nonlinear soil-foundation interaction in design of new structures and

retrofit of existing structures (e.g., Comartin et al., 2000, Martin and Lam, 2000, Pecker and Pender, 2000, Gazetas, 2006, and Mergos and Kawashima, 2005). The concerns about deformations beneath the foundation, uncertainty associated with foundation load and moment capacities, and the lack of practical reliable models to predict the nonlinear soil-foundation system behavior have hindered the use of foundation rocking as an efficient energy dissipation mechanism.

Shallow foundations can be designed to rock on their supporting soil during seismic loading and shearing of soil beneath the foundation will dissipate energy through friction during rocking. Furthermore, because soil consists of uncemented particles, properly compacted soil is a much more ductile material than concrete or welded steel. Experimental research findings reveal that properly designed shallow foundations, with controlled rocking, possess many desirable characteristics, such as, well defined capacities, ductility, energy dissipation, isolation, and self-centering mechanisms, and hence there is promise to use rocking footings in place of, or in combination with, structural energy dissipation devices to improve the performance of structural systems during seismic loading (e.g., Taylor et al., 1981, Faccioli et al, 2000, Gajan et al., 2005, Ugalde et al., 2007, Paolucci et al., 2007, and Gajan and Kutter, 2008a, 2009b). It has been observed that after some earthquakes in Japan, a number of structures resting on spread footings responded to seismic excitation by rocking on their foundations and the rocking mechanism enabled them to avoid failure (Mergos and Kawashima, 2005). Despite all the mounting experimental and field case history evidences, foundation rocking and soil yielding still remain as an unreliable/unproven energy dissipation mechanism for reducing ductility demands on the structure.

1.2. Scope of the Research

1.2.1. Objectives

The objectives of this thesis are two-fold: (1) to compare the effectiveness of different structural energy dissipation devices using numerical simulations and (2) to compare the effectiveness of foundation energy dissipation (during footing rocking) with that of structural devices using experimental results and numerical simulation results.

1.2.2. Methodology

In this study, beam-column frame structures are numerically modeled to simulate a series of shaking table experiments of fixed-base structures with and without passive energy dissipation devices. These shaking table experiments were conducted in Italy as part of MANSIDE (Memory Alloys for New Seismic Isolation Devices) project (Dolce et al., 2005 and 2007b). Finite element simulations are carried out using OpenSees (Open System for Earthquake Engineering Simulations) (OpenSees, 2009) to analyze the behavior of structural systems with and without energy dissipation mechanisms in structures. Four types of frames are modeled and analyzed:

- Bare frame
- Frame with steel energy dissipating braces
- Frame with Shape Memory Alloy (SMA) based braces
- Frame with SMA base isolation

In each case, the models are shaken by several, but consistent, ground motions with varying magnitudes.

Numerical simulation results for energy dissipation and force and displacement demands on the structure are compared with the energy dissipation characteristics of rocking shallow foundations recorded in centrifuge experiments. Results from two series of centrifuge experiments, where shallow foundations were allowed to rock on soil, are considered for comparison: (1) rigid shear wall-footing model tests (Gajan and Kutter, 2008a), and (2) flexible bridge deck-column-footing model tests (Ugalde et al., 2007). These centrifuge experiments were conducted in University of California, Davis. These experimental results are used to compare the effectiveness of energy dissipation in foundation soil with the effectiveness of structural energy dissipation devices as obtained from numerical simulations. The flow chart of research approach is shown in Fig. 1.1.

1.3. Organization of Thesis

There are seven chapters in this thesis. The description of each chapter is as follows:

- Chapter 1: Provides introduction and scope of the research and organization of the thesis.
- Chapter 2: Presents literature review on structural energy dissipation devices.
- Chapter 3: Presents literature review on foundation rocking and on energy dissipation due to foundation rocking.
- Chapter 4: Presents the numerical simulations of structures with and without energy dissipation devices.

- Chapter 5: Presents energy dissipation in foundation soil due to rocking and the comparison of energy dissipation in soil with that of in structural energy dissipation devices.
- Chapter 6: Presents the summary and conclusions.
- Chapter 7: Presents recommendations for future research work

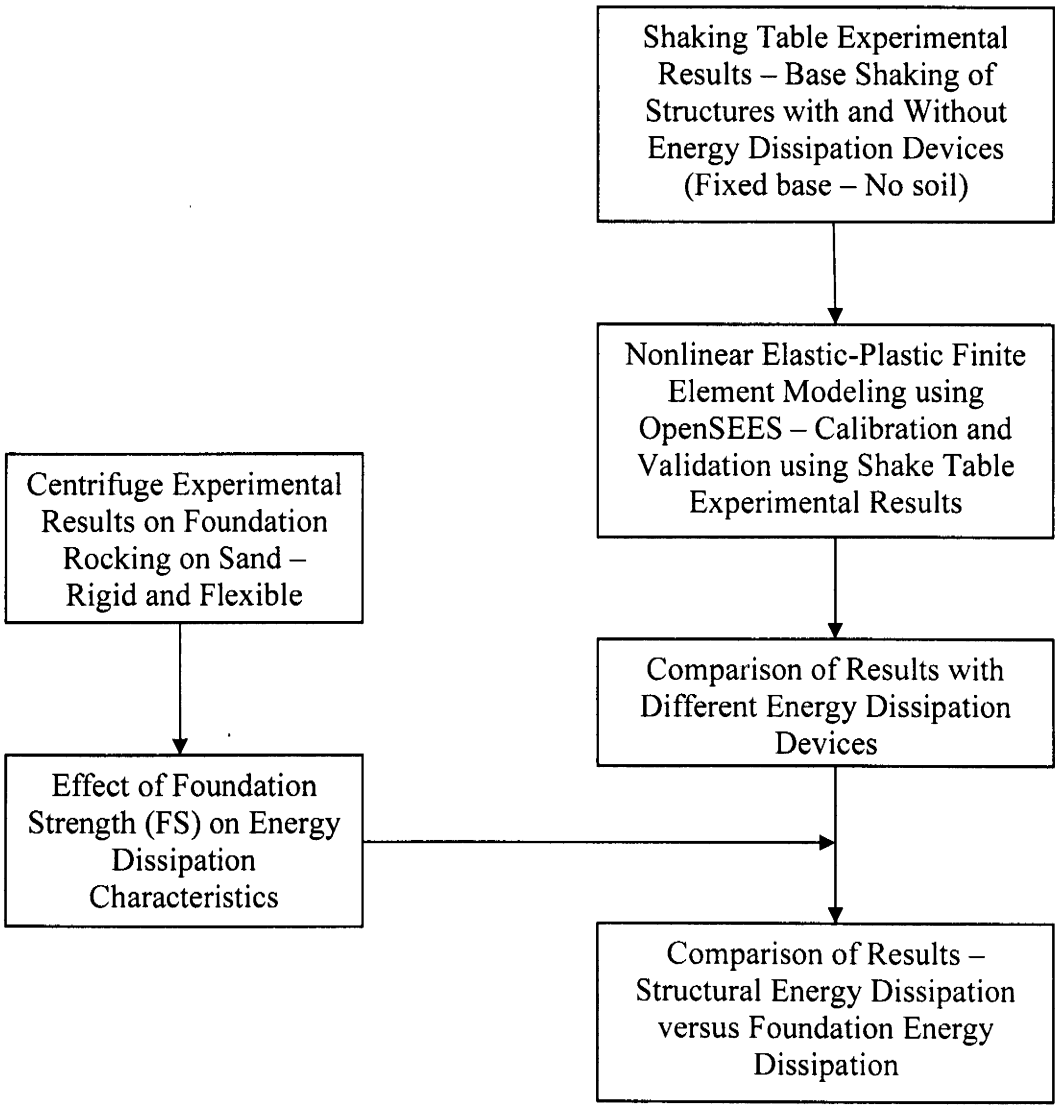

Fig. 1.1. Flow chart of research approach

CHAPTER 2. STRUCTURAL ENERGY DISSIPATION

The vibration control of civil structures to external dynamic loading can be pursued by using active control, semi-active control, and passive control (Housner, 1997; Soong and Spencer, 2002; Song et al., 2006). In the active control mode, an external power source controls actuators to apply forces to the object structures. For a passive control system, no external power source is required and the impact forces are developed in response to the motion of the structures. The semi-active control devices use considerably less energy to adjust the structural properties than the active control devices (Song et al., 2006). Only passive control systems are discussed in this section.

Selection between current passive control applications, base isolation or energy dissipation systems, should be made on the beginning of the design and primarily depend on the required performance level at specified level of earthquake demand (FEMA, 2000). Table 2.1 provides some simple guidance on the performance levels for which isolation and energy dissipation systems should be considered as possible design strategies for building rehabilitation.

Table 2.1. Applicability of isolation and energy dissipation systems (FEMA, 2000)

Performance Level	Performance Range	Isolation	Energy Dissipation
Operational	Damage Control	Very Likely	Limited
Immediate Occupancy		Likely	Likely
Life Safety	Limited Safety	Limited	Likely
Collapse Prevention		Not Practical	Limited

In general, isolation systems provide significant protection to the building structure, nonstructural components, and contents (FEMA, 2000 and Dolce et al., 2003), but, at a higher cost (FEMA, 2000). However, for the tall buildings isolation systems may not be feasible.

2.1. The Energy Equation

This section introduces energy related terms and their definitions. Energy equation can be derived from equation of motion for a single decree of freedom structure, subjected to a horizontal earthquake motion (Shen and Akbas, 1999), which is shown in Fig.2.1.

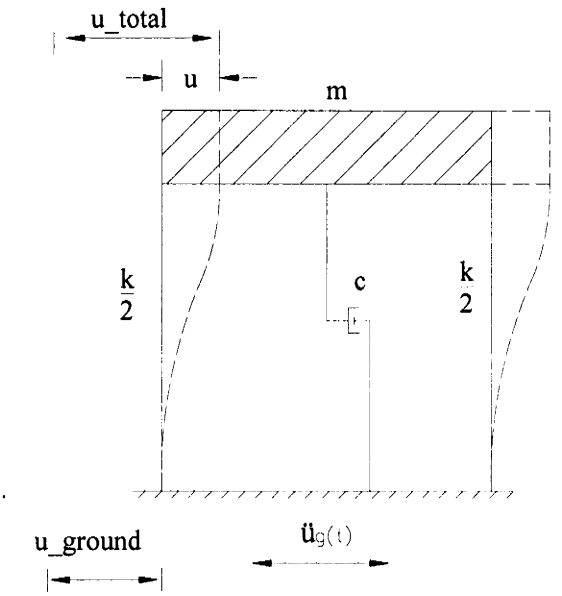

Fig. 2.1. Single Decree of Freedom Structure

From equation of motion,

$$m\ddot{u}_t + c\dot{u} + f_s = 0 \qquad \text{(Eq.2.1.1)}$$

where 'm' is mass of the structure, 'c' is viscous damping coefficient, 'f_s' is restoring force, 'u_t' is total or absolute displacement of mass, and 'u' is relative displacement of mass with respect to ground.

So, u_t can be written as,

$$u_t = u + u_g \qquad \text{(Eq.2.1.2)}$$

From Eq.2.1.1 and Eq.2.1.2,

$$m\ddot{u} + c\dot{u} + f_s = -m\ddot{u}_g \qquad \text{(Eq.2.1.3)}$$

Eq.2.1.1 can be used to calculate relative energy equation where as Eq.2.1.3 is used to calculate absolute energy. Uang and Bertero (1990) studied both these energy equations and found that absolute energy equation is physically more meaningful. So, absolute energy terms are chosen to analyze in this analysis rather than relative energy terms.

By integrating Eq.2.1.3 with respect to 'u' from the time that the ground motion excitation starts,

$$\int m\,\ddot{u}_t du + \int c\,\dot{v} du + \int f_s\, du = 0 \qquad \text{(Eq.2.1.4)}$$

From Eq.2.1.2 and first term in Eq.2.1.4,

$$\int m\,\ddot{u}_t du = \int m\,\ddot{u}_t(du_t - du_g) = \int m\frac{d\dot{v}_t}{dt} dv_t - \int m\,\ddot{v}_t dv_g \qquad \text{(Eq.2.1.5)}$$

Thus Eq.2.1.4 can be written as,

$$\frac{m(\dot{u}_t)^2}{2} + \int c\dot{u}du + \int f_s du = \int m\ddot{u}_t\, dv_g \qquad \text{(Eq.2.1.6)}$$

On the left side of Eq.2.1.6, the first term indicates kinetic energy (E_k), the second term gives energy dissipated by viscous damping (E_D), and the third term is sum of hysteretic energy (E_h) and elastic strain energy (Es). The right side of Eq.2.1.6 is input energy (E_I). So, Eq. 2.1.6 can be rewritten as,

$$E_k(t) + E_D(t) + E_s(t) + E_h(t) = E_I(t) \qquad \text{(Eq.2.1.7)}$$

The input energy is always positive because it is equal to the sum of kinetic, damping, strain, and hysteretic energy. However, input energy does not always increase because the change in ground displacement may be in the opposite direction to the absolute acceleration (Wong and Yang, 2002).

In Eq.2.1.7, kinetic energy and elastic energy are related to instant response of the system, very small compare to hysteretic and damping energy, and vanish at the end of vibration in an inelastic system (Shen and Akbas, 1999). So, Eq.2.1.7 may reduce to the form of,

$$E_D(t) + E_h(t) \cong E_I(t) \qquad \text{(Eq.2.1.8)}$$

According to Uang and Bertero (1989) the input energy for a multiple degree structure can be written as,

$$E_i = \int (\sum_{i=1}^{N} m_i \ddot{v}_{ti})\, dv_g \qquad \text{(Eq.2.1.9)}$$

where, N is no of story.

Uang and Bertero (1990) used a six story frame for shaking table test. They used the 1978 Miyagi-Ken-Oki (MO) earthquake ground motion as the input ground motion. The energy time histories of the model during the collapse level test, which had measured peak base horizontal acceleration of 0.65g, is shown in Fig. 2.2. The energy time histories show that hysteretic energy and viscous energy are the major part in dissipating the input energy, and kinetic energy and strain energy portions are relatively very small.

Wong and Yang (2002) proposed a computational method to characterize energy and transfer among energy forms in structure during earthquake. They used a moment resisting frame, six stories and three bays, model and computed energy time histories. They

showed that most of the input energy dissipated by hysteretic energy/plastic energy (PE) and damping energy. Therefore, strain and kinetic energies are not too large.

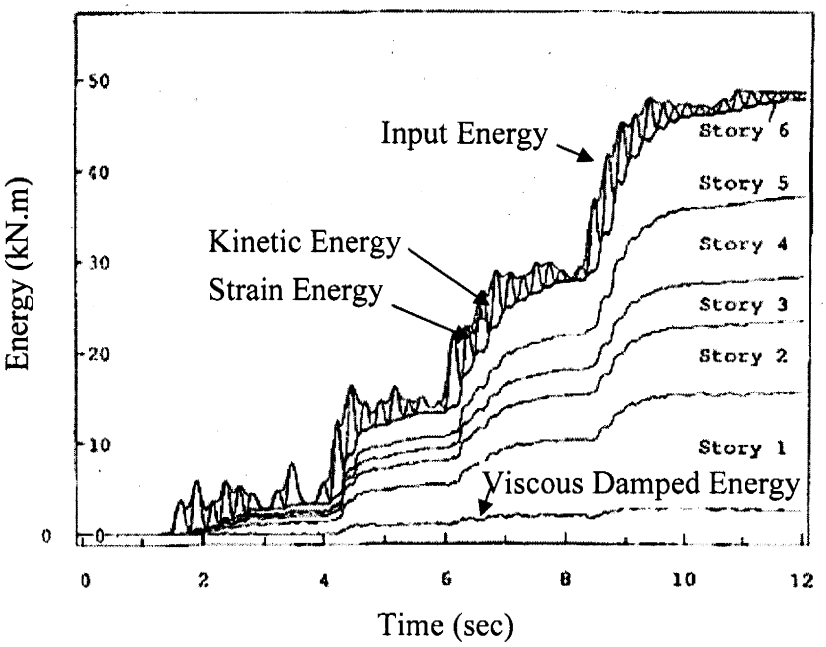

Fig. 2.2. The energy time histories of the six story frame model for peak base ground acceleration of 0.65g (Uang, and Bertero, 1990)

2.2. Seismic Isolators

Seismic isolators are classified as elastomeric/rubber isolators and sliding isolators (FEMA, 2000, Dolce and Cardone, 2006). The main drawbacks of currently available isolators are related to the bad control of the force transmitted to the superstructure and the large residual displacements at the end of an earthquake (Dolce and Cardone, 2006). However, SMA-based isolation systems which have the superelastic behavior can limit the force transmitted to the superstructure and recover the initial position at the end of a strong earthquake (Dolce and Cardone, 2006).

This section gives brief discussion on elastomeric/rubber isolators and sliding isolators, specifically, based on FEMA (2000). SMA isolator is discussed together with SMA based devices.

2.2.1. Elastomeric Isolators

Elastomeric isolators are typically made of layers of rubber separated by steel shims (Dolce and Cardone, 2006). Elastomeric isolators are high-damping rubber bearings (HDR), low-damping rubber bearings (RB) and low-damping rubber bearings with a lead core (LRB) (FEMA, 2000).

Behavior of Lead rubber bearings can be represented by a bilinear hysteretic model. The model needs three parameter to define; the post-yield stiffness k_p, the yield force F_y, and the yield displacement D_y High-damping rubber bearings are made of specially compounded rubber that exhibits effective damping between 0.10 and 0.20 of critical (FEMA, 2000). The increase in effective damping of high-damping rubber is achieved by the addition of chemical compounds that may also affect other mechanical properties of rubber (FEMA, 2000).

2.2.2. Sliding Isolators

Sliding isolators are flat assemblies or have a curved surface, such as the friction pendulum system (FPS) and Rolling systems shall be characterized as a subset of sliding systems (FEMA, 2000). Sliding bearings are typically made of PTFE (polytetrafluoroethylene or Teflon) or PTFE-based composites in contact with polished stainless steel (Dolce and Cardone, 2006). Also, combinations of either low-damping

elastomeric or FPBs with viscous dampers , combinations of low-damping elastomeric and flat sliding bearings, and combinations of flat sliding bearings and elastoplastic devices, especially in bridge applications, are in use today (Dolce et al., 2007b).

Sliding bearings will tend to limit the transmission of force to an isolated structure to a predetermined level (FEMA, 2000). Force-deformation response properties of sliding isolators is based on contact pressure, rate of loading or velocity, bilateral deformation, temperature, contamination, and other environmental loads and aging effects over the design life of the isolator (FEMA, 2000). Fig. 2.3 shows idealized force-displacement loops of sliding bearings with flat, spherical, and conical surfaces. Sliding bearings with either a flat or single curvature spherical sliding surface are typically made of PTFE or PTFE-based composites in contact with polished stainless steel.

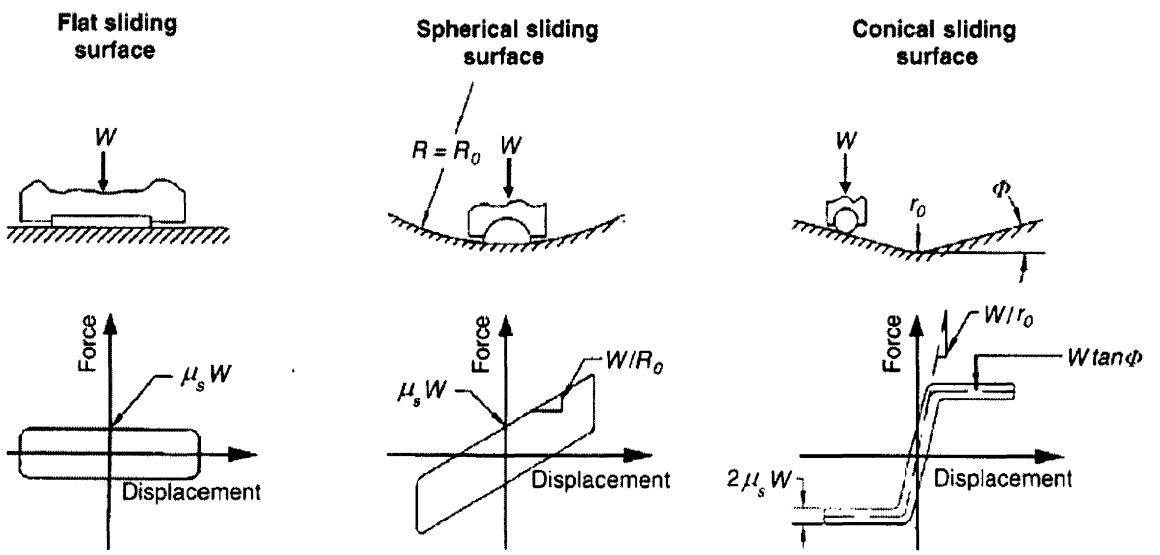

Fig. 2.3. Idealized force-displacement loops of sliding bearings (FEMA, 2000)

2.3. Passive Energy Dissipation Systems

Passive energy dissipation devices dissipate the seismic energy through hysteresis behavior and sometimes add stiffness to the building. Passive energy dissipation devices

reduce drift of the structure by a factor of about two to three or higher in case the device also adds stiffness to the structure (FEMA, 2000). The most common passive energy dissipation devices used to seismic protection of structures are metallic dampers, friction dampers, viscous fluid dampers, viscoelastic solid dampers, phase transformation dampers and re-centering dampers. Other devices which could be classified as passive energy dissipation devices are tuned mass and tuned liquid dampers, which are primarily applicable to wind vibration control. This section presents literature review for metallic dampers and other dampers are discussed briefly. Phase transformation dampers, based on shape memory alloys, are discussed in next section.

2.3.1. Metallic Dampers

Dissipating input energy using the yielding of metal, especially steel, is more than 30 years old (Skinner et al., 1975). Metallic dampers can be investigated as two different categories: Added Damping and Stiffness (ADAS) (Skinner et al., 1975; Whittaker et al., 1991; Xia and Hanson, 1992; Tsai et al., 1993; Braga and D'Anzi, 1994; D'Anzi et al., 1996; Braga et al., 1996; and Braga et al., 2002) and Buckling Resistance Braces (BRB) (Black et al., 2004). Skinner et al. (1975) considered torsional beams, flexural beams, and other structural mechanisms as the basis for energy dissipation devices for seismic protection of structures. But later braces with an array of mild steel plates, in triangular or 'X' shape, have been proposed (Whittaker et al., 1991; Tsai et al., 1993; and D'Anzi et al., 1996). Triangular or 'X' shape is chose because it yields uniformly over its height and plastic deformation is distributed uniformly over the height of the plate. All these studies show that both ADAS element and BRB are effectively dissipates substantial amount of

input energy. Generally, braces are arranged in echelon formation in order to limit the variations of the axial force in columns. Moreover, the steel brackets are shaped in such a way that the axes of braces, beams and columns converge to the same point, in order to avoid additional shear and moment stresses in beams and columns (Dolce et al., 2005).

Skinner et al. (1975) developed high capacity and low cost hysteretic dampers based on the plastic deformation of steel beams, nowadays called as metallic yield dampers, which are suitable for earthquake resistance structure. Inelastic deformation of those beams, with square or rectangle or circular section, was through various combination of torsional, flexural and shearing. Also, they explained about suitable locations of hysteretic dampers for different structures. Their idea was, for the economic way of hysteretic dampers, a structure should have a pair of nearby points which undergo substantial relative displacements during severe earthquakes. Moreover, to avoid the interference of normal structural loads on dampers, the dampers should be located in laterally flexible buildings in such a way that they are loaded only during lateral loads.

Whittaker et al. (1991) evaluated the seismic performance of steel plate elements, Added Damping and Stiffness (ADAS), kind of metallic damper, though a series of sub-assemblage experiments and by the earthquake simulator testing of a three storey flexible Moment Resisting Frame (MRF) upgraded with ADAS elements. The ADAS elements investigated in their research program were composed of X-shaped plates because it yields uniformly over its height and plastic deformation is distributed uniformly over the height of the plate. They found that the strength and stiffness of ADAS did not degrade after many cycles of loading. They compared the behavior of frames with and without ADAS in terms of strength demand, maximum inter storey drift, and energy dissipation (Table 2.2). Fig.2.4

shows energy time histories of input energy, energy dissipated by ADAS elements in each storey and energy dissipated by structural elements. The shaded area is represented by energy dissipated by inelastic deformation in the MRF and by equivalent viscous damping. The ADAS elements dissipated approximately 74% of the total input energy and the remaining being dissipated by inelastic deformation in the MRF and by equivalent viscous damping. Also, they indicated that the addition of the ADAS system clearly improve the response of the test structure by increasing its stiffness, damping and energy dissipation capacity. They concluded that the hysteretic behavior of ADAS element is dependent on its yield strength and yield displacement, and the degree of restraint at the head and base of the element. Finally, they suggested that ADAS can be effectively employed in structures like Concentrically Braced Frames (CBFs), eccentrically braced frames and coupled-reinforced concrete structural walls other than flexible MRF.

Table 2.2. Comparison of results between with and without ADAS systems (Whittaker et al., 1991)

Structure	Flexible MRF without ADAS Systems			Flexible MRF with ADAS Systems					
Max. Ground Acceleration	0.13g			0.13g			0.56g		
Storey Level	1	2	3	1	2	3	1	2	3
Max. Lateral Displacement (in.)	2.21	1.69	0.89	0.71	0.56	0.32	2.63	2.16	1.30
Max. Inter-storey Drift (%)	0.84	1.30	1.11	0.27	0.39	0.40	0.90	1.40	1.62
Storey Shear (kips)	12.4	21.3	25.0	8.7	14.0	17.6	21.6	34.7	46.8
Over turning Moment (kips-in.)	795	2159	4145	555	1446	2798	1383	3596	7020

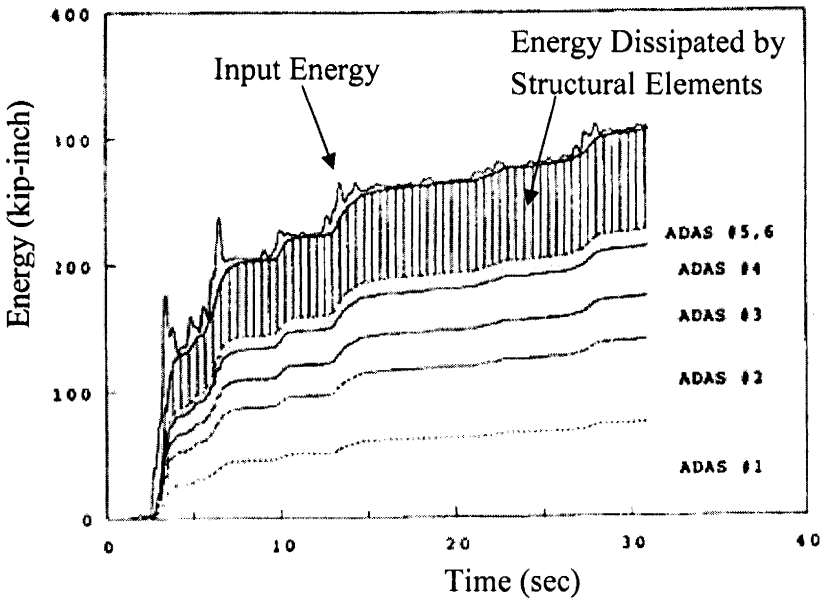

Fig. 2.4. Energy time histories (Whittaker et al., 1991)

Xia and Hanson (1992) studied the ADAS elements, ADAS device and two bracing members that support the device, and aimed to use their results as a source document for the design of building structures with ADAS elements. Yield force, yield displacement, strain-hardening ratio, ratio of the design stiffness to the bracing member stiffness, and ratio of device stiffness to structural storey stiffness without the device in place were identified as the most important parameters to characterize the performance of this device by them. They analyzed the influence of these parameters on earthquake response of three ten storey moment frame structure through numerical analysis using DRAIN-2D program. They used three different ground motions for their analysis. They suggested that the selection of device yield force should consider both strength and energy demands based on the expected earthquake ground motion intensity and duration at the building site. They concluded that the ADAS device can substantially increase the energy dissipation capacity of a structure and significantly reduce the energy dissipation demand on the framing members of a structure.

Tsai et al. (1993) presented their research findings on effectiveness of using steel triangular plates welded as the ADAS device for earthquake resistance structures. They carry out cyclic loading tests on eleven welded triangular ADAS devices and they indicated that a properly welded steel triangular plate ADAS device can sustain a large number of yielding reversals without any stiffness or strength degradation. They further investigated the effectiveness of the triangular ADAS device for building in high seismic risk using pseudo-dynamic testing procedures for a two storey steel frame. They compared the experimental results with analytically predicted response and found good agreement. In order to gain insight into the effects of some important parameters on the seismic response of ADAS structural systems they analyzed nonlinear response spectra for Single Degree of Freedom (SDOF) systems. They discussed the effects of the ratio of the triangular ADAS element stiffness to that of the bare frame, and the ratio of the entire frame yield strength to that associated with the triangular ADAS element on the seismic response of the ADAS structures. Based on their experimental and analytical studies, they developed a design methodology and an example for the design of beams, columns, and braces in structures using the triangle ADAS device as primary energy dissipating system.

Braga and D'Anzi (1994) presented a design strategy to define brace stiffness and slip load of the energy dissipating system, steel braces and steel yielding plates, in order to minimize the deformation of Reinforcing Concrete (R/C) structure. They carried out numerical tests to verify the proposed method. They proved that properly designed steel braces with energy absorbing devices are a reliable, effective and economical way to minimize the deformation of R.C building. Also, they suggested to use steel chains along the beams to absorb the large tension load induces because of seismic activity. They

recommended their presented method to both retrofit/upgrade R/C existing frames and to design new buildings.

D'Anzi et al. (1996) tested two ¼ scale 4-storey 2-span R/C fames, designed only for gravity loads. The main purpose of their tests was to verify the capability of the design method proposed by Braga and D'Anzi (1994) through experimental tests. One of the two models was upgraded with Energy Dissipating Braces (EDBs), which were fabricated from a pair of steel T-sections and "X" shape steel yielding plate, while the other one was bare frame for comparison. They found a good agreement with all the theoretical assumption and the design method for the bracing system performed very well. They found that there was no damage and no need to repair or replace them even after a strong earthquake. Also they showed the effectiveness of the connection to the mounting bracket which was used to connect the braces with R/C frame.

Braga et al. (1996) carried out numerical simulations to better understand the overall and local behavior of the tested experimental models by D'Anzi et al. (1996). Drain-2DX was used to implement detailed numerical model. They showed excellent agreement of numerical results such as displacements and accelerations with experimental results.

Braga et al. (2002) assessed the efficiency of steel hysteretic dissipating devices embodied into steel braces, called as Energy Dissipating Braces (EDBs), to upgrade R/C framed buildings to seismic actions through experimental (D'Anzi et al., 1996) and numerical (Braga et al., 1996) investigations. They found that, EDBs were very effective in improving seismic behavior of the model. Bare frame started to collapse at 0.24g where as model with EDBs, withstand up to 0.94g. Storey drift registered for un-braced model of

0.33g shake test were 2.30%, 1.10%, 0.40% and 0.07% at first, second, third and forth storey levels respectively where as for braced model of 0.92g test, they were 0.63%, 0.28%, 0.27% and 0.19%. Also, they confirmed the importance of pre-tensioned steel tie rods to counteract the induced tensile forces and to exert a beneficial effect of confinement on beam-column joints. Moreover, they found that the presence of the braces introduces large axial force variations, even greater than the initial compressive stress, in the external columns from their numerical analysis. They showed that 85% of the total energy dissipation is due to plastic energy component and the rest is viscous part.

Black et al. (2004) reported on the results from a comprehensive component testing program on a type of buckling restrained brace known as the unbonded brace. They suggested Bouc-Wen model, proposed by Bouc (1971) and subsequently extended by Wen (1975, 1976), as the suitable model to approximate the nonlinear hysteretic behavior of an unbonded brace. From their comprehensive experimental results they found that the unbonded braces deliver ductile, stable and repeatable hysteretic behavior. Also they found that unbonded braces are capable of providing both the rigidity needed to satisfy structural drift limits, while delivering a stable and substantial energy absorption capability. They concluded that unbonded braces represent a reliable and practical alternative to conventional framing systems to enhance the earthquake resistance of existing and new structures.

Donatello et al. (2004) carried out an extensive program of shaking table tests on ¼-scale three dimensional R/C frames to evaluate the effectiveness of passive control bracing systems for the seismic retrofit of R/C frames designed for gravity loads only. EDBs were one type of braces they considered. Dissipating unite of the brace consist of four double

flag-shaped steel elements connecting the C-sections with the bottom steel bracket was used by them. They followed the procedure proposed by Braga and D'Anzi (1994) to design EDBs. They studied the effectiveness of braces in two different conditions. First condition is unidirectional motion, mass and stiffness centers coincident and the other one is bidirectional motion and eccentric mass. They showed that the stiffness of the model was increased by braces and, therefore, the natural frequency of the model also increased. They concluded that the steel braces are very effective in limiting the inter-storey drift, and thus the structural damage, even under earthquake much stronger than design earthquake. However, they point out one possible problem that is requirement of heavy, large size, and thus expensive, brace system to satisfy their stiffness requirement.

2.3.2. Friction Dampers

Many researchers have studied friction dampers as an effective mean to dissipate energy via sliding friction across the interface between two solid bodies and reduce the inelastic behavior of main structure (Pall and Marsh, 1982; Aiken et al., 1993). At the sliding interface between the steel plates, special materials may be utilized to promote stable coefficients of friction. The deformations of the structural framing are largely restricted until the friction force is overcome. Thus, the dampers add initial stiffness to the structural system (Symans et al., 2008). All the friction dampers generate rectangular hysteresis loops except one, the Fluor-Daniel EDR (Energy Dissipating Restrained). Rectangular loops indicate that significant energy can be dissipated per cycle of motion and the cyclic behavior of friction dampers is strongly nonlinear. Pall and Marsh (1982) showed that friction damper in the bracing of the steel framed buildings can significantly

enhance their earthquake resistance. Pall friction damper is intended to be mounted in X-bracing.

Aiken et al. (1993) ensured the improvement of structure during seismic action through the inclusion of the friction damper. Aiken et al. (1993) used the friction damper developed by Sumitomo Metal Industries, Ltd., a cylindrical device with friction pads that slid directly on the inner surface of the steel casing of the device, and the friction devices were attached to the frame model, the underside of the floor beams and connected to chevron brace assemblages. Fluor Daniel, Inc., has developed and tested a unique type of friction device, called the Energy Dissipating Restraint (EDR) (Hanson et al., 1993). Hysteresis loops of Fluor-Daniel EDR have self-centering capabilities, and the slip load is proportional to the displacement. The friction surfaces in this device are bronze wedges sliding on a steel barrel.

2.3.3. Viscous Fluid Dampers

Fluid can be used to dissipate energy and several device configurations have been proposed (Hanson et al., 1993; Constantinou et al., 2001; Hwang et al., 2008; Lu et al., 2008). One kind of proposed device involves the concept of a viscous damping wall (Hanson et al., 1993; Lu et al., 2008). This kind of dampers are proposed as an alternative to brace-type damper devices, specially to overcome the stress concentrations which usually take place at the connection between a brace-type damper and its joining RC members (Lu et al., 2008). Another class involves the use of a cylindrical piston immersed in a viscous fluid (Hanson et al., 1993; Constantinou et al., 2001; Hwang et al., 2008; Symans 2008). Viscous fluid dampers generally consist of a piston in the damper housing

filled with a compound of silicone or similar type of oil. It dissipates energy through movement of the piston in the highly viscous fluid, fluid orificing (Housner et al., 1997). The increasing temperature in the device may be of concern due to the potential for heat-induced damage to the damper seals. In this case, the temperature rise can be reduced by reducing the pressure differential across the piston head (Symans at al., 2008).

Commonly used installation schemes are diagonal brace, chevron brace, upper toggle brace, and lower toggle brace (Hwang et al., 2008). Constantinou et al. (2001) described configurations of energy dissipation devices which are based on the toggle mechanism and which results in device displacements that are larger than the structural drift where as diagonal and chevron brace configurations results in either equal (case of chevron brace) to or less than (case of diagonal brace) drift of story at which the devices are installed. As an alternative to viscous fluid dampers, viscoelastic fluid dampers, which are intentionally designed to provide stiffness in addition to damping, have recently become available for structural applications (Symans et al., 2008). These dampers provide damping forces via fluid orificing and restoring forces via compression of an elastomer. Thus, more accurately, the dampers may be referred to as viscoelastic fluid/solid dampers (Symans et al., 2008).

2.3.4. Viscoelastic Solid Devices

Viscoelastic dampers have been used for structural control for more than 30 years and recently extended to seismic protection (Hanson et al., 1993; Housner et al., 1997; Soong and Spencer, 2002; Symans et al., 2008). Viscoelastic solid materials can be used to dissipate energy at all deformation levels. Therefore, viscoelastic dampers can find in both

wind and seismic protection (Hanson et al., 1993). Application of viscoelastic dampers to civil engineering appears to begun in 1969 when approximately 10,000 viscoelastic dampers were installed in each of the twin towers of the World Trade Center in New York to reduce wind induced vibrations (Hanson et al., 1993; Housner et al., 1997).

Viscoelastic solid dampers generally consist of solid elastomeric pads, viscoelastic material, usually copolymers or glassy substances that dissipate energy through shear deformation, bonded to steel plates. The steel plates are attached to the structure within diagonal bracing or chevron bracing. As one end of the damper displaces with respect to the other, the viscoelastic material is sheared resulting in the development of heat which is dissipated to the environment (Symans et al., 2008).

Chang et al., (1995) carried out experimental and numerical studies on the seismic behavior of steel frame with viscoelastic dampers with various ambient temperatures and showed that the viscoelastic dampers are effective in attenuating seismic structural response under mild and strong earthquake ground motions. Viscoelastic solid devices can be modeled using a spring and dashpot in parallel which is Kelvin model of viscoelasticity (FEMA, 2000; Symans et al., 2008). The cyclic response of viscoelastic materials are generally dependent on level of shear deformation in the material, frequency of loading, and the operating temperature, including temperature rise due to excitation (Hanson et al., 1993; FEMA, 2000).

2.4. SMA Based Devices

2.4.1. Material Behavior of SMAs

The Shape Memory Alloys (SMAs) are smart materials which are able to undergo large strains (Grasser and Cowzzarelli, 1991). Properties of SMAs are strictly related to a reversible solid-to-solid phase transformation, which can be thermal-induced or stress-induced (Dolce and Cardone, 2001). This micromechanical phase transition process is capable of producing a high damping capacity in SMAs as compared to conventional metals (Grasser and Cowzzarelli, 1991; Dolce and Cardone, 2001; Song et al., 2006). This result from a first order martensitic phase transformation which is commonly refers to a broad family of diffusionless transformation in metals (Grasser and Cowzzarelli, 1991). Behavior of SMAs is broadly explained in Dolce and Cardone (2001), Dolce et al (2000), Grasser and Cowzzarelli (1991), and Song et al. (2006).

2.4.2. Development of SMA Based Devices

Innovative techniques for controlling structural response are searching for smart materials which can introduce new possibilities in earthquake protection methods. One class of such materials is metallic alloys known as Shape Memory Alloys (SMAs) which is in use for a long time in medical sciences and electrical and mechanical engineering (Dolce et al., 2000, and Dolce and Cardone, 2001).

Grasser and Cowzzarelli (1991) presented experimental results and analytical material modeling for SMAs material. They used nickel-titanium SMA known as Nitinol. A heat treatment was specified by them such that a hysteretic material response close to that of super-elasticity was attained. They reformulated Ozdemir's one-dimensional model

of rate-independent force-deformation behavior in terms of stress and strain, and then modified to allow for the simulation of hysteretic behavior of SMAs. Also they obtained the experimental results for the cyclic behavior of a nickel-titanium SMA for varying levels of strain and strain rate. Finally they evaluated the capability of the model of SMA behavior using experimental results. From their results, they demonstrated the usefulness of SMAs in earthquake engineering. From their cyclic loading of Nitinol, It can be noticed that residual strain is very small when the stress is reached zero during unloading process. Another point which they noticed is, yield points are not the same during tension and compression. Also they noted the hysteresis loop shifting by small increments for each cycle. They noted two important points regarding strain rate behavior in Nitinol: the axial yield points for tension and compression did not show a pronounced sensitivity to the varying levels of strain rate that were applied; the inelastic uniaxial response to Nitinol is rate-dependent and affects the overall shape of the fully developed cyclic hysteresis.

Wilde et al. (2000) used the model explained in Grasser and Cowzzarelli (1991) for their analysis and extended it to represent the hardening of the SMA after the transition to martensite is completed. Also, Wilde et al. (2000) presented a design of a SMA bar damper added to the laminated rubber bearing isolation system. They presented the performance of the proposed smart isolation system together with the conventional isolation system using laminated rubber bearing with lead core and an additional stopper device, referred to as an NZ system. They concluded that The SMA isolation system provides stiff connection between the pier and the deck for small external loading. For a medium size earthquake, the SMA bars increase the damping capacity of the isolation due to stress induced martensitic transformation of the alloy. For the largest considered earthquake, the SMA bars provide

hysteretic damping and, in addition, act as a displacement controlling device due to hardening of the alloys after completeness of the phase transformation. The damage energy, summation of kinetic energy of pier and deck, and strain energy of the pier and laminated rubber bearing, of the bridge with SMA isolation system is small, even though the input energy to the structure is larger than to a bridge with lead rubber bearings. One drawback of adding SMAs is an increase in acceleration response. They have explained this sudden jump in acceleration as a result of the nonlinear characteristics of SMAs, particularly during the transition from "plastic" response to the elastic one.

Dolce et al. (2000) described the conceptual design process; the functioning mechanism of SMA based devices, braces and base isolation, and the results of an extensive experimental investigation. Dolce et al. (2000) defined three fundamental preliminary steps in the conceptual design process of SMA devices. Those are selection of the most suitable alloy for the SMA kernel components; selection of the shape of SMA kernel components; and selection of the stress mode of SMA kernel components. They tested five different alloy types, comparing their mechanical and durability properties, and NiTi (nickel-titanium) also called as Nitinol was selected as the most suitable SMAs for passive control devices because of their better super-elastic properties, lower sensitivity to temperature, higher resistance to corrosion and fatigue.

Since there is limitation on workability of the material, kernel components for devices can only be drawn from wires or bars (Dolce et al., 2000). Nitinol wires can only be used in their austenitic phase, as super-elasticity allows them to undergo large deformation without any residual strain. On the contrary Nitinol bars can be employed either in their martensitic or in their austenitic state (Dolce et al., 2000). Under bending or

torsion stress mode, martensite bars shows almost same behavior which has good energy dissipation capacity but partially super-elasticity (Dolce et al., 2000).

Dolce et al. (2000) considered full re-centering and good energy dissipation as the main targets of the conceptual design. A wide range of mechanical behaviors can be obtained with the same device, by simply varying the number and/or the characteristics of the SMA elements of both groups, as well as the pre-tensioning levels of the re-centering wires. Dolce et al. (2000) classified the resulting devices into three categories based on the residual displacement at the end of the action or the eventual supplemental recovering force. Those are, Supplemental Re-Centering Devices (SRCD), Not Re-Centering Devices (NRCD), Re-Centering Devices (RCD). They found that the mechanical features of device can be calibrated according to the desired features and fit the specific needs mainly due to the modularity of the two groups of elements governing the two aspects, re-centering and energy dissipation.

Dolce and Cardone (2001) investigated the mechanical behavior of several specimens of Nitinol SMA, subjected to torsion tests, through a large experimental test program and numerical simulations in order to verify their possible use of kernel components of seismic protection devices. They tested martensite and austenite, wires and bars with different diameter, with different alloy composition and thermo-mechanical. They used different stress mode like tension, torsion, bending and shear. They found that the martensite bars provide large energy dissipation and extraordinary fatigue resistance capabilities than austenite bars where as austenite bars shows negligible residual deformation at the end of the action (superelasticity). They concluded that the SMA bars

subjected to torsion have a good potential for their use as kernel components in seismic devices.

Dolce et al. (2000), and Dolce and Cardone (2001) concluded many basic features of SMA devices, such as great versatility (the possibility to obtain a wide range of cyclic behaviors), simplicity of the functioning mechanism (in spite of their sophisticated behavior), Self-centering capability, high stiffness for small displacements, good energy dissipation capability, extraordinary fatigue resistance, long-term reliability (due to the absolutely negligible relaxation effects of the pre-tensioned SMA wires), high durability (an excellent corrosion resistance of Nitinol alloys and no degradation due to ageing).

Dolce and Cardone (2003) examined the advantages and drawbacks of different types of isolation systems considering the protection of internal components (secondary systems). They considered rubber isolators, steel-hysteretic isolators, and re-centering SMA isolators. In their study, internal system was considered as elastic single degree of freedom system by them. They evaluated the capacity of fixed-base and base isolated models with different isolation systems to protect light secondary system by comparing the floor response spectra obtained from the storey accelerations recorded during the shaking table tests. They confirmed the effectiveness of seismic isolation in reducing the accelerations on the internal content of the structures. However, they pointed out that each type of isolation system can result more or less effective in certain frequency ranges, depending on their dynamic behavior. They explained the possibility of tuning effects which should be considered. They suggested that the choice of the type of isolation system as well as its design must be optimized with respect to the type and the dynamic characteristics of the internal content to be protected.

Dolce et al. (2004) demonstrated the effectiveness of re-centering devices based to retrofit existing old buildings which were designed only for gravity load. They carried out experimental test on an existing old two storey, one bay, R/C building to be demolished, which was designed in the seventieth for gravity load only. They used re-centering SMA devices (RCD) which had austenitic Nitinol wires. They carried out quasi-static cyclic tests and release tests on both bare and braced frame. They demonstrated that the passive protection system based on SMA wires behaves as expected and increase the safety of the structure.

Dolce et al. (2005) presented a comprehensive overview of the main results of the shaking table tests carried out on Reinforce Concrete (R/C) frame models with and without energy dissipating braces which were based on the hysteretic behavior of steel components (EDBs) and on the super-elastic properties of Shape Memory Alloys (SMAs). They compared the performances of the SMAs braces to steel EDBs. Up to certain seismic intensities (0.3g PGA) the model equipped with SMA and steel braces exhibited similar response in terms of storey accelerations and inter-story drifts. Also they found that the new SMA braces can provide performances at least comparable to those provided by currently used devices, but the SMA devices do not need to be substituted after a strong earthquake because those have high low fatigue resistance.

Song et al. (2006) presented a review of effectiveness and feasibility of SMA devices, both isolation system and energy dissipation system. They summarized the basic properties of Nitinol SMA and their application in passive structural control, active frequency tuning (semi-active) and active damage control.

Dolce and Cardone (2006) provided an overview of the main results achieved, consisting of the conceptual design, implementation, and testing of three families of SMA based devices, namely: special braces for framed structure, seismic isolation devices for buildings and bridges, and smart ties for arches and vaults. They demonstrated following as the basic features of SMA ties: accurate calibration of the stress in the tie, reduction of the force changes caused by temperature variations, ability of applying the force in the tie anchorages without jerks during an earthquake, dissipation of a considerable amount of energy during an earthquake, high stiffness for large displacements in order to limit the maximum deformations in the structure under unexpected earthquakes, and capacity of avoiding buckling under negative displacements. Also they proved full applicability and reliability of the SMA devices under real conditions through some demonstrative release tests on two real buildings equipped with SMA based isolation systems and SMA based bracing system.

Dolce et al. (2007a) assessed the effectiveness of SMA isolation systems in reducing structural seismic vibrations trough shaking table tests on reduced scale R/C models. They compared the structural response of the models equipped with SMA isolation system to that of fixed base systems and of models equipped with more common isolation devices, that is rubber isolators and steel hysteretic devices. They showed that the SMA isolation can provide outstanding structural performance as other common isolators. Dolce et al. (2007b) tested the applicability of SMA isolators for bridges.

Nitinol is fairly sensitive to temperature changes with respect to its hysteretic cycle and loses its superelastic behavior in cold temperatures (Zhang et al., 2008). Zhang et al. (2008) examined the suitably of superelastic copper-aluminum-beryllium (Cu-Al-Be) ally

wires for the seismic protection of bridges. They carried out uniaxial cyclic tests as well as monotonic testing of superelastic Cu-Al-Be wires at cold temperature using a temperature chamber. They found that Cu-Al-Be alloy shows better results for different temperatures. It maintains its superelastic behavior within very wide range of temperature from -85° C to 100° C.

Motahari et al. (2007) introduced a single damper in order to obtain the most efficient behavior of the structure instead of using different combinations of complicated dampers as proposed by Dolce et al. (2000). They achieved the optimized behavior of the SMA damper by numerical studies performed with different configurations for SMA material in the damper using the constitutive model proposed by Motahari and Ghassemieh (2006). They used two phases of SMA, austenite and martensite, in the damper in order to achieve an efficient behavior of both the re-centering and high energy dissipating capability. They considered one bay three storey frame and four different SMA dampers in their analytical study. They compared the results of four SMA dampers with buckling resistant steel braces. They utilized the idea of damage indicator to attain a comparative basis for the different systems. They showed the effectiveness of the implementation of SMA dampers especially in reduction of the residual deformations on the structure even after very high ground motions.

Zhang and Zhu (2008) presented a simulation-based benchmark control study in which NiTi based SMA wire dampers were utilized to control the seismic response of a three-storey nonlinear steel frame building. They used the modified version of the Wilde model for analytical modeling of the load-displacement behavior of the SMA wire damper. They studied the SMA wire dampers with prestrained and un-prestrained. They showed

that the SMA wire dampers can reduce the peak drift ratios of the seismically excited three-storey nonlinear structure but tend to amplify the peak acceleration of the three-storey structure building.

Motahari and Ghassemieh (2006) proposed simplified constitutive model which is able to predict superelasticity and detwinning process of SMAs under both isothermal and adiabatic conditions. It is a simple multi-linear one-dimensional thermodynamics constitutive model for modeling the behavior of SMAs under different loading conditions, low rate and high rate, and at different temperatures. They found that the ability of the proposed model to simulate the behavior of SMAs under high rate loading conditions, especially Nitinol, makes it appropriate for use in seismic applications. Also they verified the model with experimental data and found good match.

The major drawback of SMA based dampers is high cost (Christopoulos et al., 2008). But the price of SMA material may decrease due to the increase in demand in different emerging applications and technologies (Motahari et al. 2007).

CHAPTER 3. FOUNDATION ENERGY DISSIPATION

This section summarizes experimental and numerical studies of combine loading on shallow foundations and consequence energy dissipation available in literature. Taylor et al. (1981) did experiments on sand and on clay soils for a rigid rectangular surface footing. Georgiadis and Butterfield (1988) presented the results of an experimental investigation of the displacements of rectangular surface footing on sand. Gottardi et al. (1999) presented plastic response of circular footing on sand under general planar loading. Gajan et al., (2005) performed 20-g centrifuge model test on shallow foundations, on sand and clay, subjected to vertical, lateral slow cyclic and dynamic loading. Gajan and Kutter (2008) presented the findings of tests conducted on shallow footings, attached to a shear wall structure, subjected to slow lateral cyclic and dynamic loading at 20g centrifugal acceleration. They mainly discussed the interrelation of the ratio of the footing area to the footing contact area required to support the applied vertical loads (A/Ac) with moment capacity, energy dissipation, and permanent settlement measured in centrifuged and 1-g model tests.

Nova and Montrasio (1991); and Houlsby and Cassidy (2002) presented macro-element model to evaluate settlements and rotations of rigid shallow foundations for monotonic loading. Cremer et al., (2001) developed non-linear soil-structure interaction macro-element model for cyclic loading. Gajan and Kutter, 2008 introduced a new Contact Interface Model to provide nonlinear relations between cyclic loads and displacements of the footing-soil system during combine cyclic loading. Contact interface model is based on the concept that the modeling of the cyclic load-deformation behavior of a rocking footing can be based upon modeling and tracking the shape of the deformed soil surface beneath

the footing, the locations where the footing is in contact with the underlying soil, and the size and location of gaps between the footing and soil.

3.1. Experimental Studies from Literature

Taylor et al. (1981) presented the moment-rotation-settlement relationships for a rigid rectangular surface footing (0.50m x 0.25m) on sand and clay soils. A simple theory was proposed based on Winkler model. They investigated both extended Winkler model results and experimental results. They found that correlation between extended Winkler model and experiment is, in general, reasonably close. Experiment results show that the rocking along longer axis produces more displacement and the displacement increases with reduction in vertical factor of safety (FS_v) which is the ratio of the ultimate vertical load to applied vertical load. The settlement at the largest amplitude and the hysteretic energy loss were continuous during cyclic loading. They recommended more study for footing on sand for rocking loading because this study was carried out for the footings on surface which is not common. They found for FS_v=3 foundation on clay soil, the test results shows that small vertical displacement continues with the successive cycle of loading, even though the extended Winkler model prediction was permanent vertical displacement would occur only in the first cycle of loading. Repeated cyclic loading reduces the rotational stiffness as well as the maximum moment, as a result of degradation of clay. Also with increasing amplitude of the applied rotation, rotational stiffness reduces. They recommended that the yielding of soil at high amplitude and at successive cycles, during earthquake, can be used as a beneficiary activity for earthquake resistant design. Also, by designing spread footing

which will yield in rotation at an applied moment less than the moment capacity of the column, column hinging can be avoided.

Georgiadis and Butterfield (1988) presented the results of an experimental investigation of the displacements of surface footing (0.40 m x 0.05 m) subjected to eccentric and inclined loads on sand. The experimental results were analyzed and interpreted using elastic theory which then augmented to provide the complete nonlinear footing response. They compared the relationship between vertical and horizontal ultimate loads, ultimate vertical loads and ultimate applied moment achieved in the test with experimental results of other several investigators and tests from literature. Almost all the results were compared with Pragash (1981) who developed an empirical nonlinear method for predicting the vertical displacement and rotation of vertically and eccentrically loaded footings on sand. They also proposed an empirical equation for bearing capacity which includes the combined effect of eccentricity and inclination using interaction diagrams between vertical loads, horizontal loads and moments. They found that the horizontal displacement of all footing were almost zero until failure condition were approached. Also the larger the load eccentricity is the smaller the horizontal displacement. The research revealed that as the load inclination increases the vertical displacement of the footing decreases and the horizontal displacement increases. They developed a method for predicting displacements of footings subjected to inclined and eccentric loads.

Gottardi and Butterfield (1995) presented extensive data on the load-displacement response of vertical, horizontal and rotational displacement trajectories of a model surface footing (0.5 m x 0.1 m), derived from a series of 1-g monotonic loading and unloading experiments carried out at the University of Pavoda. Particularly, information from the

load-displacement records and a proposed extension of the interaction diagram analysis to establish a basis for modeling the footing response at lower loads. They applied the concept of interaction diagram to the V-H-M/B load components acting on a footing which was lead to a failure envelope that is all load points causing failure of the footing lie on a surface in V-H-M/B space. They represented the whole failure envelope by a single equation which gives parabolic failure surface. The surface which is corresponded to ultimate vertical load gives the yield surface. They found that, by scaling conjugately the displacements generated by radial load tests and plotting them in normalized V-H-M planes, a unified diagram was obtained in which identical pairs of load inclination (tan α) and eccentricity (e/B) generate identical displacement trajectories.

Gottardi et al. (1999) presented plastic response of circular footing on sand under general planar loading. They mainly focused on the tests, which were designed to provide the information necessary to construct a complete model of the footing behavior, based on the concepts of plasticity theory. Particularly, the tests provide detailed information about the shape of the yield surface, and also allow generalization of bearing capacity calculations to cases of combine loading. Test results are relevant to surface footing and the tests were done by displacement control method. The adapted hypothesis is that, after a given penetration of the footing, a yield surface will be established in Vertical force (V), Moment (M/2R, where R is radius of circular footing) and Horizontal force (H) space. Within this surface, the displacement would be substantially elastic. If the footing is pushed further into the ground, the yield surface expands. They did three types of tests on dense sand. Vertical loading test was conducted to establish the vertical load displacement relationship up to the relevant maximum penetration and to find the information about the

vertical elastic stiffness of the footing. Another test conducted is called swipe test. At specific vertical load, if the footing is driven purely horizontally, while the horizontal load increases, the vertical load decreases, then the load path sweeps out a track in V- M/2R-H space. In the same way pure rotation is applied then moment is developed. This type of tests called a swipe test which was allowed to direct investigation of the shape of the yield surface at a given penetration. The other test is radial displacement test which involved in application of a straight displacement path in vertical displacement, horizontal displacement and rotation space. Through these tests they came to a conclusion that the shape of yield surface in V- M/2R- H space is well described by a parabolic ellipsoid. Also they stated that the hardening behavior can be defined by expressing the size of the yield surface as a function of plastic vertical penetration. And the tests can be successfully interpreted in the context of hardening plasticity theory in terms of force resultant and overall footing displacements.

Gajan et al. (2005) performed 20-g centrifuge model test on shallow foundations, on sand and clay, attached to a rigid shear wall subjected to vertical, lateral slow cyclic and dynamic loading. They carried out five series of tests including forty model shear wall footings to study the effect of footing dimensions, depth of embedment, and initial static vertical factor of safety on soil-foundation system response. Initial static vertical factor of safety was changed by changing the structural weight and footing dimensions. They found that the moment rotation behaviors during lateral slow cyclic and dynamic tests agree very well. So, slow cyclic tests may be appropriate for simulating moment rotation behavior in dynamic events. However there was no clear trend in terms of the effect of vertical factor of safety on rotational stiffness reduction. Their test results in cyclic and dynamic tests

showed that the footing tends to accumulate vertical settlement as the movement and shear loads were cycled. They indicated that a consistent reduction in rotational stiffness due to uplift and separation of the base of the footing from the soil through the slope of the curve in the intermediate region of any moment-rotation plot becomes less steep with larger deformations. They showed that their experimental results agreed with the failure envelopes developed by Cremer et al (2001), and Houlsby and Cassidy (2002) indicating that previously developed analytical expression can be used for modeling of shallow foundations subjected to combined moment, shear, and axial loading. Also the changing location of the resultant of bearing pressure distribution with the rotation of footing dictates the moment-rotation behavior. They observed the occurrence of rounding of soil beneath the footing as the building rocks, which is consistent with the observed reduction in moment-rotation stiffness associated with the uplift of the footing.

Gajan and Kutter (2008a) presented the findings of tests conducted on shallow footings (2.8 m x 0.65 m and 2.7 m x 0.65 m), supported by medium dense to dense sand and clay soil stratums, attached to a shear wall structure subjected to slow lateral cyclic and dynamic loading at 20g centrifugal acceleration. They mainly discussed the interrelation of the ratio of the footing area to the footing contact area required to support the applied vertical loads (A/Ac) with moment capacity, energy dissipation, and permanent settlement measured in centrifuged and 1-g model tests. Considering slow cyclic tests, their results show that while A/Ac increases, moment capacity increases, and energy dissipation due to soil inelasticity and permanent settlement decrease. They observed similar moment-rotation-settlement behavior in footings on clayey soil and sandy soil for slow cyclic test. They found that designing footings with a large A/Ac ratio with uplift allowed, allow

considerable amount of energy dissipation of the footing and minimal permanent settlement. It was found that the effect of shaking intensity on the dynamic load-displacement behavior of footing could be compared to the effect of the magnitude of applied rotation on the behavior of footing in slow lateral cyclic loading tests. Through their analysis results they recommended soil yielding instead of structural damping mechanisms or combination of soil yielding and structural damping mechanisms to improve the performance of the structure during cyclic loading.

3.2. Numerical Analysis from Literature

3.2.1. Winkler-Based Modeling

One of the common method used when modeling soil-foundation-interaction is the Winkler model (Harden et al., 2005; Houlsby et al., 2005; Allotey and Naggar, 2008; Raychowdhury and Hutchinson, 2009).

Raychowdhury and Hutchinson (2009) proposed a beam-on-nonlinear-Winkler-foundation (BNWF) approach for modeling shallow foundation behavior under seismic loading. The proposed model builds upon that of Harden et al. (2005) and complements that of Allotey and Naggar (2003, 2008). The proposed two-dimensional BNWF model is constructed with a mesh of closely spaced, independent nonlinear spring elements placed vertically along the length of the footing and horizontally at the ends of the footing. A region of increased stiffness is provided at the end of the footing such that the rotational stiffness is appropriately accounted for. Raychowdhury and Hutchinson (2009) mentioned that the model has the following attributes: backbone curves of the spring models are calibrated against shallow footing tests, elastic stiffness are directly adopted to characterize

the spring curve, nominal tension capacity is allowed in the model, a variable vertical stiffness distribution along the base of the model is incorporated to capture rotational stiffness, and the model is able to capture experimentally observed behavior for a broad range of shallow footings, soil types, vertical factors of safety and loading histories.

3.2.2. Macro-element Model

Nova and Montrasio (1991) presented a macro-element model to evaluate settlements and rotations of rigid shallow foundations on sand under the combined action of inclined and eccentric loads. They defined the non-dimensional forces (F_V, F_H, and F_M) and displacements (U_V, U_H, U_M) in such a way that forces and displacements satisfy the expression of the work density. They did two series of tests. One test series was with horizontal and vertical loads and another was with eccentric vertical loads. The analytical expressions of failure locus are given in equation 3.2.1 and equation 3.2.2

$$f(F_V, F_H) = F_H - F_V(1-F_V)^{\beta} \qquad 3.2.1$$

$$f(F_V, F_M) = F_M - F_V(1-F_V)^{\beta} \qquad 3.2.2$$

Where, β is a parameter which controls the position of the maximum horizontal load. For eccentric and inclined loading conditions, combined (V-H-M) loading, the failure envelope is as follow,

$$f(F_V, F_H, F_M) = F_H^2 + F_M^2 - F_V^2(1-F_V)^{2\beta} \qquad 3.2.3$$

Nova and Montrasio (1991) showed that the theory based on strain-hardening plasticity describes the observed behavior of model shallow foundations on sand with reasonable accuracy. Especially they indicated the model prediction of increased vertical

displacement while the vertical load decreased. Nova and Montrasio (1991) model is applicable for monotonic loading.

Houlsby and Cassidy (2002) described a complete theoretical model, based on work hardening plasticity theory, for the behavior of rigid circular footings on sand, when subjected to combine vertical, horizontal and moment loading. They specified the precise form of the hardening law by a relationship between the size of the yield surface and the plastic vertical deformation. However, Houlsby and Cassidy (2002) model is applicable only for monotonic loading.

Cremer et al. (2001) presented a non-linear soil-structure interaction macro-element model for shallow foundation on cohesive soil. The macro-element reproduces the cyclic behavior of the foundation, including the effects of non-linearity occurring in the near field. They modeled the yielding of the soil under the foundation through a plasticity model and contact non-linearity induced by the uplift of the foundation as uplift model. Both those model are coupled together even though developed separately. They showed that macro-element is a practical and efficient tool that ensures the accurate integration of the effect of soil-structure interaction.

3.2.3. Contact Interface Model

Gajan and Kutter (2009a) presented a new Contact Interface Model (CIM) to provide nonlinear relations between cyclic loads and displacements of the footing-soil system during combine cyclic loading. CIM is based on the concept that the modeling of the cyclic load-deformation behavior of a rocking footing can be based upon modeling and tracking the shape of the deformed soil surface beneath the footing, the locations where the

footing is in contact with the underlying soil, and the size and location of gaps between the footing and soil (Gajan and Kutter, 2009a).

Gajan and Kutter (2009a) mentioned that the most important parameter governing load capacities, settlement, sliding, and rotation is critical contact area ratio (A/Ac) which defines the geometry and kinematics of the moving contact problem. The CIM is placed at the footing-soil interface, replacing the rigid footing and surrounding soil in the zone of influence (Gajan and Kutter, 2009a). The CIM incorporates the coupling between forces and displacements in V-H-M space and captures the essential features of moment-rotation-settlement and shear-sliding-settlement relationships (Gajan and Kutter, 2009a). Also, Gajan and Kutter (2009a) showed that the CIM predictions for moment and shear capacities, stiffness degradation, energy dissipation, and displacements compare well with the experimental results.

The CIM can be utilized in OpenSeeS. SoilFootingSection2D, a two-dimensional section material that represents the CIM in OpenSees, material is used with a ZeroLengthSection element to represent the two-dimensional footing-soil interface that has three degrees of freedom of forces and displacements (Gajan and Kutter, 2008b). Node 1 and node 2 connects the ZeroLengthSection element while node 1 is fixed in all three degrees of freedom and node 2 is free to settle, slide, and rotate (Gajan and Kutter, 2008b). The CIM requires six user-defined parameters, described in Gajan and Kutter (2009a) and those are follows,

1. Ultimate vertical load (Vult): Vult calculation can be included the effects of embedment of the footing, surface surcharge, and shape of the footing.

2. Length of the footing (L): Linear dimension of the footing in plane of rocking.

3. Initial Vertical Stiffness (Kv): Initial vertical stiffness of the foundation when the footing is in full contact with soil for pure vertical loading. It is considered as elastic vertical stiffness of the entire footing. The initial elastic vertical stiffness is given by,

$$Kv = \frac{4.G.R}{1-v} \qquad \text{Eq.3.3.6}$$

Where G is shear modulus of the soil, R is effective radius of the footing, and v is Poisson's ratio of the soil.

4. Initial Horizontal Stiffness (Kh): Initial horizontal stiffness of the foundation when the footing is in full contact with soil for pure shear loading. It is considered as elastic horizontal stiffness of the entire footing. The initial elastic shear stiffness is given by,

$$Kh = \frac{8.G.R}{2-v} \qquad \text{Eq.3.3.7}$$

5. Rebound Ratio (Rv_o): It is an empirical parameter to account for the elastic rebound and bulging of soil into the gap associated with plastic compression in neighboring loaded areas. The value may differ as it fits to particular problem.

6. *Internal Node Spacing (ΔL):* Specifies the distance between the footing-soil interface nodes internally created in the CIM. It should be chosen to be significantly smaller than the critical contact length.

Gajan et al. (2010) reviewed both BNWF and CIM. They compared the predicted responses for the model building. They discussed relative strengths and limitations of foundation-soil models. Also, they summarized their suggestions for practical implications of both numerical models.

CHAPTER 4. STRUCTURAL NUMERICAL SIMULATIONS

This chapter presents the details of shaking table experiments of fixed base frame structures carried out under MANSIDE (Memory Alloys for New Seismic Isolation and Energy Dissipation Devices) project in Italy (Dolce et al., 2005, 2007b) and numerical simulations of those experimental models using OpenSees finite element framework. Experimental models include 3-story frame structures with and without seismic energy dissipation devices. Structural energy dissipation devices include steel and shape memory alloy (SMA) braces and SMA base isolation systems.

4.1. Shake Table Experiments

Shaking table experiments on frame structures with and without passive energy dissipation devices were conducted as part of the MANSIDE project (Memory Alloys for New Seismic Isolation and Energy Dissipation Devices) in University of Basilicata, Italy (Dolce et al., 2005, 2007b). Three types of structures were subjected to dynamic base shaking loading: (1) fixed-base bare frame structures, (2) fixed-base frame structures with steel or shape memory alloy (SMA) energy dissipating braces, and (3) frame structures with SMA base-isolation systems. Structures were designed in reduced scale (scale factor = 1/3.3) to obtain geometrically similar characteristics of full-scale prototype structures (Dolce et al., 2005, 2007b). Fig. 4.1 shows the schematic of the bare frame model structure tested in shaking table experiments together with the cross sections of the typical column and beam. Fig. 4.2 shows the schematics of the frame with energy dissipating braces and the frame with base isolation system.

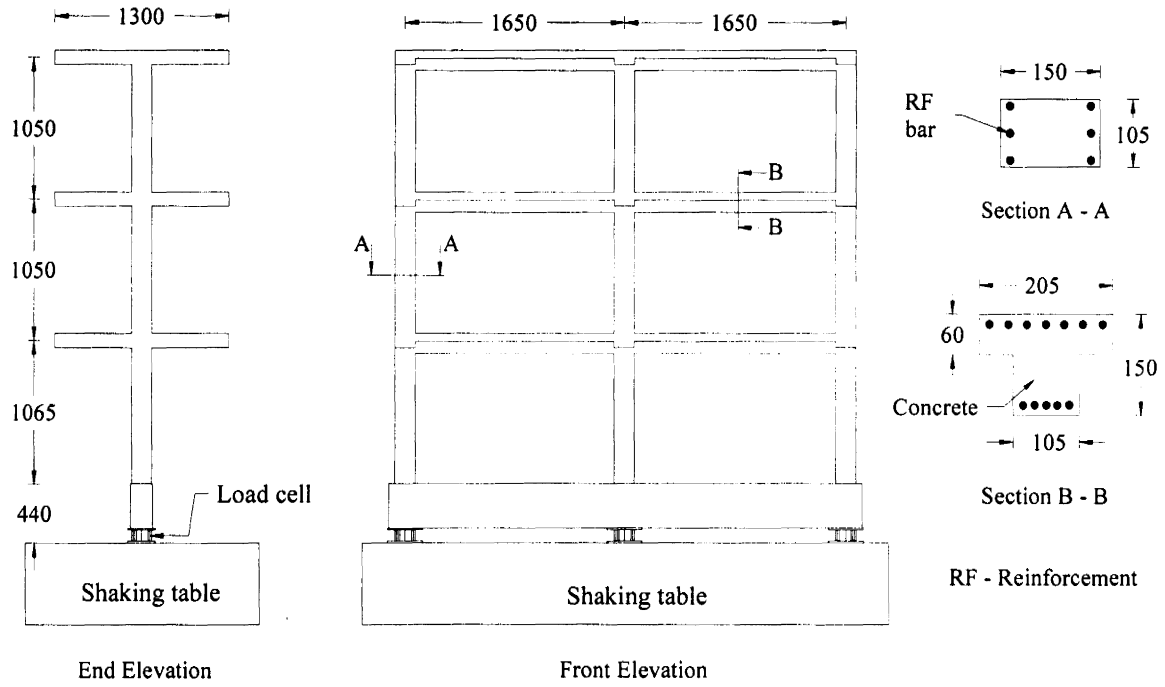

Fig. 4.1. Schematic of the shaking table experimental model of bare frame structure (conducted in University of Basilicata, Italy) (All dimensions are in mm)

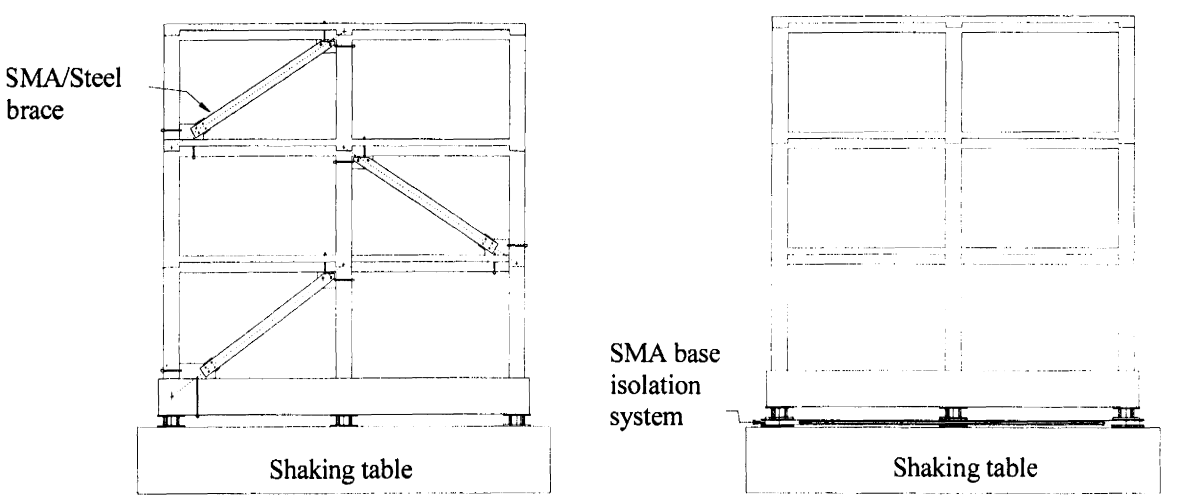

Fig. 4.2. Schematic of the shaking table experimental model of frame with braces (left) and frame with base isolation system (right)

The dimensions and the cross sections of beams and columns of all three structures were identical. A strong beam at the base was used to provide the fixed-base condition and it was supported on load cells. The total weight of the bare-frame structure was 101.2 kN,

compressive strength of the concrete used in the experiments was 34.2 MPa, and the yield stress of the reinforcement bar (4 mm diameter bars) was 560 MPa (Dolce et al., 2005, 2007b).

For the structures with passive energy dissipating devices, two types of braces were used: (1) steel braces and (2) SMA braces. The core components of the steel braces consisted of X-shaped steel plates that have different geometry at each storey level, so as to provide the device with the required design stiffness and yielding force (Dolce et al., 2005). The core components of the SMA braces consist of pre-tensioned Nickel–Titanium (NiTi) austenite super elastic wires arranged in two different ways, in order to provide the device with both self-centering and energy dissipating capacity (double-flag-shaped hysteretic loops) (Dolce et al., 2005). The area of the steel braces was 2700 mm^2 while it was 1100 mm^2 for SMA braces (Dolce, et al., 2005).

The base isolation systems included three steel–PTFE sliding bearings, supporting the total weight of the structure while accommodating large lateral displacements, and an isolation device. The core energy dissipating components of the SMA base isolation system were similar to SMA brace (Dolce et al., 2007b).

Fig. 4.3 shows the normalized time history and response spectra (with 5% damping ratio) of the applied base acceleration in the experiments. The acceleration time history was scaled to obtain maximum peak accelerations varying from 0.07g to 0.74g, without altering the frequency contents. Table 4.1 presents the fundamental periods of all the structures for first three modes. The first mode natural period of the structures vary from 0.1 sec to 0.3 sec, indicating that the structures are very sensitive to the selected ground motion (see the response spectra in Fig. 4.3). The inclusion of energy dissipating braces essentially makes

the structure stiffer and hence the reduction in natural period, whereas the base-isolation system lengthens the natural period of the structure, as expected. Note that the natural periods are calculated based on the initial stiffness of the structural system (elastic) in OpenSees. For large displacements, the natural period of the structure with base-isolation system increases even higher as can be seen in the displacement time history of the structure (presented later). Dimensions and results that are related to shaking table experiments are presented in model scale unless otherwise stated. More details of these experiments can be found in Dolce et al. (2005 and 2007b).

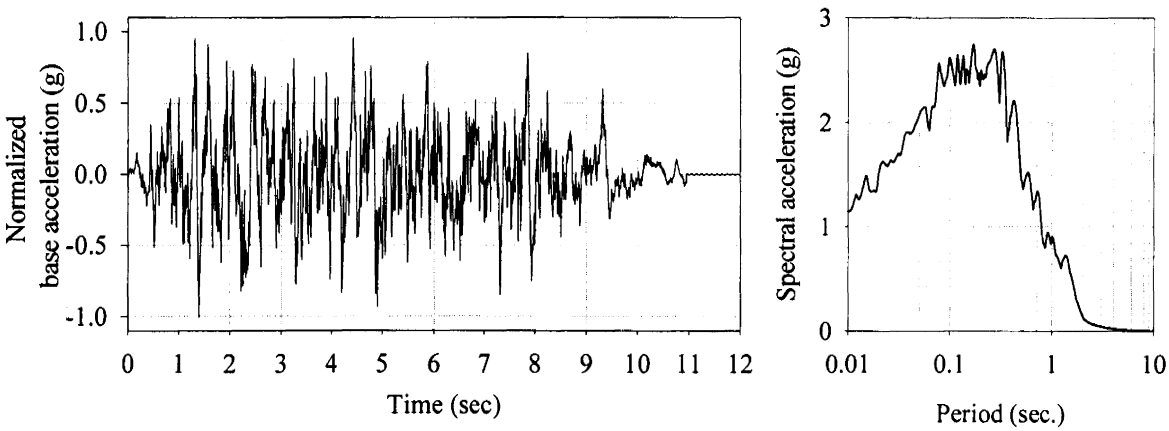

Fig. 4.3. Time history (left) and response spectra (right) of acceleration applied in the shake table experiments (time history is normalized by the peak acceleration)

Table 4.1. Fundamental periods of structures

Structure	Period		
	1st mode	2nd mode	3rd mode
BF	0.293	0.089	0.048
BR_SMA	0.112	0.043	0.026
BR_ST	0.116	0.041	0.028
BI_SMA	0.314	0.095	0.050

4.2. Material Constitutive Models

4.2.1. Steel_02 material model

The well-known nonlinear hysteretic nodel of Menegotto and Pinto (1973), as extended by Filippou et al. (1983), is adopted in OpenSees as Steel_02 material model. The model is computationally efficient and capable of reproducing experimental results with accuracy (Monti et al. 1993; Orakcal et al., 2006). The Menegotto and Pinto (1973) model is shown in Fig. 4.4. The model relationship is in the form of curved transitions, from a straight line asymptote with slope of modulus of elasticity (E_0) to another straight line asymptote with slope of yield modulus (E_1) where the strain-hardening ratio is *b*. A cyclic curvature parameter R governs the curvature between the two asymptotes and it permits the Bauchinger effect to be represented (Monti et al. 1993). Eq. 4.2.1 represents the curved transition.

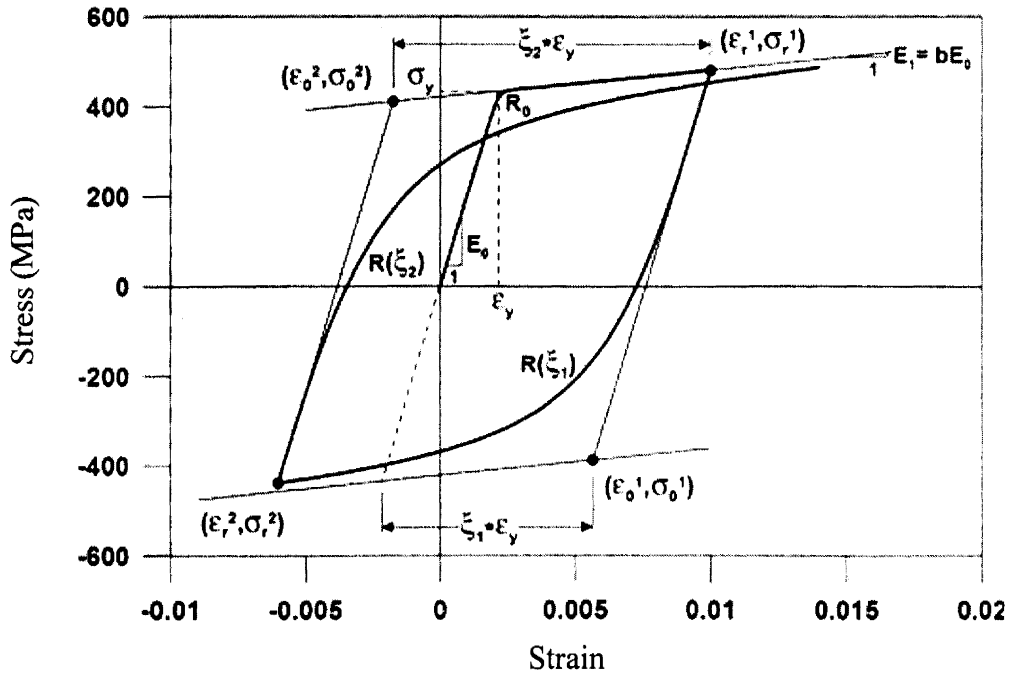

Fig. 4.4. Menegotto and Pinto (1973) constitutive model for steel (Monti et al. 1993)

$$\sigma^* = b \cdot \varepsilon^* + \frac{(1-b) \cdot \varepsilon^*}{(1+\varepsilon^{*R})^{1/R}} \qquad \text{Eq. 4.2.1}$$

where,

$$\varepsilon^* = \frac{\varepsilon - \varepsilon_r}{\varepsilon_0 - \varepsilon_r} \qquad \text{Eq. 4.2.2}$$

and

$$\sigma^* = \frac{\sigma - \sigma_r}{\sigma_0 - \sigma_r} \qquad \text{Eq. 4.2.3}$$

In Fig. 4.4, (σ_0, ε_0) and (σ_r, ε_r) are the set of stress and strain at the point where the two asymptotes of the branch under consideration meet and the point where the last strain reversal took place, respectively. These stress and strain values are updated after each strain reversal. R is considered depended on the strain difference between the current asymptote intersection point and the previous load reversal point with maximum or minimum strain depending on weather the corresponding steel stress is positive or negative (Monti et al. 1993). The expression for R takes the form suggested in Menegotto and Pinto (1973),

$$R = R_0 - \frac{a_1 \cdot \xi}{a_2 + \xi} \qquad \text{Eq. 4.2.4}$$

where ξ is updated following a strain reversal. R_0 is the value of the parameter R during first loading and a_1, a_2 are experimentally determined parameters to be defined together with R_0. The definition of ξ remains valid in case that reloading occurs after partial unloading (Monti et al. 1993). Filippou et al. (1983) proposed a stress shift in the linear yield asymptote as a function of the maximum plastic strain to account for isotropic hardening, however, the model used in this study was implemented without the isotropic strain hardening option (Monti et al. 1993; OpenSees, 2008). Typical hysteretic behavior of Steel_02 material without isotropic hardening is shown in Fig. 4.5, given in OpenSees manual (OpenSees, 2008). For reinforcement bars the parameter values are: R0=18,

a_1=0.925, a_2=0.15 as recommended by OpenSees Manual (OpenSees, 2008), and in case of special devices, these values are back calculated using the individual cyclic loading test results of those devices.

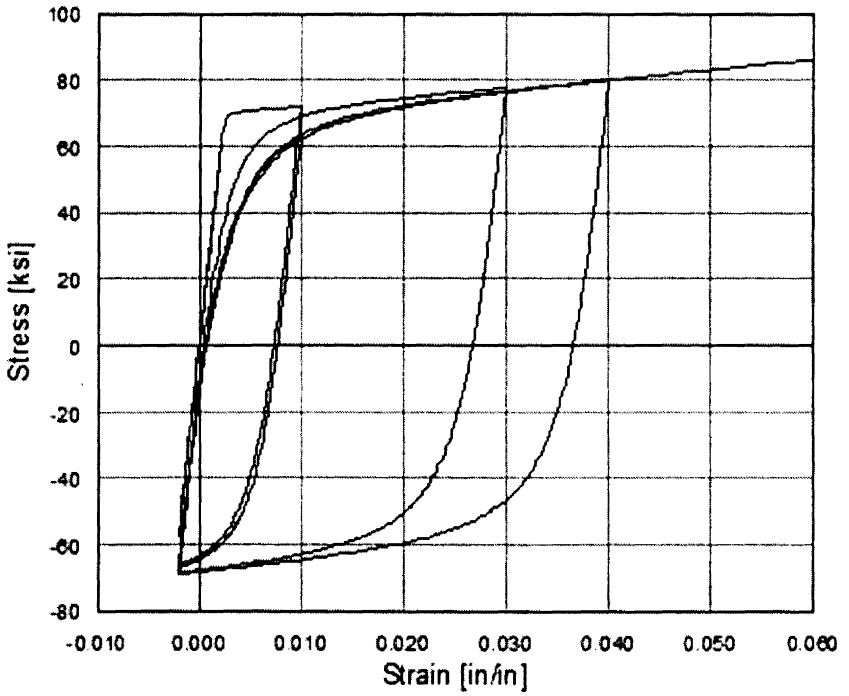

Fig. 4.5. Typical hysteretic behavior of Steel02 material without isotropic hardening (OpenSees, 2008)

4.2.2. Concrete_02 material model

A uniaxial hysteretic model proposed by Yassin (1994) is available in OpenSees as Concrete_02 material model (Fig. 4.6). The model takes into account concrete damage and hysteresis, while retaining computational efficiency (Orakcal et al., 2006). The monotonic envelope curve of the hysteretic model for concrete in compression follows the monotonic stress-strain relation model of Kent and Park (1971) as extended by Scott et al. (1982), called modified Kent and Park model, offers a good balance between simplicity and accuracy, and is widely used (Orakcal et al., 2006). The model proposed by Yassin (1994) is briefly described here as in Orakcal et al., 2006.

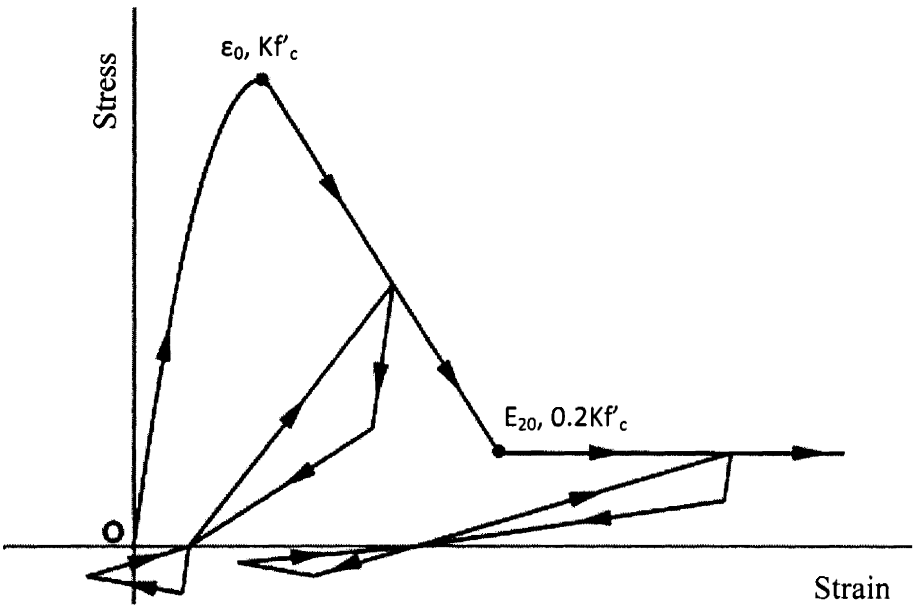

Fig. 4.6. Hysteretic unloading and reloading rules of model by Yassin (1994) (Orakcal et al., 2006)

The monotonic concrete stress-strain relation in compression is described by three regions as follows (compression is positive) (Orakcal et al., 2006),

Region 0A: $\varepsilon_c \leq \varepsilon_0$ $\sigma_c = Kf_c' \left[2\left(\frac{\varepsilon_c}{\varepsilon_0}\right) - \left(\frac{\varepsilon_c}{\varepsilon_0}\right)^2\right]$ Eq. 4.2.5

Region AB: $\varepsilon_c \leq \varepsilon_c \leq \varepsilon_{20}$ $\sigma_c = Kf_c'[1 - Z(\varepsilon_c - \varepsilon_0)]$ Eq. 4.2.6

Region BC: $\varepsilon_c \geq \varepsilon_{20}$ $\sigma_c = 0.2Kf_c'$ Eq. 4.2.7

The corresponding tangent moduli (E_t) are given by the following expressions:

$\varepsilon_c \leq \varepsilon_0$ $E_t = \frac{2Kf_c'}{\varepsilon_0}\left[1 - \frac{\varepsilon_c}{\varepsilon_0}\right]$ Eq. 4.2.8

$\varepsilon_c \leq \varepsilon_c \leq \varepsilon_{20}$ $E_t = -ZKf_c'$ Eq. 4.2.9

$\varepsilon_c \geq \varepsilon_{20}$ $E_t = 0$ Eq. 4.2.10

where

$\varepsilon_0 = 0.002K$ Eq. 4.2.11

$$K = 1 + \frac{\rho_s f_{yh}}{f_c'} \qquad \text{Eq. 4.2.12}$$

$$Z = \frac{0.5}{\frac{3 + 0.29 f_c'}{145 f_c' - 1000} + 0.75 \rho_s \sqrt{\frac{h'}{s_h}} - 0.002K} \qquad \text{Eq. 4.2.13}$$

In the equations above, ε_0 is the concrete strain at maximum compressive stress, ε_{20} is the concrete strain at 20% of maximum compressive stress, K is a factor that accounts for the strength increase due to confinement, Z is the strain softening slope, f_c' is the concrete compressive cylinder strength (unconfined peak compressive stress) in MPa, f_{yh} is the yield strength of transverse reinforcement in MPa, ρ_s is the ratio of the volume of transverse reinforcement to the volume of concrete core measured to the outside of stirrups, h' is the width of concrete core measured to the outside of stirrups, and s_h is the center to center spacing of stirrups or hoop sets (Orakcal et al., 2006).

The hysteretic unloading and reloading rules proposed by Yassin (1994) are a set of linear stress-strain relations, as shown in Fig. 4.6 (Orakcal et al., 2006). Although the compressive and tensile hysteresis loops are continuous, they are discussed separately for the sake of clarity. For compression, successive stiffness degradation for both unloading and reloading, for increasing values of maximum strain, are shown in Fig. 4.7. The stiffness degradation is such that the projections of all reloading lines intersect at a common point R. Point R is determined by the intersection of the tangent to the monotonic envelope curve at the origin and the projection of the unloading line from point B, which corresponds to a concrete strength $0.2\, f_c'$. The strain and stress at the intersection point are given by the following expressions (Orakcal et al., 2006):

$$\varepsilon_r = \frac{0.2K f_c' - E_{20}\varepsilon_{20}}{E_c - E_{20}} \qquad \text{Eq. 4.2.14}$$

$$\sigma_r = E_c \varepsilon_r \qquad \text{Eq. 4.2.15}$$

where *Ec* is the tangent modulus of the monotonic envelope curve at the origin, and E_{20} is the unloading modulus at point B of the monotonic envelope curve with a compressive stress of 0.2 f_c'. The magnitude of E_{20} has to be determined experimentally; a value of 10% of *c E* was used by Yassin (1994) (Orakcal et al., 2006).

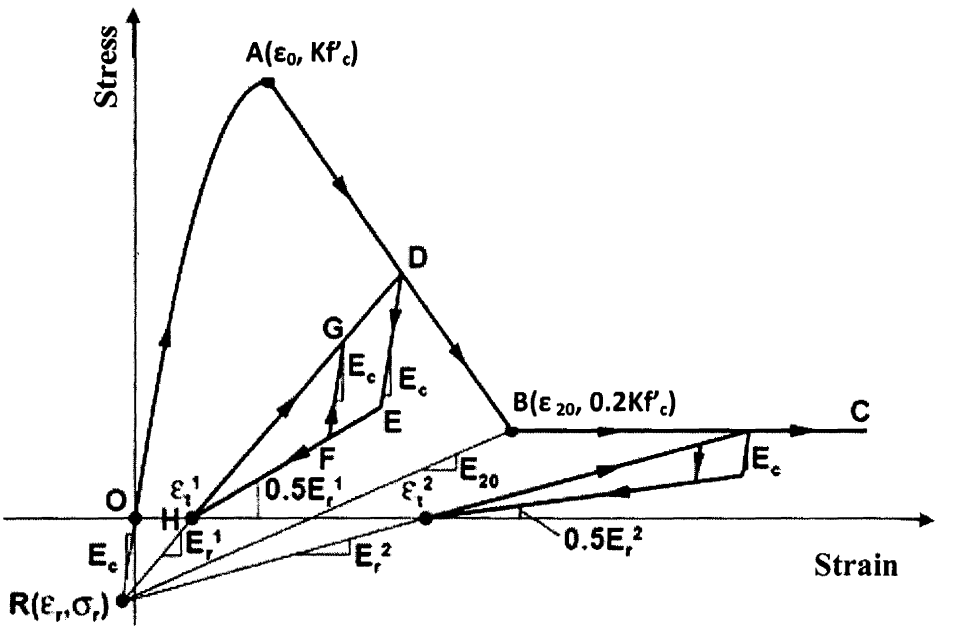

Fig. 4.7. Hysteretic parameters of model by Yassin (1994) (Orakcal et al., 2006)

Upon unloading from and reloading to a point on the compressive monotonic envelope (point D in Fig. 4.7), and above the zero stress axis (point H in Fig. 4.7), the model response follows two hysteretic branches that are defined by the following equations (Orakcal et al., 2006):

Maximum branch (line HD): $\sigma_{max} = \sigma_m + E_r(\varepsilon_c - \varepsilon_m)$ Eq. 4.2.16

Minimum branch (line HE): $\sigma_{min} = 0.5E_r(\varepsilon_c - \varepsilon_m)$ Eq. 4.2.17

Where

$$E_r = \frac{\sigma_m - \sigma_r}{\varepsilon_m - \varepsilon_r} \qquad \text{Eq. 4.2.18}$$

$$\varepsilon_t = \varepsilon_m - \frac{\sigma_m}{E_r} \qquad \text{Eq. 4.2.19}$$

Parameters σ_m and ε_m are the stress and strain at the unloading point on the compressive monotonic envelope, respectively. Therefore, the position of the unloading and reloading loop depends on the position of the unloading point. For partial loading and unloading cycles within the loops, the model follows a straight line with slope E_c. In the numerical implementation, a trial stress and tangent modulus are assumed based on the linear elastic behavior with slope E_c (Orakcal et al., 2006):

$$\sigma_c^T = \sigma_c' + E_c \Delta\varepsilon_c \qquad \text{Eq. 4.2.20}$$

where σ_c^T is the new trial stress, σ_c' is the previous stress state, and $\Delta\varepsilon_c$ is the strain increment. The following rules are then used to determine actual stress and tangent modulus of the model (Orakcal et al., 2006):

$$\text{if} \quad \sigma_{min} \leq \sigma_c^T \leq \sigma_{\max} \quad \text{then} \quad \sigma_c = \sigma_c^T \quad \text{and} \quad E_t = E_c \qquad \text{Eq. 4.2.21}$$

$$\text{if} \quad \sigma_c^T < \sigma_{\min} \quad \text{then} \quad \sigma_c = \sigma_{\min} \quad \text{and} \quad E_t = 0.5E_r \qquad \text{Eq. 4.2.21}$$

$$\text{if} \quad \sigma_c^T > \sigma_{\max} \quad \text{then} \quad \sigma_c = \sigma_{\max} \quad \text{and} \quad E_t = E_r \qquad \text{Eq. 4.2.21}$$

The tensile behavior of the model (Fig. 4.8) takes into account tension stiffening and the degradation of the unloading and reloading stiffness for increasing values of maximum tensile strain after initial cracking. The maximum tensile strength of concrete is assumed to be equal to (Orakcal et al., 2006):

$$f_t' = 0.623\sqrt{f_c'} \qquad \text{Eq. 42.22}$$

where f_t' and f_c' are expressed in MPa. Fig. 4.8 shows two consecutive tensile hysteresis loops, which are part of a sample cyclic history that also includes compressive stresses. The model assumes that tensile stress can occur anywhere along the strain axis, either as a result of initial tensile loading or as a result of unloading from a compressive state. In the latter

case, a tensile stress occurs under a compressive strain. The tensile stress-strain relation is defined by three points with coordinates (ε_t, 0), (ε_n, 0) and (ε_u, 0) in Fig. 4.8.

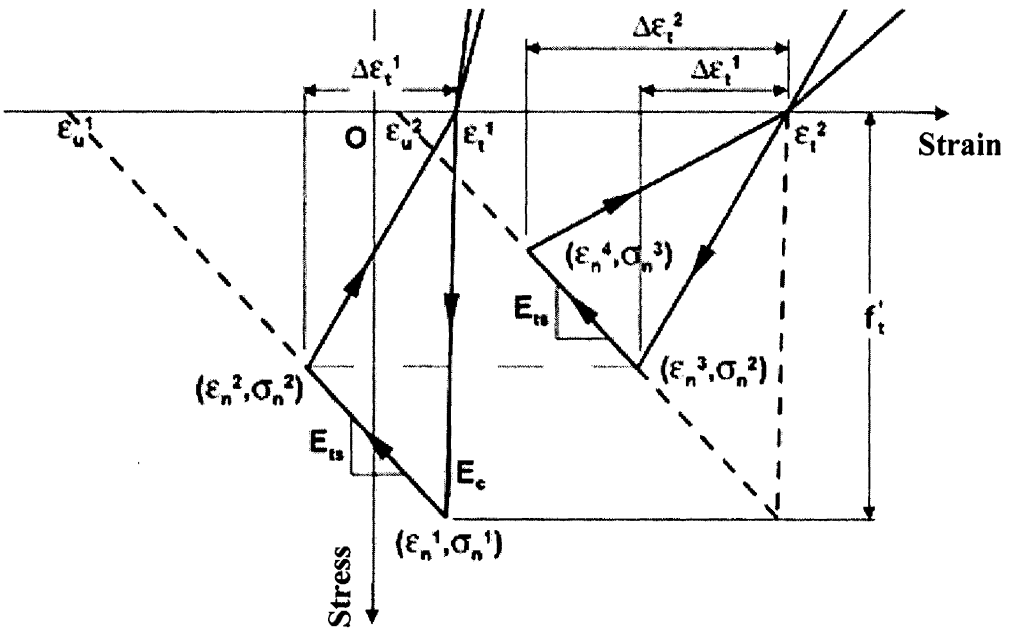

Fig. 4.8. Hysteretic loops in tension (Orakcal et al., 2006)

Parameter ε_t is the strain at the point where the unloading line from the compressive stress region crosses the strain axis and changes with maximum compressive strain. Parameters ε_n and ε_u are the strain and stress at the peak of the tensile stress-strain relation and are given by the following expressions:

$$\varepsilon_n = \varepsilon_t + \Delta\varepsilon_t \qquad \text{Eq. 4.2.23}$$

$$\sigma_n = f_t'\left(1 + \frac{E_{ts}}{E_c}\right) - E_{ts}\Delta\varepsilon_t \qquad \text{Eq. 4.2.24}$$

where $\Delta\varepsilon_t$ is the previous maximum differential between tensile strain and ε_t as shown in Fig. 4.8. Before initial cracking, $\Delta\varepsilon_t$ is equal tof_t'/E_c . Parameter E_{ts} is the tension stiffening modulus, a value of 5% of E_c was used for E_{ts} by Yassin (1994) (Orakcal

et al., 2006). Parameter ε_u is the strain at the point where the tensile stress is reduced to zero and is given by the expression:

$$\varepsilon_u = \varepsilon_t + f_t' \left(\frac{1}{E_{ts}} + \frac{1}{E_c}\right) \qquad \text{Eq. 4.2.25}$$

Given these control points, the tensile stress-strain relation and the tangent moduli are defined by the following equations (assuming the convention that tension is positive):

$$\varepsilon_t < \varepsilon_c \leq \varepsilon_n \qquad \sigma_c = E_t(\varepsilon_c - \varepsilon_t) \qquad E_t = \frac{\sigma_n}{\varepsilon_n - \varepsilon_t} \qquad \text{Eq. 4.2.26}$$

$$\varepsilon_n < \varepsilon_c \leq \varepsilon_u \qquad \sigma_c = \sigma_n + E_t(\varepsilon_c - \varepsilon_0) \qquad E_t = -E_{ts} \qquad \text{Eq. 4.2.27}$$

$$\varepsilon_c > \varepsilon_u \qquad \sigma_c = 0 \qquad E_t = 0 \qquad \text{Eq. 4.2.28}$$

If $\varepsilon_n \geq \varepsilon_u$, then σ_n, σ_c and E_t are all assumed to be zero. The modulus E_{ts} controls the degree of tension stiffening (the contribution of tensile concrete resistance between cracks) by controlling the slope the region $\varepsilon_n < \varepsilon_c \leq \varepsilon_u$. Tensile unloading and reloading are governed by the equation for the region $\varepsilon_t < \varepsilon_c \leq \varepsilon_n$, which also includes stiffness degradation for increasing values strain differential $\Delta\varepsilon_t$. The value of $\Delta\varepsilon_t$ changes whenever $\varepsilon_c > \varepsilon_n$ (Orakcal et al., 2006).

Typical hysteretic behavior of Concrete_02 material is shown in Fig. 4.9 as given in OpenSees manual (OpenSees, 2008).

4.2.3. Self-Centering Material

Self-centering material is primarily used to model a self-centering energy-dissipative brace (Christopoulos et al., 2008) which has flag shape force-deformation curve as shown in Fig. 4.10. The material has a high initial stiffness (k_1), until the force reaches the pretensioning force, and low post yield stiffness (k_2), once the pretensioning force is

overcome (Christopoulos et al., 2008). Beta (β) is the energy dissipation capacity parameter and controls the unloading path (Tremblay et al., 2008). This material has the option to model the slippage of an external friction fuse (which causes non-recoverable deformation above a given brace strain) of the brace (OpenSees, 2008). The bearing option is used to approximately model the effect of bolt bearing in the brace or external fuse mechanisms, which causes a steep increase in the stiffness of the brace (OpenSees, 2008). This material type could potentially be used for any comparable self-centering system that exhibits a flag-shaped hysteretic response (OpenSees, 2008). Self-centering material is available in OpenSees to construct a uniaxial self-centering (flag-shaped) material object with optional non-recoverable slip behavior and an optional stiffness increase at high strains (bearing behavior). In this study, slip and bearing behavior of the material are not used since those behaviors are not noticed in the devices under study.

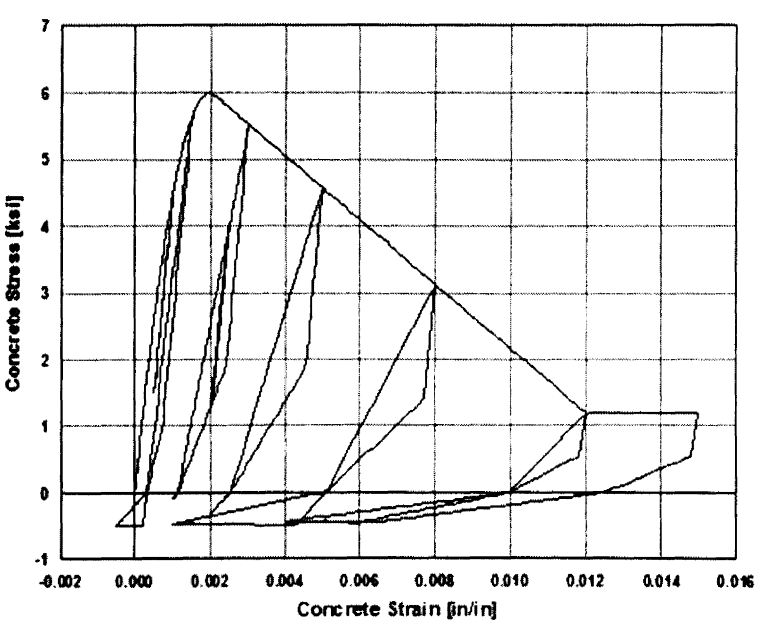

Fig. 4.9. Typical hysteretic behavior of Concrete_02 material (OpenSees, 2008)

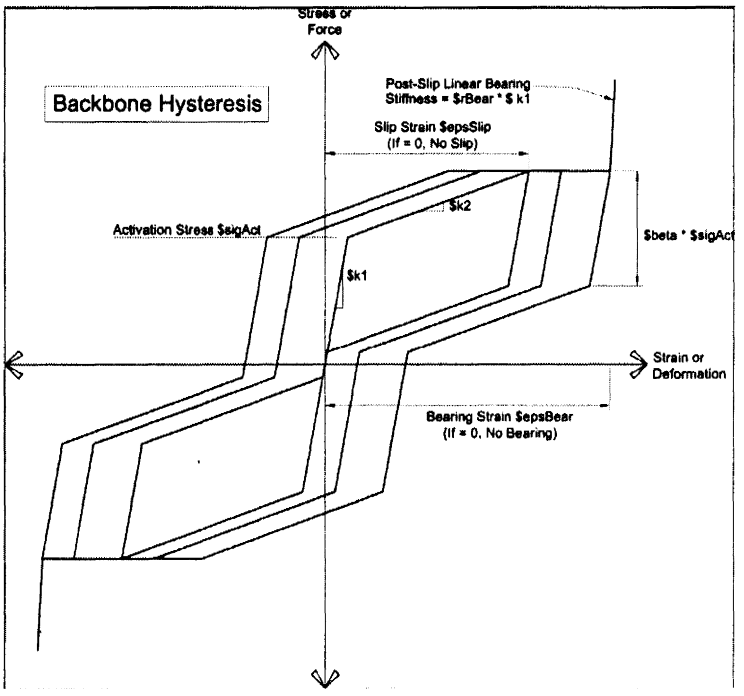

Fig. 4.10. General backbone hysteresis showing parameters of self-centering material (OpenSees, 2008)

4.2.4. Elastic Perfectly Plastic (ElasticPP) Material

This material is used to construct elastic perfectly plastic behavior. Fig. 4.11 shows parameters that control the force-deformation curve.

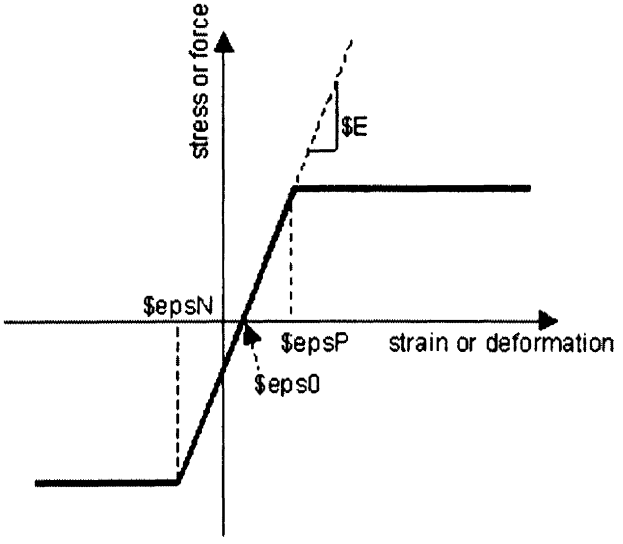

4.11. Force-Deformation curve of Elastic Perfectly Plastic material (OpenSees, 2008)

Initial tangent E, strain/deformation at which material reaches plastic state in tension and compression epsP and epsN, respectively; and initial strain eps0. In this study, uniform force-deformation is considered in tension and compression that is, epsP is equal to epsN. Also, initial strain is considered as zero.

4.3. Numerical Simulations

The OpenSees finite element framework (Open System for Earthquake Engineering Simulations) is used for numerical modeling of shaking table experiments (OpenSees, 2008). OpenSees was developed by Pacific Earthquake Engineering Research Center (PEER, 2008). It has the capabilities of performing static and dynamic finite element simulations for structural and geotechnical applications. OpenSees includes different material models (constitutive models) and elements that are capable of performing linear and nonlinear finite element simulations. The object-oriented nature of OpenSees allows one to choose different materials, elements, and solution algorithms that are most suitable to simulate a particular analysis. Fig. 4.12 shows one of the finite element meshes used to model the bare-frame structure in OpenSees simulations. The mass of the model is lumped at each node as shown in Fig. 4.12. Table 4.2 presents the details of the elements, sections, and material models used to simulate the behavior of beams, columns, and energy dissipating devices in OpenSees simulations. Bottom nodes of all three base columns (load cells) are fixed in all three degrees of freedom in order to simulate fixed base condition except for frame with base isolation. In case of frame with base isolation, vertical displacement and rotation of bottom nodes of all three base columns are fixed and

horizontal displacement is controlled by material models, explained later in this section. Example files for OpenSees codes are given in Appendix for each model.

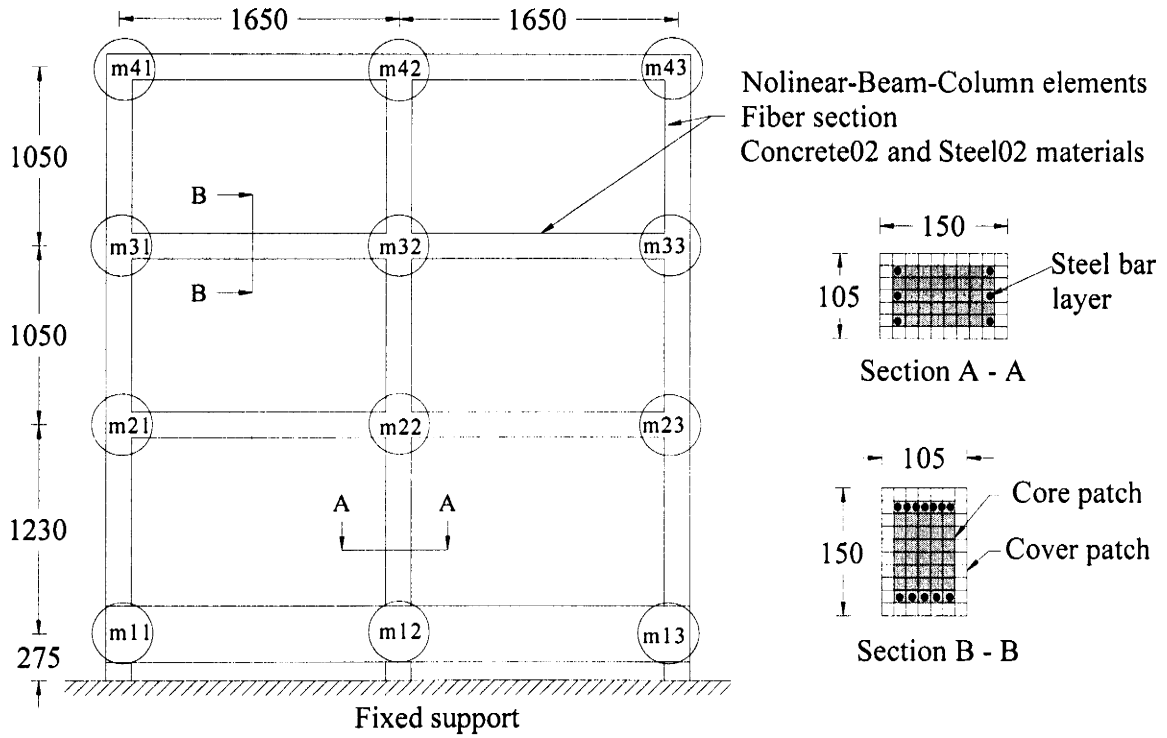

Fig. 4.12. Numerical model of bare frame structure together with the section details of beams and columns (m: point mass; dimensions are in mm)

Table 4.2. Details of the OpenSees finite element model

Component		Element	Section	Material
Beam and Column		NBC[1]	Fiber	Steel_02 (r/f bars) and Concrete_02 (Concrete)
Braces	Steel	NBC[1]	Fiber	Steel_02
	SMA	NBC[1]	Fiber	SC[3] and Steel_02
Base Isolation		ZLE[2]	-	SC[3], Steel_02, and EPP[4]
NBC[1]: Nonlinear-Beam-Column Element, ZLE[2]: Zero-Length-Element, SC[3]: Self-Centering Material, EPP[4]: Elastic-Perfectly-Plastic Material				

4.3.1. Elements and Sections

Beams and columns of the frame structure are modeled using nonlinear-beam-column elements available in OpenSees. Nonlinear-beam-column element is a fiber beam-column element for the non-linear static and dynamic analysis of reinforced concrete frames (Spacone et al., 1996). It is assumed that plane section remains plane and normal to the longitudinal axis. The element formulation is flexibility-based and relies on force interpolation functions that strictly satisfy the equilibrium of bending moments and axial force along the element (Spacone et al., 1996). This element is capable of tracing very well the highly non-linear behavior of R/C members under cyclic load combinations of bending moment and axial forces (Spacone et al., 1996). The non-linear hysteretic behavior of the element derives from the constitutive relations of concrete and reinforcing steel fibers into which each section is divided. Fig. 4.12 shows fiber sections used to include the steel reinforcement bars and concrete in beam and column elements.

Energy dissipating braces are modeled using nonlinear-beam-column elements; however, different behaviors of braces are obtained by using different material model combinations. Both steel and SMA braces are modeled using circular fiber sections as shown in Fig. 4.13 and diameters of sections are 29.32 mm and 18.71 mm, respectively.

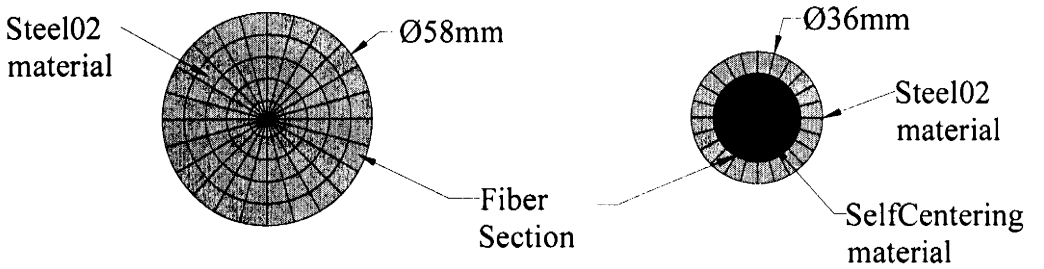

Fig. 4.13. Fiber section of (a) Steel brace and (b) SMA brace

The zero-length element is used to model the base isolation system. The zero-Length element is defined by two nodes at the same location. The nodes can be connected by multiple material models to represent the force-deformation relationship for the element. The load cell is modeled using elastic-beam-column elements, as they are relatively rigid compared to the frame.

4.3.2. Material Models

Stress-strain behaviors of concrete and steel materials are simulated by Concrete_02 and Steel_02 material models respectively, available in OpenSees. Their constitutive models with required input parameters are shown in Fig. 4.14. Steel_02 material is used for steel energy dissipating braces; however, the behavior of SMA braces could not be captured by single material model due to its super elastic behavior combined with energy dissipation. In order to capture the self-centering behavior and energy dissipation behavior of SMA braces, self-centering material model is combined with Steel_02 material model as shown in Fig. 4.15. The self-centering material is developed (by Christopoulos et al., 2008) for self-centering energy dissipative steel brace which has pretension wires on it (Tremblay et al. 2008 and Christopoulos et al., 2008) similar to SMA devices considered in this study. Therefore, the self-centering material is capable to simulate the behavior of pretension wires in SMA devices (braces and base isolation).

Typically base isolators have high stiffness in vertical direction and law stiffness in horizontal direction in order to support the structure in vertical direction and to undergo large horizontal displacement. Also, the isolator system has three sliding bearings on it.

Therefore, all three bottom columns (bottom of load cells) are fixed in vertical direction and allowed to slide in horizontal direction as shown in Fig. 4.16.

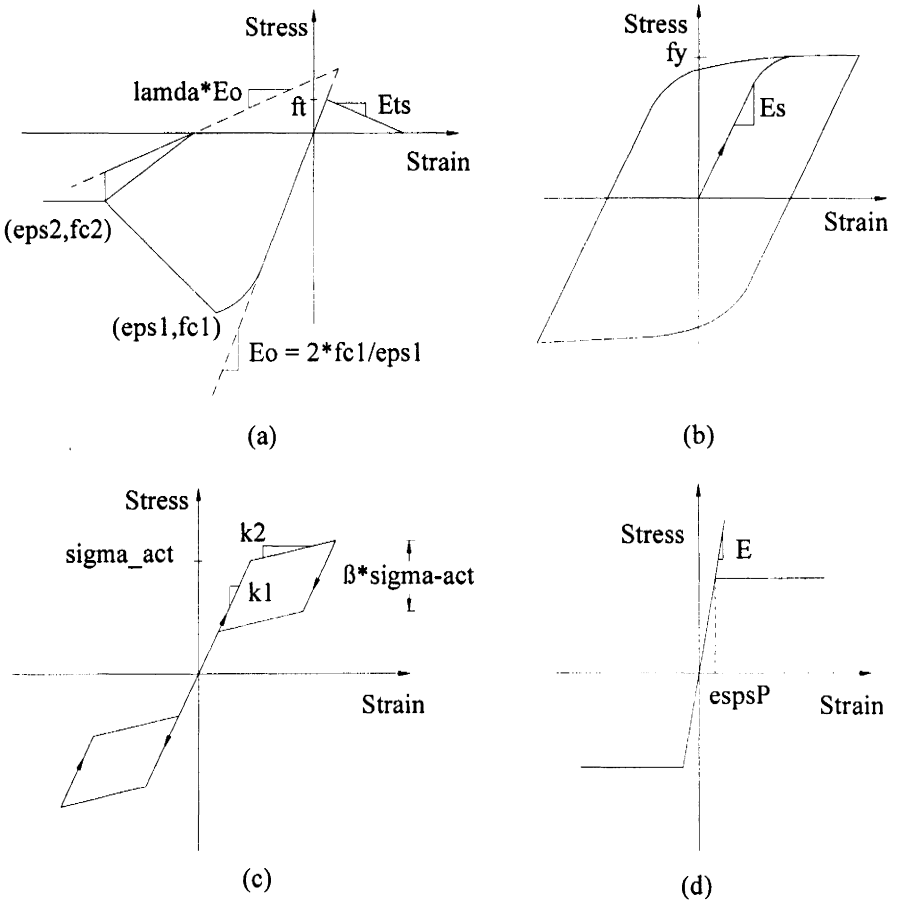

Fig. 4.14. Stress-strain relationships for marial models: (a) Concrete_02, (b) Steel_02, (c) Self-Centering, and (d) Elastic Perpectly Plastic

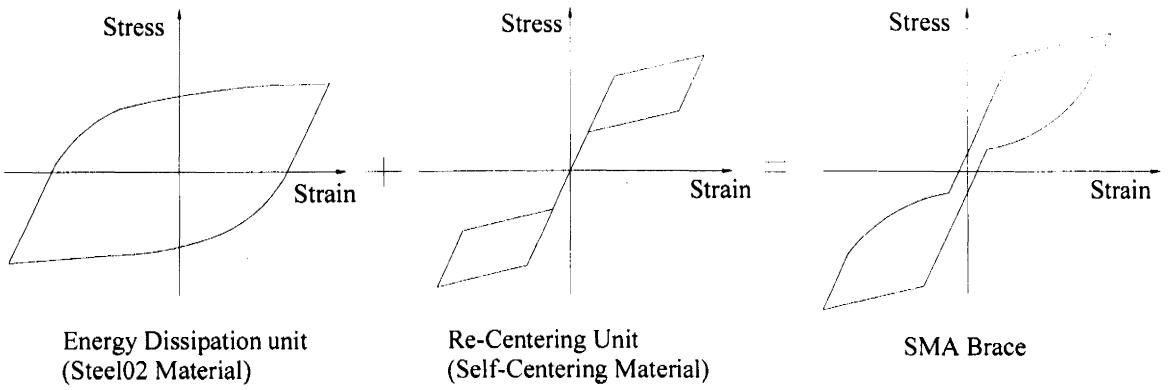

Fig. 4.15. Idealized behavior of SMA brace

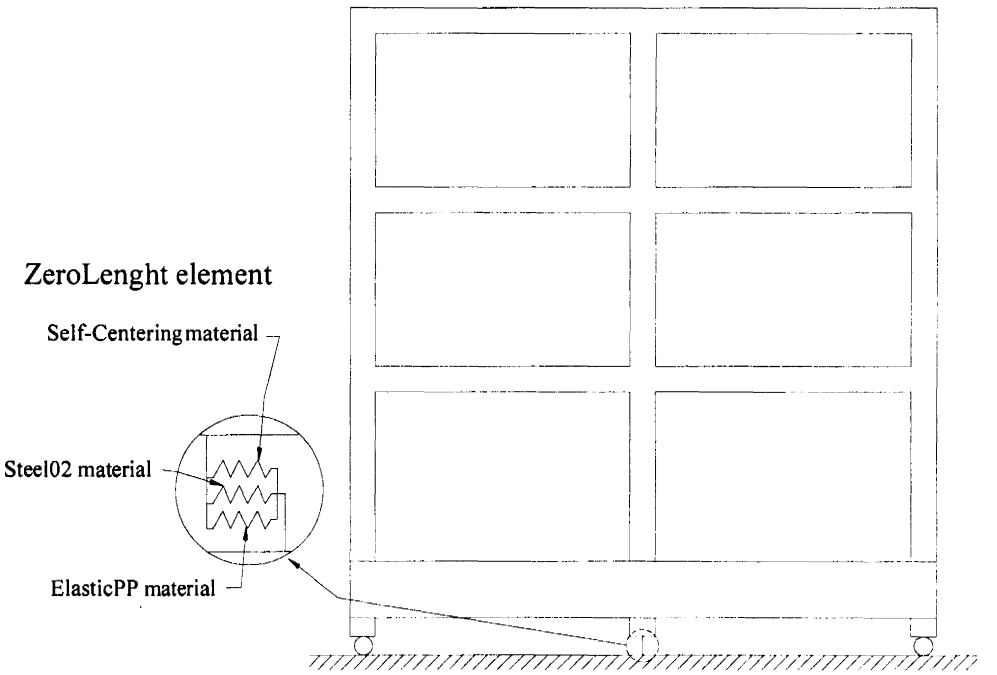

Fig. 4.16. Numerical model of brace with base isolation system

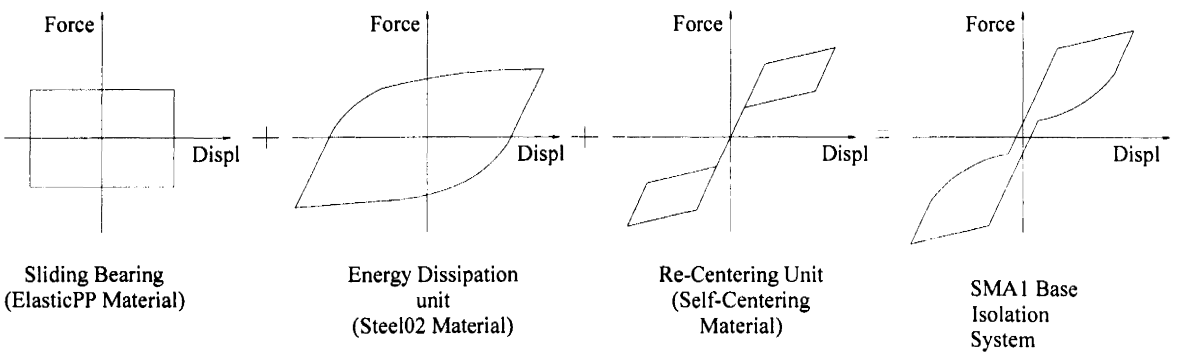

Fig. 4.17. Idealized behavior of SMA base isolation system

The zero-length element is used to define the horizontal force-deformation behavior at bottom of center column for base-isolation. Idealized behavior of SMA base-isolation system is similar to SMA brace behavior except that it has a higher deformation range (nearly ten times larger than the brace deformation range) and sliding bearings. In order to capture the sliding bearing behavior in addition to the self-centering and energy dissipation behavior, elastic perfectly plastic material model is combined with self-centering material

and Steel_02 material to model the behavior of base isolation system as shown in Fig. 4.17. These three materials are connected in parallel in horizontal direction.

4.3.3. Analysis Tools

The self-weight of the structure is applied at each node as gravitational force. After the self-weight of the structure is applied, the acceleration time histories used in the shake table experiments are applied at the fixed base nodes in OpenSees simulations. The Newmark integrator and Newton algorithm, available in OpenSees, are used for dynamic calculations in the simulations. OpenSees recorders are used to record the acceleration and displacement at each node and the forces and moments of each element of the structure. Viscous damping is included in numerical simulations using Rayleigh damping in the form of eq. 4.3.1 (Shen and Akbas, 1999, and Chopra, 2006),

$$C = \alpha \cdot M + \beta \cdot K \qquad \text{(Eq.4.3.1)}$$

where C, M and K are damping, mass, and stiffness matrix, respectively. To calculate the coefficients α and β, a uniform damping ratio (2%) and first and third mode of frequencies of the structure are used (Shen and Akbas, 1999).

In order to make the energy dissipation calculations and comparisons meaningful (presented later in the thesis), numerical simulations are also carried out without Rayleigh damping. Table 4.3 presents the test matrix of shake table experiments used in numerical simulations. The test name indicates the type of structure and the peak ground acceleration applied in the simulation. Note that additional numerical simulations are carried out for energy dissipation comparisons.

4.3.4. Model Parameter Calibration

The input parameters used for Steel_02 and Concrete_02 materials used to represent beam and column elements are presented in Table 4.4. These material parameters were obtained directly from the properties of the physical models used in the experiments (presented in Dolce et al., 2005). The input parameters used for steel and SMA brace materials are presented in Table 4.5 and Table 4.6 respectively. These material parameters are obtained from the experimental model details presented in Dolce et al. (2005) and by back-calculation of some of the experimental results.

Table 4.3. Test matrix (shake table experiments and numerical simulations)

Bare Frame	Frames with braces		Frames with base isolation
	SMA brace	Steel brace	SMA1
BF_07			
BF_09*	BR_SMA_09	BR_ST_09	
BF_14			
BF_15*		BR_ST_16	BI_SMA1_15
BF_17*	BR_SMA_17		
BF_24*	BR_SMA_24	BR_ST_23	
BF_28			
BF_30*		BR_ST_31	BI_SMA1_30
BF_33*	BR_SMA_33		
BF_39*			BI_SMA1_39
BF_48			
BF_46*	BR_SMA_46		
BF_50*	BR_SMA_51	BR_ST_50*	BI_SMA1_50

BF – Bare Frame, BI – Base Isolation, BR- Brace, ST- Steel, SMA- Shape Memory Alloy. The tests' names indicate type of structure and peak ground acceleration. For example, BF_48 imply Bare Frame (BF) and peak ground acceleration 0.48g (48). *Only numerical test

Fig. 4.18 and Fig. 4.19 present the experimental and numerical simulation results of the cyclic load-displacement behavior of steel brace and SMA brace respectively used at each story level. These cyclic load-displacement experiments and simulations were conducted independently on the brace elements for the purpose of calibration (not attached with the structures). As can be seen from those figures, capacity and stiffness differ at each story level, and are back-calculated using the cyclic loading experimental results in order to reproduce the similar behavior in numerical simulations. This back-calculation enabled the inclusion of stiffness added by the steel brackets which were used to connect braces in the numerical models.

Table 4.4. Material parameters used for beams and columns (OpenSees, 2008)

<table>
<tr><td colspan="5">Material parameter</td></tr>
<tr><td colspan="3">Concrete_02 material</td><td colspan="2" rowspan="2">Steel_02 material</td></tr>
<tr><td></td><td>Unconfined concrete</td><td>Confined concrete</td></tr>
<tr><td>Compressive strength (fc1) (MPa) (Tension positive)</td><td>-34.2 (Dolce et al. 2005)</td><td>-44.46</td><td colspan="2">Yield stress (Fy) (MPa) (Dolce et al. 2005)</td><td>560</td></tr>
<tr><td>Crushing strength (fc2) (MPa)</td><td>-6.84</td><td>-8.892</td><td colspan="2">Modulus of steel (Es) (GPa)</td><td>200</td></tr>
<tr><td>Elastic Modulus (Ec) (GPa) (Dolce et al. 2005, 2007)</td><td>22.5</td><td>22.5</td><td colspan="2">Strain-hardening ratio (b)</td><td>0.01</td></tr>
<tr><td>Strain at maximum strength (eps1)</td><td>-0.003</td><td>-0.00395</td><td rowspan="4">Constants (control the transition from elastic to plastic branches)</td><td rowspan="2">R_0</td><td rowspan="2">18</td></tr>
<tr><td>Strain at crushing strength (eps2)</td><td>-0.01</td><td>-0.079</td></tr>
<tr><td>Tensile strength (ft) MPa)</td><td>4.79</td><td>6.22</td><td rowspan="2">cR1</td><td rowspan="2">0.925</td></tr>
<tr><td>Tension softening stiffness (Ets) (GPa)</td><td>2.4</td><td>2.4</td></tr>
<tr><td>Ratio between unloading slope at eps2 and initial slope Ec (lambda)</td><td>0.1</td><td>0.1</td><td>cR2</td><td>0.15</td></tr>
</table>

Table 4.5. Material parameters used for steel braces

Steel brace				
Steel02 material				
Story Level		1st	2nd	3rd
Initial stiffness (Es) (GPa)		56.7	55.7	56.1
Yield stress (Fy) (MPa)		5.55	3.7	2.96
Strain-hardening ratio (b)		0.085	0.053	0.0125
Constants (control the transition from elastic to plastic branches)	R_0	40		
	cR1	0.925		
	cR2	0.55		

Table 4.6. Material parameters used for SMA braces

SMA brace							
Self-Centering material				Steel02 material			
Story Level	1st	2nd	3rd	Story Level		1st	2nd	3rd
Initial stiffness (k1) (GPa)	280	380	160	Initial stiffness (Es) (GPa)		15.59		
Post-Activation stiffness (k2) (GPa)	16	9	4	Yield stress (Fy) (MPa)		21.59	15	7.273
Forward activation stress (σ_{act}) (MPa)	45	28	10	Strain-hardening ratio (b)		0.015		
Ratio of forward to reverse activation stress (β)	0.67	0.78	0.38	Constants (control the transition from elastic to plastic branches)	R_0	40		
					cR1	0.925		
					cR2	0.15		

Fig. 4.20 presents the experimental and numerical simulation results of the cyclic load-displacement behavior of SMA base isolation system. Similar back-calculations were carried out to calibrate the material parameters for the SMA base-isolation model and the parameters are presented in Table 4.7.

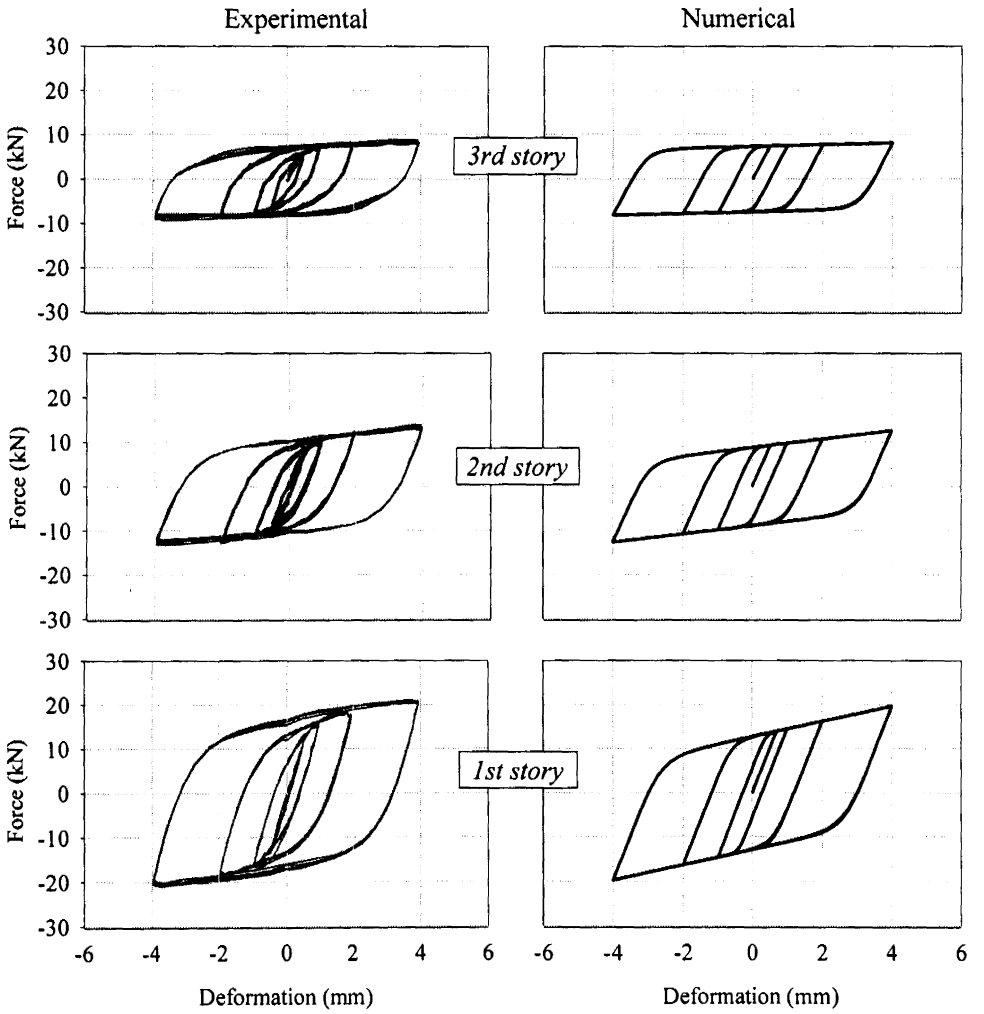

Fig. 4.18. Cyclic load-displacement behavior of steel braces: experimental and numerical (experimental results are after Dolce et al., 2005)

Table 4.7. Material parameters used for SMA base isolation

Self-Centering material		Steel02 material			ElasticPP material	
Initial stiffness (k1) (MNm^{-1})	2	Initial stiffness (Es) (MNm^{-1})	0.84		Tangent (E) (MNm^{-1})	35
Post-Activation stiffness (k2) (MNm^{-1})	0.15	Yielding Load (Fy) (kN)	1.75			
Forward activation Force (σ_{act}) (kN)	5.4	Strain-hardening ratio (b)	0.01		Deformation at which material reaches plastic state (epsyP) (10^{-4})	0.5
Ratio of forward to reverse activation Force (β)	0.2	Constants (control the transition from elastic to plastic branches)	R_0	40		
			cR1	0.93		
			cR2	0.15		

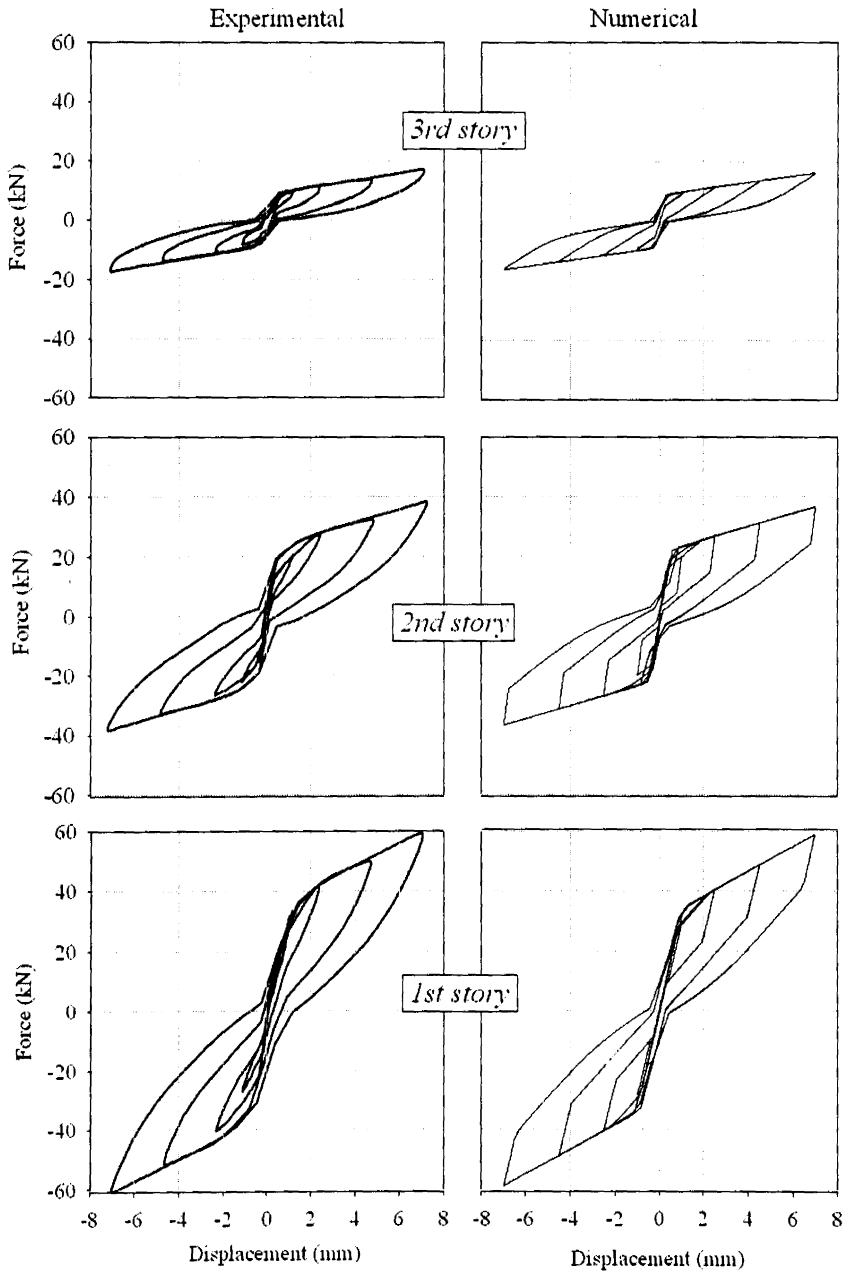

Fig. 4.19. Cyclic load-displacement behavior of SMA braces (experimental results are after Dolce et al., 2005)

4.3.5. Model Performance Validation

Validation of the numerical model is carried out using the experimental results available in Dolce et al. (2005, 2007b). Base shear versus 1st story displacement

relationships for experimental bare frame structure (Dolce et al., 2005) is compared with numerical simulation results for three different shakes in Fig. 4.21. The numerical simulation results in general show good comparisons with experimental results though simulation results for shear force are slightly smaller than those of the experiments, particularly for a_base_max = 0.28 g shake.

Maximum cyclic displacement and maximum acceleration at each story level of numerical simulation results for bare frame structure is compared with experimental results in Fig. 4.22. All four test results with varying maximum base shake intensities from 0.07g to 0.28g are included. The numerical simulation results of maximum cyclic displacement of story level shows very good match with experimental results. In case of maximum acceleration at story level, shows very good agreement except for 1st story level results of tests with a_base_max=0.14g and 0.28g. The lateral force-displacement relationships of base isolation system for frame with base isolation (Dolce et al., 2007b) is compared with numerical simulations results during shakes with 0.30g and 0.50g maximum base acceleration in Fig. 4.23, and simulation results are in good agreement with experimental results.

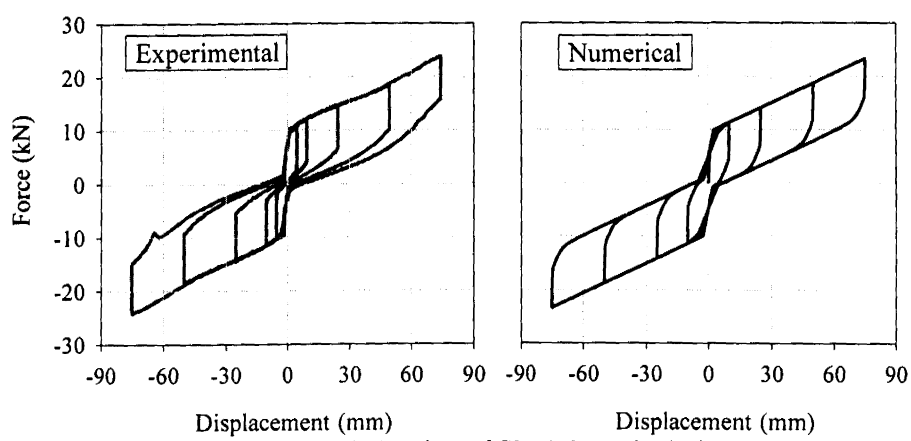

Fig. 4.20. Cyclic load-displacement behavior of SMA base isolation (experimental results are after Dolce et al., 2007b)

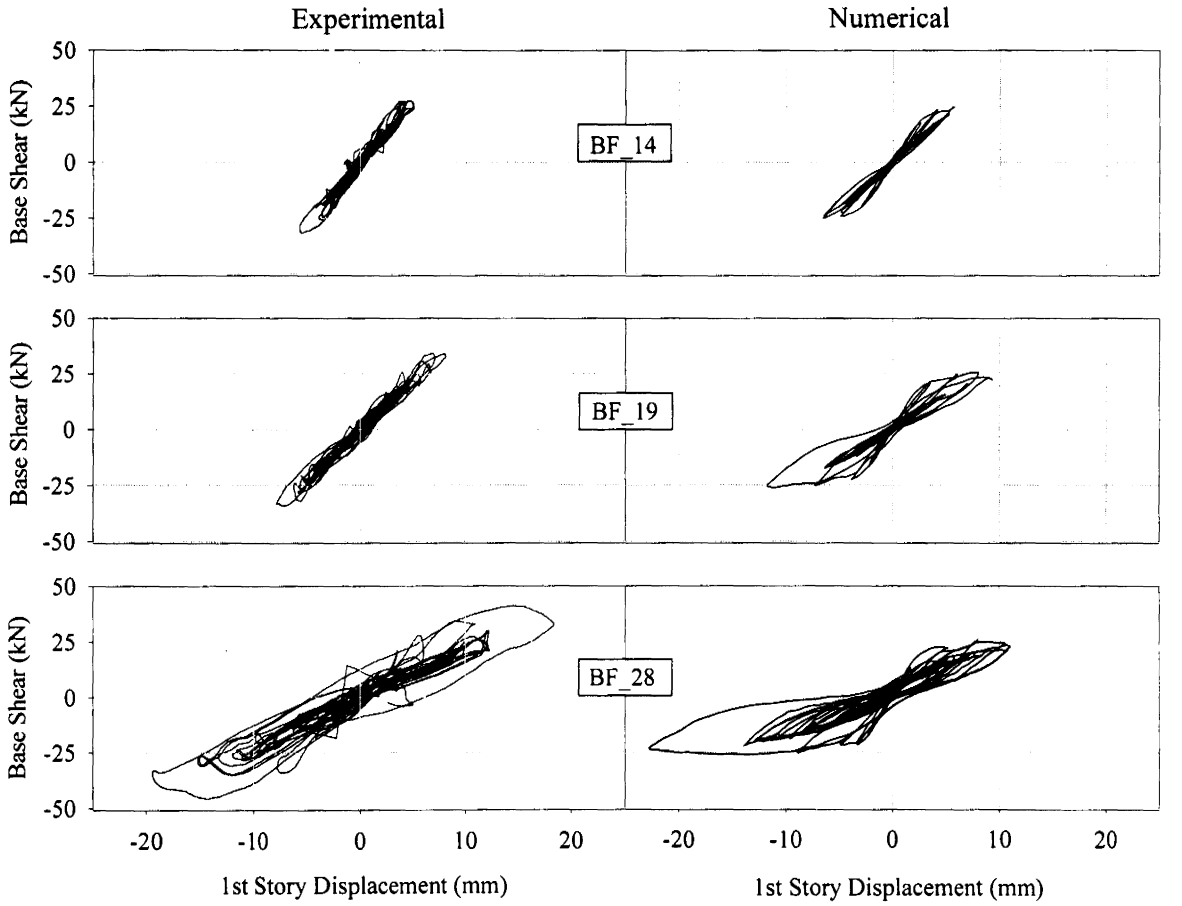

Fig. 4.21. Base shear versus 1st story displacement relationships of bare frame structure during different shaking events (experimental results are after Dolce et al., 2005)

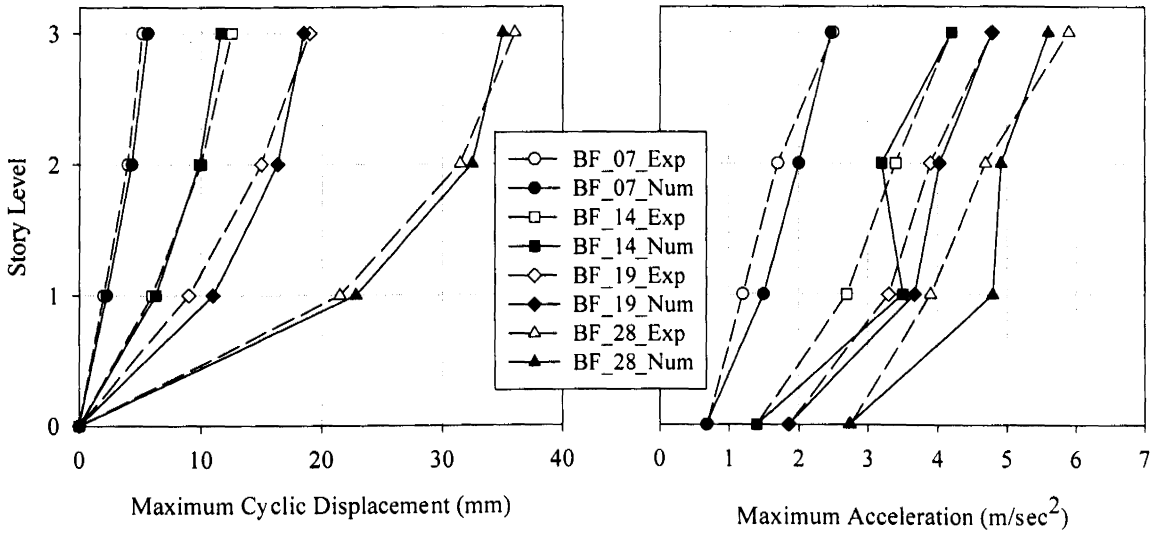

Fig. 4.22. Validation of Bare Frame (BF) structure: simulation results with experimental results (experimental results are after Dolce et al., 2005)

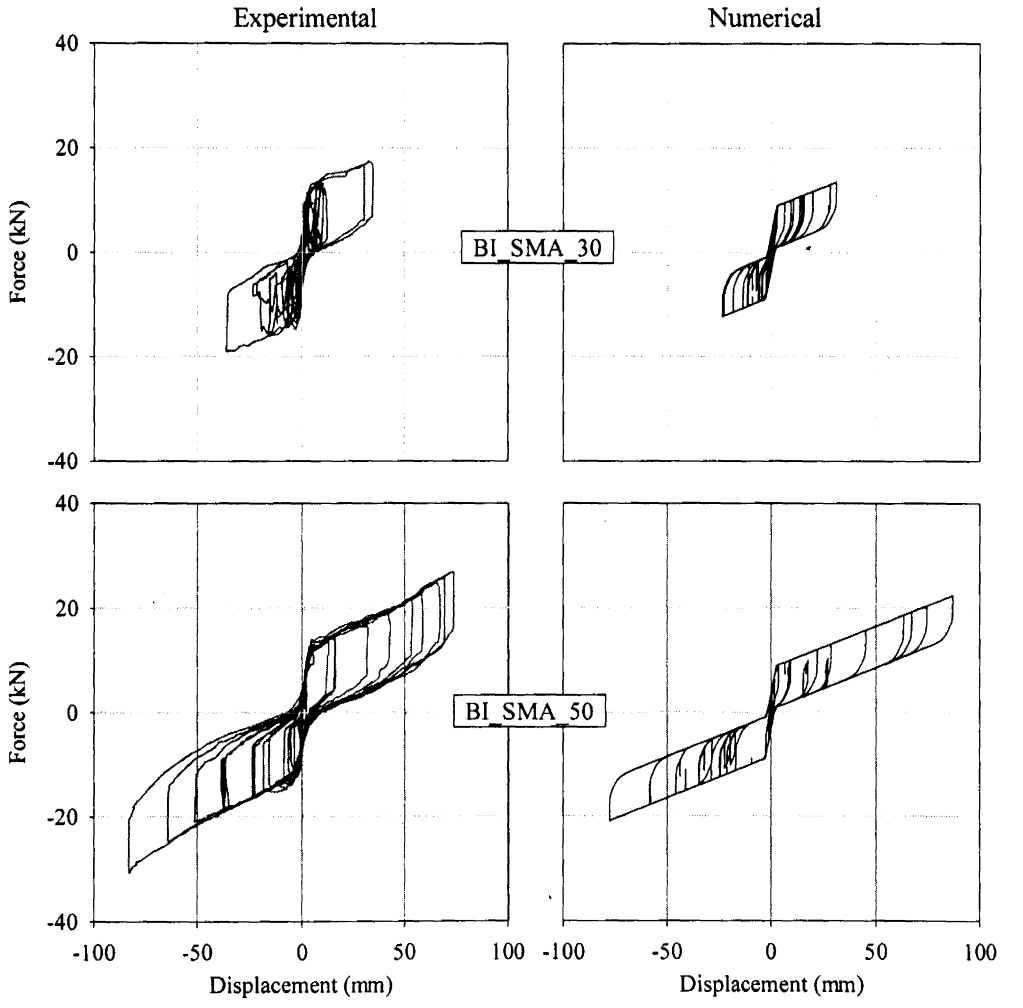

Fig. 4.23. Lateral force-displacement relationships of base isolation system during different shaking events (experimental results are after Dolce et al., 2007b)

Fig. 4.24 presents the Experimental and numerical simulation results of the time histories of the base displacement of the structure with base isolation system during shakes with 0.30g and 0.50g maximum base acceleration. Apart from minor deviations, numerical simulation results compare well with experimental results for the most part. Fig. 4.25 presents the numerical simulation results for maximum story level cyclic displacements and maximum inter-story drift ratio of structures with and without energy dissipation devices during shakes whose maximum base acceleration is approximately equal to 0.30g and

0.50g together with experimental results. Note that the experimental results are not available for all shakes and all models (only the published experimental data are included in Fig. 4.25). The maximum cyclic displacement is the absolute peak displacement of the structure at that particular story. Relative displacement of each story is dived by corresponding story height to obtain the drift ratio (%). The simulation results for maximum story level displacements and maximum inter-story drift ratio compare well with experimental results. Overall, the numerical model captures the essential features observed in the shake table experiments.

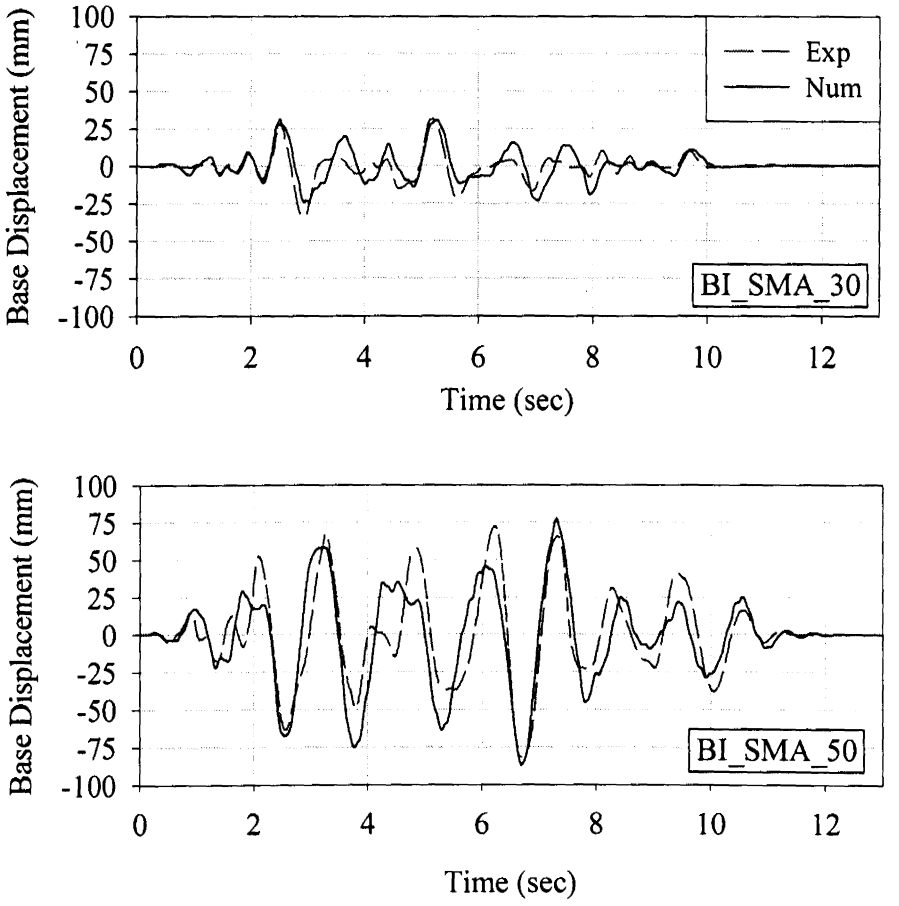

Fig. 4.24. Experimental and numerical simulation results of the time histories of the base displacement of the structure with base isolation system during different shaking events (experimental results are after Dolce et al., 2007b)

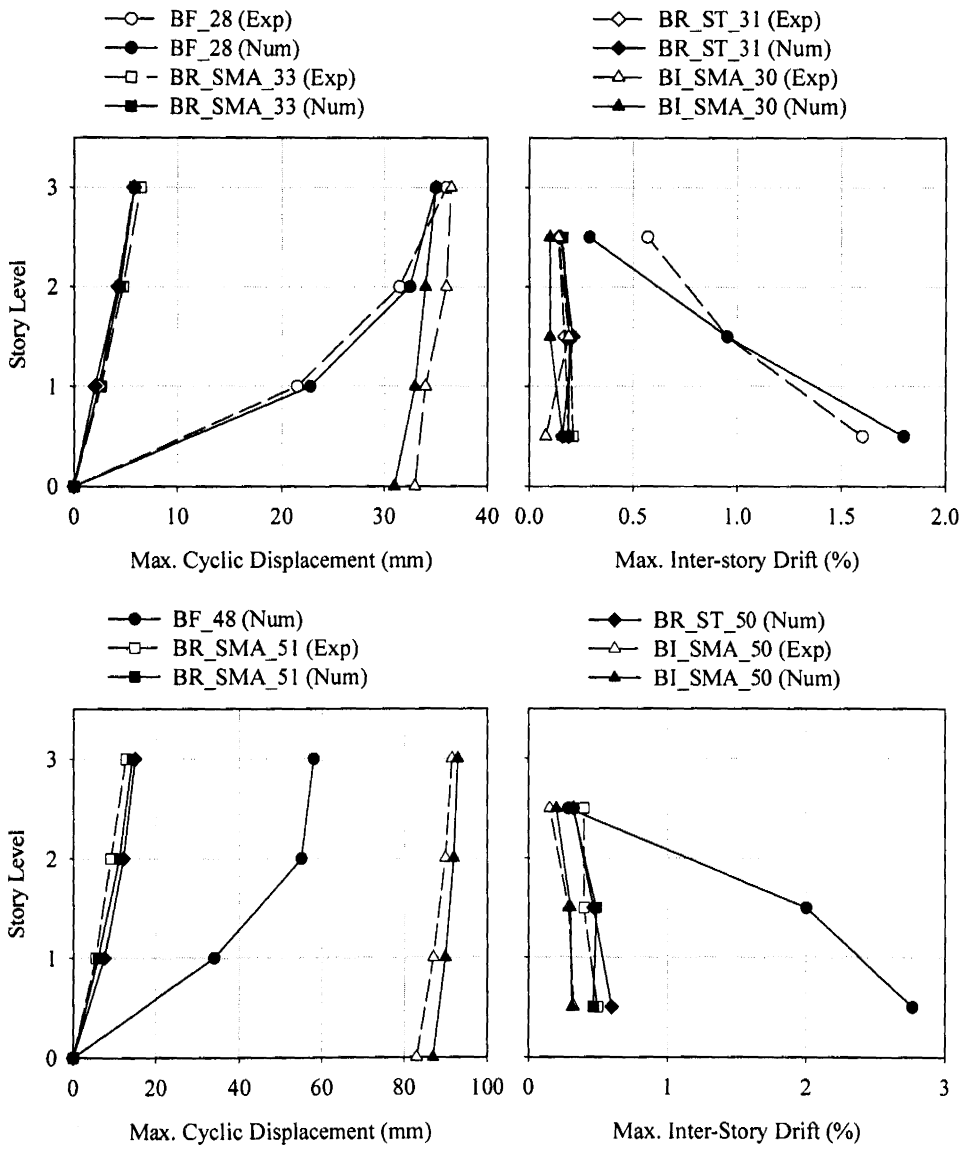

Fig. 4.25. Validation of simulation results with experimental results: Maximum cyclic displacement and maximum inter-story drift (experimental results are after Dolce et al., 2005 and 2007b)

4.4. Validity of the Numerical Model

The numerical model of reinforced concrete bare frame structure is simulated based on the experimental data published in Dolce et al., 2005. Validation of this model is shown in Fig. 4.21 and Fig. 4.22 where cyclic base shear vs. 1st story displacement curve, maximum cyclic displacement at each story level, and maximum acceleration at each story

level are considered. The comparison of numerical simulation results with experimental results from Dolce et al., 2005 shows very good agreement. It is important to point out that none of the model parameters are back calculated for the purpose of bare frame numerical simulation. So, it is reasonable to conclude that the bare frame numerical model is valid to use for any similar reinforced concrete frame structure with necessary alteration of number and/or arrangement of rebar, dimensions and/or geometry.

To simulate the behavior of special devices (Steel/SMA braces and SMA base isolation), parameters govern the force-displacement behavior of devices are back calculated using the published results of cyclic tests on special devices (in Dolce et al., 2005 and 2007b) since published data on special devices is insufficient. These experimental cyclic tests were carried out on individual devices (before attached to the main frame). Cyclic sinusoidal displacements were applied to the devices, in order to investigate their actual behavior, and their dependence on displacement amplitude, frequency of loading, temperature, and number of cycles (Dolce et al., 2000). These cyclic tests with different maximum cyclic sinusoidal displacements are used to calibrate the material parameter used to model the devices through similar cyclic loading numerical simulations on individual devices (Fig. 4.18, Fig. 4.19, and Fig. 4.20). Calibrated numerical models of devices attached to the frame model and validated using shaking table experimental results. The validation figures explained in previous section (Fig. 4.23, Fig. 4.24, and Fig. 4.25) clearly show that simulation results compare well with experimental results. However, if this numerical model is used for another case where frame with similar special devises, then special devices numerical models need to be calibrated again. But, the calibration is required only for the special device models.

4.5. Energy Dissipation in Structural Elements

For a fixed-based structure, the total seismic input energy (IE) can be written as the summation of kinetic energy (KE), energy dissipated by viscous damping (DE), hysteretic energy dissipated by the structural materials (HE), and elastic strain energy (SE), as presented in eq. 4.5.1 (Uang and Bertero, 1990).

$$KE(t) + DE(t) + SE(t) + HE(t) = IE(t) \qquad \text{(Eq. 4.5.1)}$$

In Eq.4.5.1, kinetic energy and elastic strain energy are related to the instant response of the system, negligible when compared to hysteretic energy dissipation (material damping), and vanish at the end the vibration in an inelastic system (Shen and Akbas, 1999). In order to make the comparison of energy dissipation with and without energy dissipation devices meaningful, one set of numerical simulations were conducted without any Rayleigh damping (i.e., zero viscous damping). Therefore, eq. 4.5.1 can be rewritten approximately as,

$$HE(t) \cong IE(t) \qquad \text{(Eq.4.5.2)}$$

For a multi-degree of freedom system structure, total seismic input energy can be calculated using equation 4.5.3 (Uang and Bertero, 1990).

$$IE = \int (\sum_{i=1}^{N} m_i \ddot{v}_{ti})\, dv_g \qquad \text{(Eq.4.5.3)}$$

where m is the point mass, v_t is absolute displacement of the mass, v_g is ground displacement, and N is number of stories. The hysteretic energy includes the energy dissipation in the structural elements (HE_S), such as beams and columns, and within the energy dissipating devices (HE_D). Energy dissipated by devices (HE_D) is calculated from the hysteretic force-displacement response of the devices. Fig. 4.26 shows the examples of energy dissipation within energy dissipating devices through force-deformation response,

as obtained from numerical simulations of shaking events with maximum base acceleration of 0.3g and 0.5g. Energy dissipated by beams and columns (HE_S) was obtained as the difference between IE and HE_D ($HE_S = IE - HE_D$).

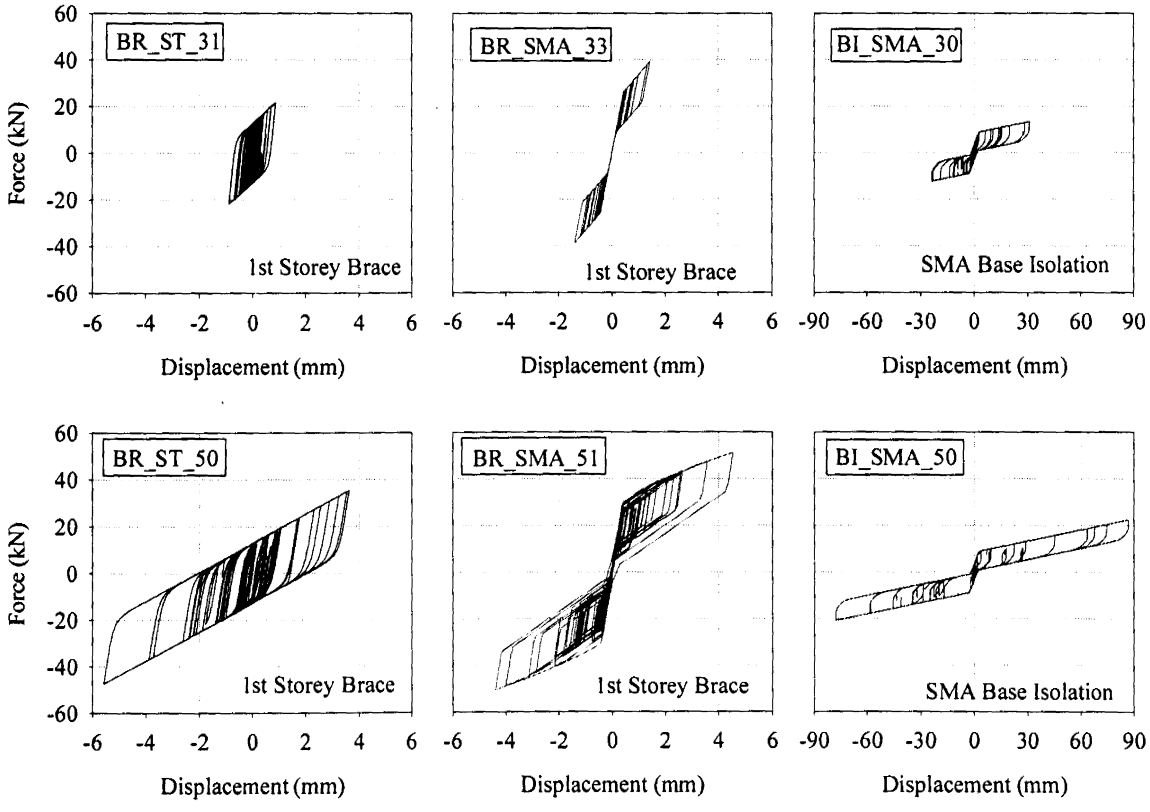

Fig. 4.26. Hysteretic energy dissipation within energy dissipating devices (steel brace, SMA brace, and SMA base-isolation system)

4.6. Results and Discussion

Fig. 4.27 presents the time histories of seismic input energy (IE), hysteretic energy dissipated in the energy dissipation devices (HE_D), and the hysteretic energy dissipated in structural elements (beams and columns) (HE_S) during shaking events with maximum base acceleration 0.3g and 0.5g. For the bare frame structures (without energy dissipation devices), the total seismic input energy was essentially dissipated by the hysteretic energy dissipation in basic structural elements (beams and columns). For the structures with

energy dissipating devices, as can be seen from Fig. 4.27, about 70% to 90% of the seismic input energy is dissipated by energy dissipating devices. Because of larger lateral displacements, base-isolation system dissipates more energy than the steel and SMA braces.

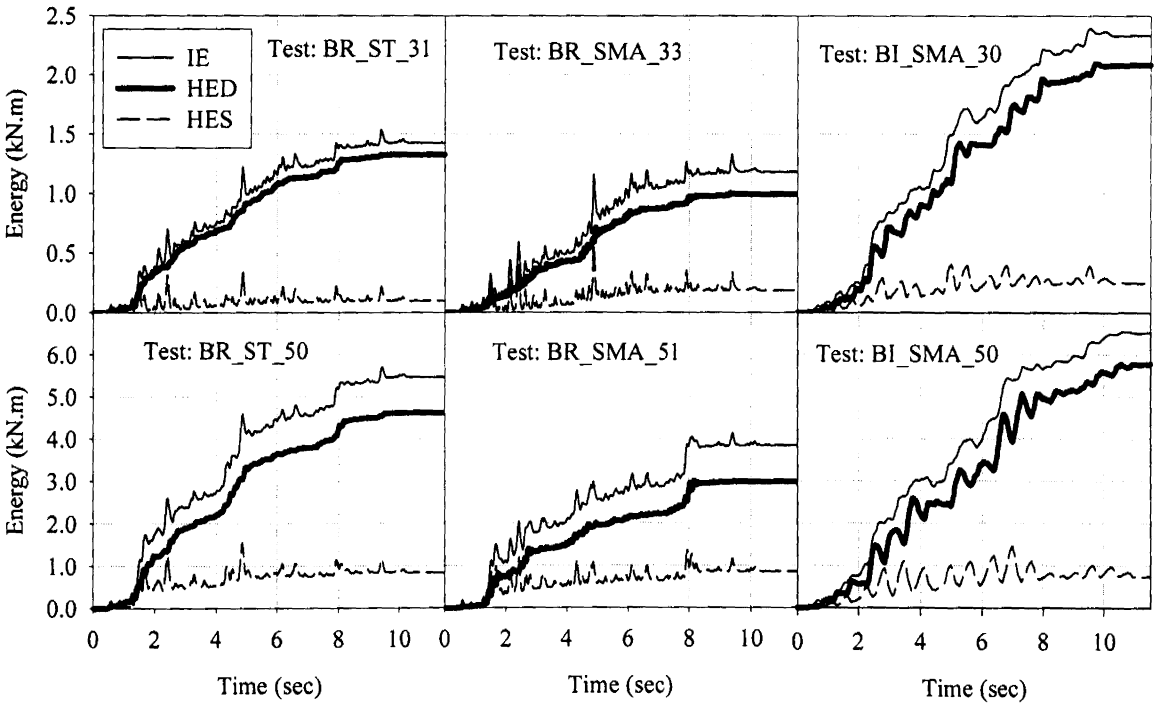

Fig. 4.27. Time histories of seismic input energy (IE), hysteretic energy dissipated in the energy dissipation device (HE_D) and the hysteretic energy dissipated in structural elements (beams and columns) (HE_S)

Fig. 4.28 compares the maximum cyclic and residual displacements of different energy dissipation devices. Maximum cyclic displacement increases as the shaking intensity increases, however the residual displacement does not show any trend with the shaking intensity. As can be seen from Fig. 4.28, the SMA brace shows minimal residual displacements due to its self-centering behavior (the maximum residual displacements of the SMA brace is about 0.03 mm regardless of the shaking intensity).

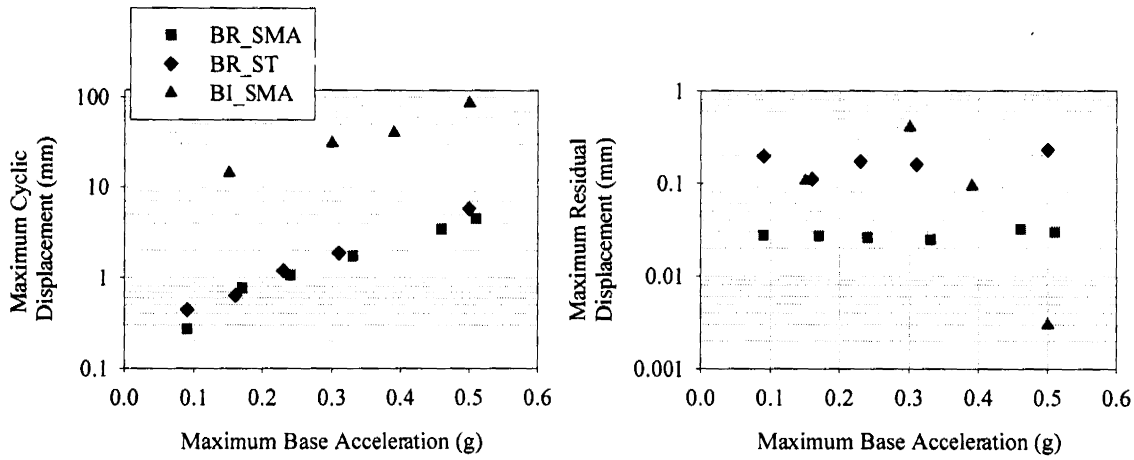

Fig. 4.28. Maximum cyclic and residual displacements of the energy dissipating devices during different shaking events

In order to compare the effectiveness of different energy dissipation devices, absolute maximum values of acceleration, cyclic displacement, cyclic drift, residual displacement, residual drift, and base shear force of the structure along with the total seismic input energy are plotted against the maximum base acceleration during different shaking events in Fig. 4.29. Note that the maximum cyclic displacements of the structure with base-isolation system are relative to the base of the structure. Available experimental results are also included in Fig. 4.29. As expected, the magnitude of all the parameters increases as the shaking intensity increases. The maximum cyclic displacement (occurs at the roof level) and maximum cyclic drift (occurs at first story level) demands of the structure are reduced when energy dissipation devices are used as most of the energy is dissipated in the devices. As for the maximum residual displacement and residual drift, wider scatter is observed in numerical simulation results (a similar scatter was also reported by Pampanin et al., 2003). The maximum residual displacement and maximum residual drift of the structure are reduced when energy dissipation devices are used during bigger shaking events (bigger than 0.2 g shakes). For smaller shaking events (smaller than 0.2 g

shakes), the inclusion of energy dissipating devices does not affect the residual displacement or drift.

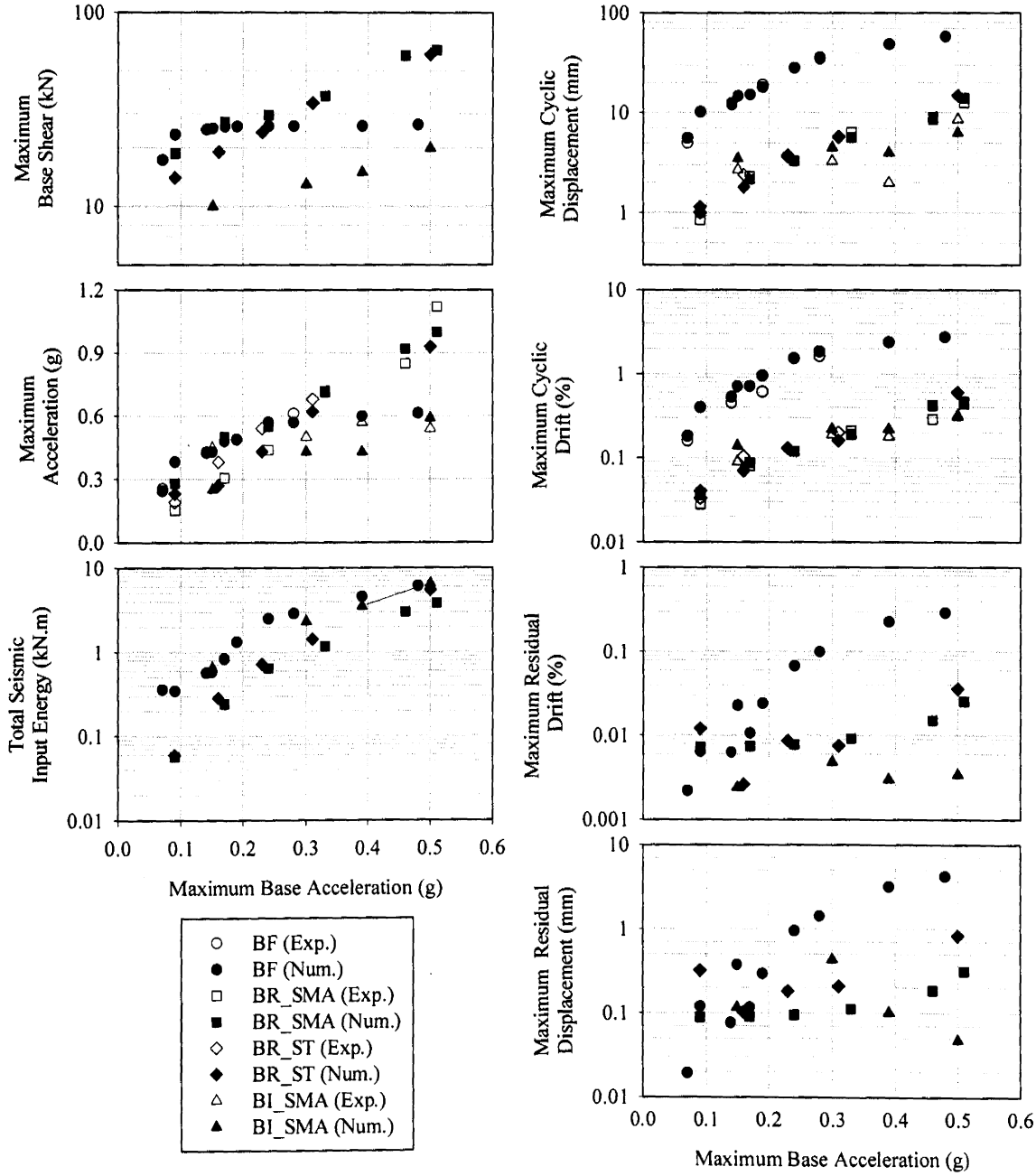

Fig. 4.29. Maximum responses of the structures during different shaking events

As can be seen from Fig. 4.29, maximum acceleration does not show significant difference between bare frame structure and structures with energy dissipation systems.

However the inclusion of steel and SMA braces increases the base shear force transmitted to the structure (increased stiffness and accelerations), while the inclusion of base-isolation system decreases the base shear force, as the lateral stiffness of the structural system decreases and the natural period increases. In addition, the total seismic input energy of the structures with energy dissipation devices is smaller than that of bare frame structures. The seismic input energy depends on ground motion characteristic, structural design parameters (including the no of floors, the height to width ratio, and the distribution of the stiffness and strength), plastic mechanisms, and high mode effects (Shen and Akbas, 1999).

To quantify the effectiveness of different energy dissipation systems, the following non-dimensional parameters are defined: (1) energy dissipation ratio (EDR): defined as energy dissipated by the energy dissipation device (brace or base-isolation) divided by the total seismic input energy, (2) displacement reduction ratio (DiRR): defined as the reduction in maximum cyclic displacement when energy dissipation devices are used divided by the maximum displacement of the bare frame structure, and (3) drift reduction ratio (DrRR): defined as the reduction in maximum cyclic drift ratio when energy dissipation devices are used divided by the maximum cyclic drift ratio of the bare frame structure. The above-mentioned parameters are defined in such a way that their values will vary between zero (for bare frame structures without energy dissipation devices) and one (for structures with ideal energy dissipation systems). Similarly, a forth non-dimensional parameter, base shear increase ratio (BSIR), is defined as the increase in maximum base shear force when energy dissipation devices are used divided by the maximum base shear force of the bare frame structure.

EDR, DiRR, DrRR, and BSIR are plotted against maximum base acceleration applied in different shaking events in Fig. 4.30. More than 85% of seismic energy is dissipated by steel braces or SMA base isolation system, whereas SMA braces dissipate about 70% to 80% of the total seismic energy (except for the smallest shaking event). Maximum cyclic displacement and drift of the structure are reduced by more than 70% and 80% respectively when energy dissipation devices are used. For the structures with energy dissipating braces, base shear force increases by as much as 150%, whereas for the structure with base-isolation system, base shear force decreases by about 25% to 50%. Also note that BSIR increases as the shaking intensity increases, while EDR, DiRR, and DrRR are relatively insensitive to the shaking intensity. Based on the numerical simulation results presented, it can be concluded that the SMA base-isolation is the most effective energy dissipation system and it is followed by steel brace and SMA brace in that order.

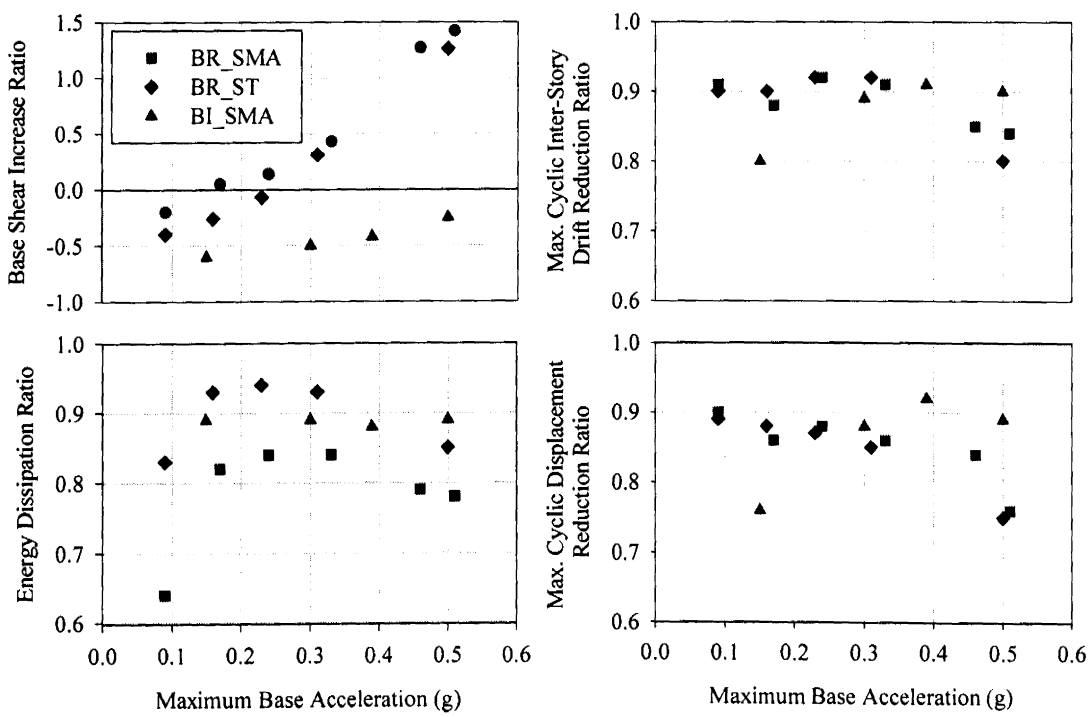

Fig. 4.30. Variation of energy dissipation ratio, displacement reduction ratio, drift reduction ratio and base shear increase ratio with maximum base acceleration

CHAPTER 5. ENERGY DISSIPATION IN FOUNDATION SOIL

In order to compare the energy dissipation in foundation soil with that in the structural energy dissipation devices, foundation energy dissipation results from two series of centrifuge experiments (SSG and JAU) are used. These centrifuge experiments were conducted in University of California at Davis. The model configurations and all the experimental results are presented using prototype-scale units. This chapter presents the centrifuge experiments and comparison of energy dissipation in soil with structural simulation results explained in previous chapter.

5.1. SSG Test Series

In SSG test series, several shear wall-footing-soil models (Fig. 5.1(left)) were subjected to dynamic base shaking loading. Shear wall and footing were made of either steel or aluminum and were relatively rigid. The footings were glued with sand to their bases to provide a rough concrete-like interface with the soil. Rectangular footings (L = 2.8 m and B = 0.65 m) supported by dry sandy soil deposit (Dr = 80% and φ = 42 degrees) were subjected to base shaking along the longer dimension (L) of the footing. The depth of embedment of the footing (D) was varied from D = 0 to D = B. The structures were freely allowed to settle, slide and rotate during shaking. Moment, rotation, and settlement at the base center point of the footing were calculated using recorded sensor readings during experiments. Detailed experimental procedure and results for all the models tested in the centrifuge tests are published in Gajan et al. (2005) and Gajan and Kutter (2008a and 2009b).

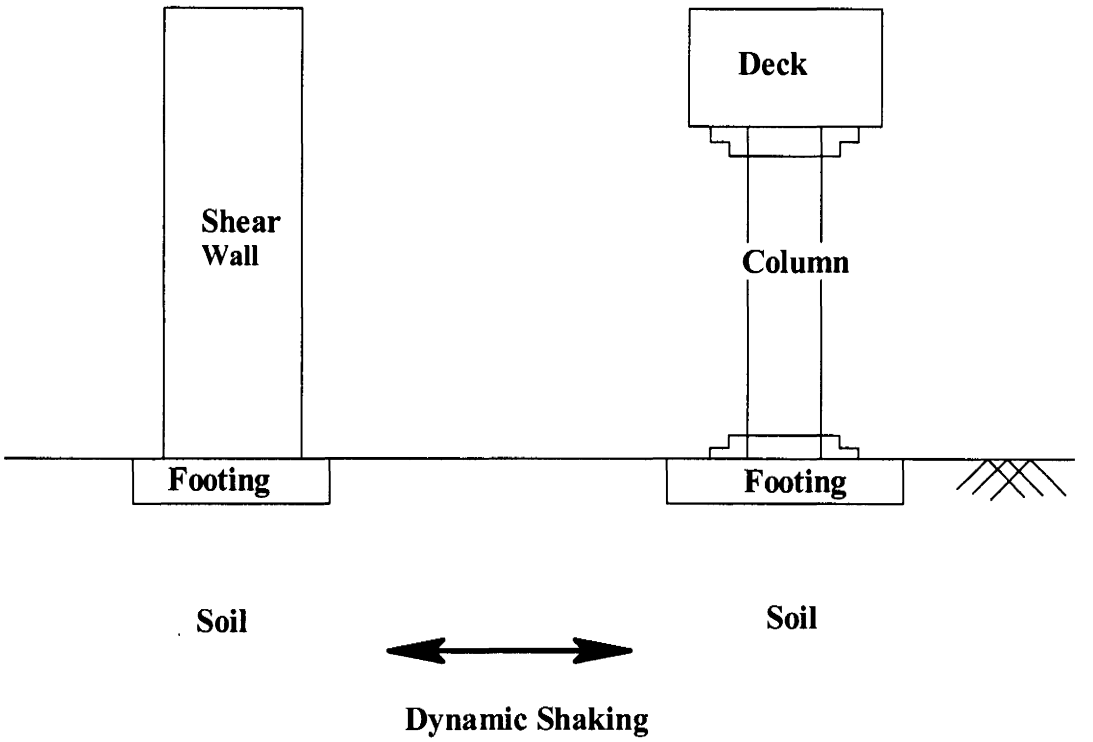

Fig. 5.1. Schematics of the centrifuge experimental models

Table 5.1 presents the details of the selected shear wall-footing structure experiments: total mass of the structure, factor of safety for static bearing capacity failure (FSv), normalized height of center of gravity, and the maximum applied base acceleration. Static vertical factor of safety against bearing capacity failure (FS_V) was calculated using the weight of the structure and conventional bearing capacity equations. The normalized height of center of gravity (hcg/L) is approximately equal to the normalized moment-to-shear ratio (M/(H·L)) at the footing-soil interface. The applied base acceleration, used in shear wall model tests, has tapered cosine cycles with increasing magnitude, with a predominant frequency of about 1.2 Hz and with higher frequency accelerations superimposed. In order to obtain different peak base accelerations in different tests, the tapered cosine displacement time history was scaled up or scaled down while maintaining the same frequency content.

Table 5.1. Details of the centrifuge experimental models

Test	Width (m)	Length (m)	Embedment (m)	Mass (Mg)	FSv	hcg/L	Max Base Acceleration (g)
SSG04_09a	0.65	2.8	0.00	58.0	2.6	1.78	0.12
SSG04_09b	0.65	2.8	0.00	58.0	2.6	1.78	0.55
SSG04_10a	0.65	2.8	0.00	36.8	4.0	1.89	0.12
SSG04_10b	0.65	2.8	0.00	36.8	4.0	1.89	0.55
SSG04_10c	0.65	2.8	0.00	36.8	4.0	1.89	0.90
SSG03_07a	0.65	2.8	0.65	58.0	7.2	1.78	0.12
SSG03_07b	0.65	2.8	0.65	58.0	7.2	1.78	0.55
SSG03_07c	0.65	2.8	0.65	58.0	7.2	1.78	0.90
SSG03_08a	0.65	2.8	0.65	36.8	11.5	1.89	0.12
SSG03_08b	0.65	2.8	0.65	36.8	11.5	1.89	0.55
SSG03_08c	0.65	2.8	0.65	36.8	11.5	1.89	0.90
JAU01_05_E_a	5.4	5.4	1.70	1090.7	17.0	2.10	0.09
JAU01_05_E_b	5.4	5.4	1.70	1090.7	17.0	2.10	0.23
JAU01_05_E_c	5.4	5.4	1.70	1090.7	17.0	2.10	0.47
JAU01_05_F_a	7.1	7.1	1.70	1172.3	31.0	1.50	0.09
JAU01_05_F_b	7.1	7.1	1.70	1172.3	31.0	1.50	0.23
JAU01_05_F_c	7.1	7.1	1.70	1172.3	31.0	1.50	0.47

5.2. JAU Test Series

In JAU test series, several bridge deck-column-footing-soil models (Fig. 5.1 (right)) were subjected to dynamic base shaking loading (Ugalde, 2005; Ugalde et al., 2007 and 2008). The prototype structure was a typical reinforced concrete single column bridge bent modeled as a "lollipop" structure with a deck mass and column connected to a shallow square spread footing. The bridge deck was modeled by a steel block; the reinforced concrete column was modeled by an aluminum tube that had a bending stiffness, EI, closely scaled to the calculated EI of the cracked section of the prototype concrete column. The footings were constructed of aluminum plates with sand glued to their bases to provide

a rough concrete-like interface with the soil. The deck and the footing were relatively rigid whereas the columns were flexible. The dimensions of the square footings were 5.4 m and 7.1 m and were supported by dry sandy soil deposit (Dr = 80% and φ = 42 degrees). The ground motions imposed on the models were scaled and filtered motions from recordings in the Tabas 1978 earthquake and a Los Gatos recording of the 1989 Loma Prieta earthquake. Table 5.1 provides other additional information of the selected centrifuge tests used in this paper. Note that the FSv values of the JAU test series are higher (17 and 31), because the footings were designed to satisfy the allowable settlement requirements (settlement controlled the design).

5.3. Centrifuge Experimental Results

The total seismic input energy is calculated using the same equation used in the previous chapter (eq. 4.5.3). The seismic input energy is dissipated by hysteretic energy dissipation in structural elements and soil and radiation damping. Energy dissipated by foundation soil is calculated from the moment-rotation hysteretic loops. Note that the M/(H.L) ratio is higher than 1.0 and hence majority of the foundation energy dissipation is through footing rocking (Gajan and Kutter, 2009b) as opposed to sliding.

Fig. 5.2 presents the time histories of the seismic input energy (IE) and the energy dissipated in soil due to footing rocking (EDF) during two centrifuge tests, while Fig. 5.3 presents the effects of foundation rocking in terms of normalized non-dimensional parameters, where energy dissipation is normalized by applied vertical load and length of the footing (V·L), settlement is normalized by the length of the footing, and energy dissipation ratio, maximum cyclic and permanent rotation of the footing (drift). The

rotation of the footing is presented in Radians. As expected all these quantities increase as the shaking intensity increases. Though energy dissipation increases as the shaking intensity increases, this increase in energy dissipation occurs at the expense of increased drift demands in the structure. Considering energy dissipation ratio in Fig. 5.3, for shear wall models (SSG test series), about 85% to 95% of the seismic input energy is dissipated in soil through footing rocking. This makes sense because the hysteretic damping in the structure is negligible (rigid structure) and also implies that the radiation damping is insignificant. For bridge models (JAU test series), about 20% to 60% of the seismic input energy is dissipated through footing rocking. This indicates the remaining energy is dissipated by yielding of the column.

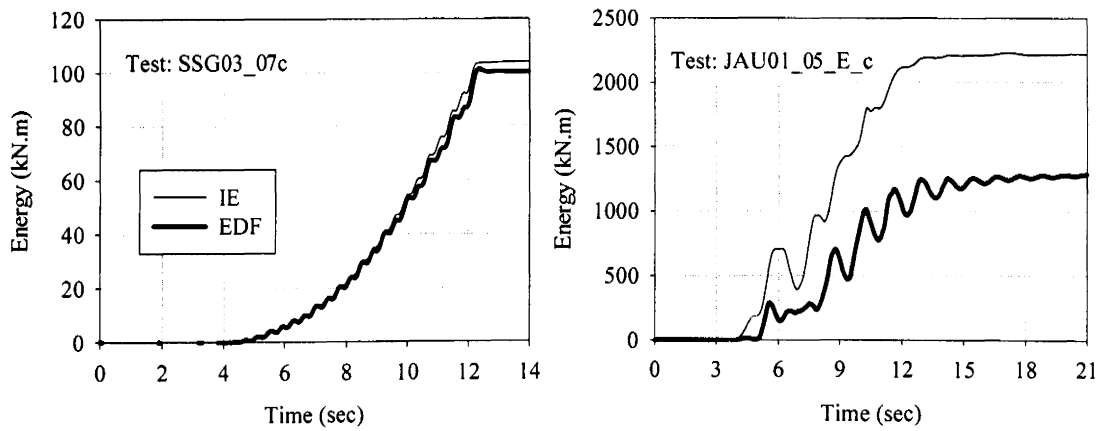

Fig. 5.2. Time histories of seismic input energy (IE) and the energy dissipation in foundation soil (EDF) during selected centrifuge experiments

Fig. 5.4 presents variation of normalized settlement, maximum cyclic rotation, energy dissipation ratio, normalized maximum moment, and normalized maximum shear where maximum moment is normalized by vertical load and length of the footing and maximum shear is normalized by vertical load.

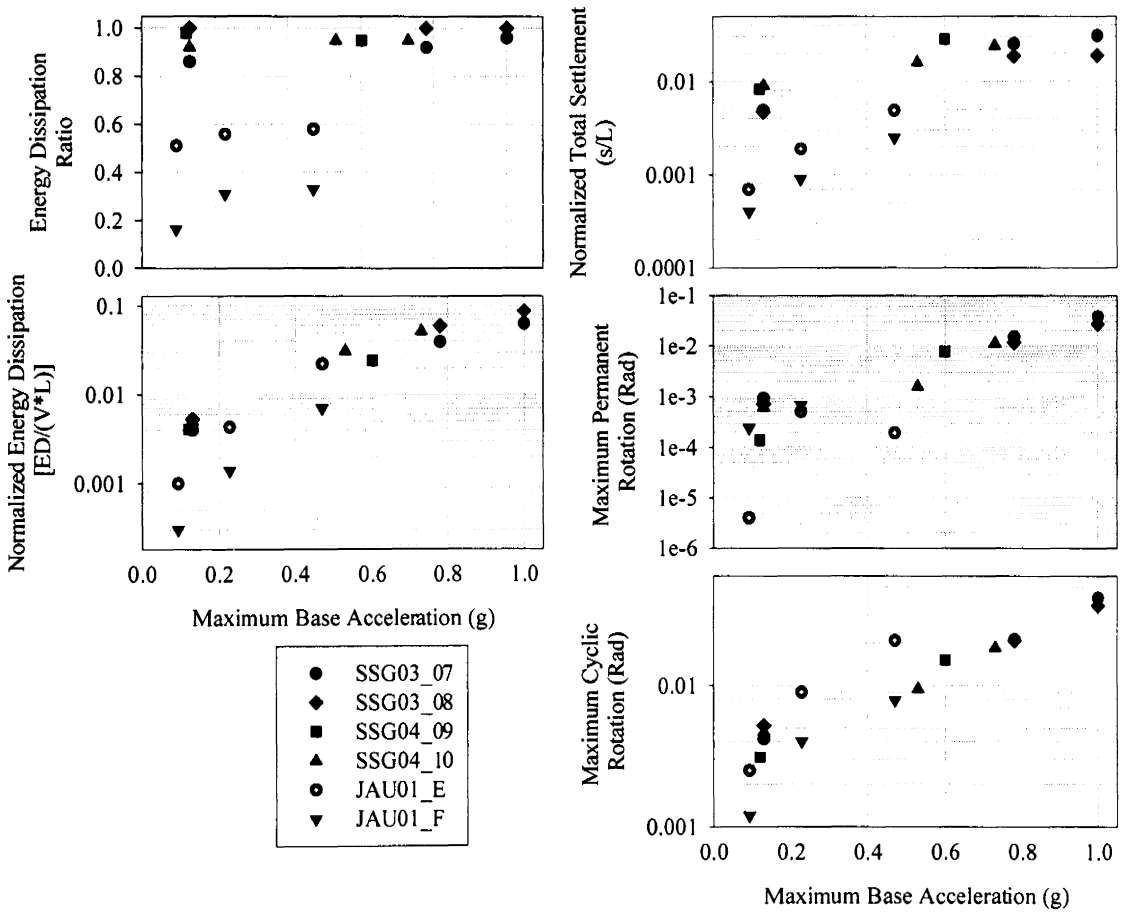

Fig. 5.3. Normalized energy dissipation and energy dissipation ratio along with consequences of footing rocking

From the Fig. 5.4, it is clear that the effects of footing rocking decreases as the factor of safety increases. Not only settlement and rotation decrease while the factor of safety increases but also the energy dissipation. More than 80% of the seismic energy is dissipated by footing rocking when FSv is less than 12, and the ratio decreases to 60% and 20% when FSv increases to 17 and 31. For strong foundations (FSv = 31), less energy is dissipated by foundation soil and more energy is dissipated by column yielding (and associated damage in the column). Normalized maximum moment and normalized maximum shear increase as factor of safety increases for SSG test series and JAU test series. Based on the centrifuge experimental results, it can be seen that an optimum FSv

can be selected where moment capacity is reasonably high, considerable energy dissipation in foundation soil, and the resulting deformations are within allowable limiting values.

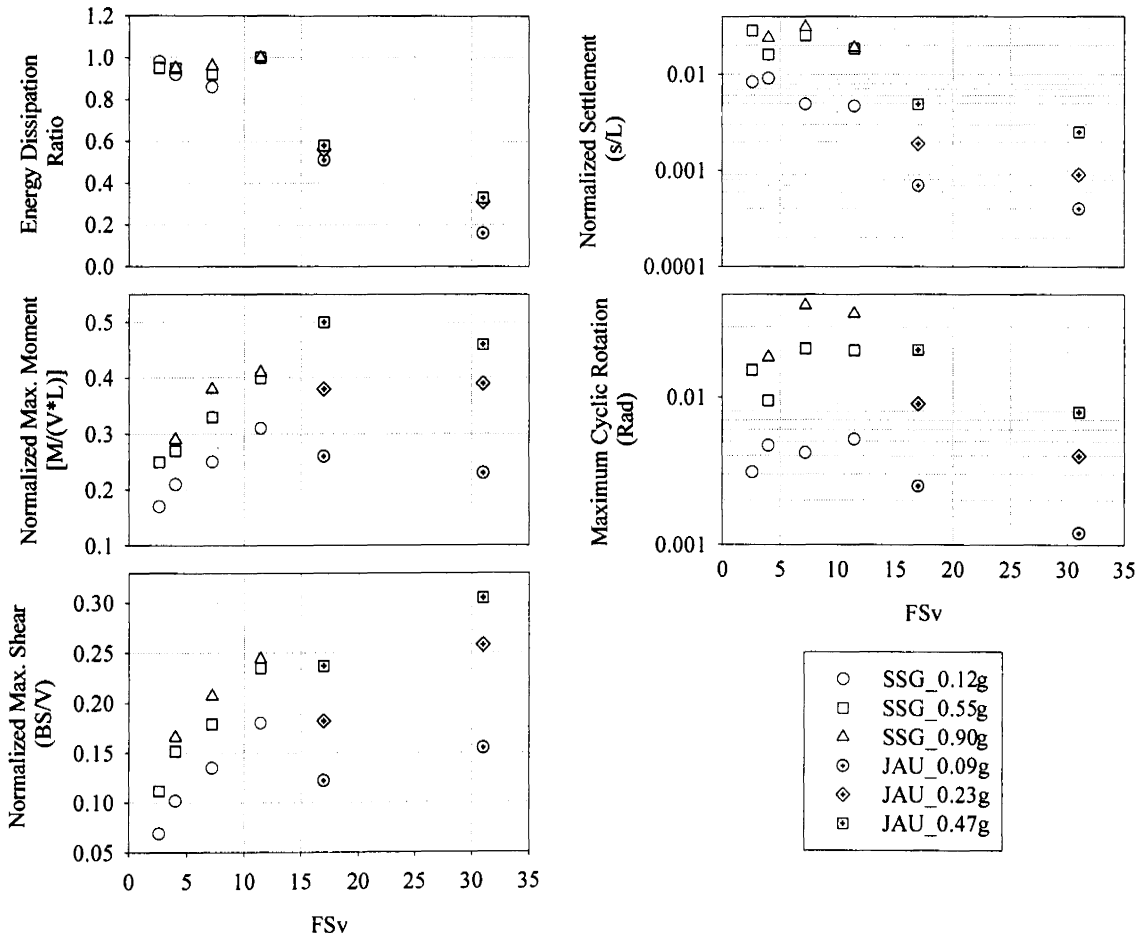

Fig. 5.4. Variation of normalized forces and deformation of footing along with static vertical factor of safety (FSv)

5.4. Comparison of Energy Dissipation in Structure and Foundation Soil

In order to compare the energy dissipation and the consequences in structural elements with those of foundation soil (due to rocking) and to quantify the effectiveness of different energy dissipation mechanisms, the following non-dimensional parameters are defined (Fig. 5.5): (1) energy dissipation ratio: defined as energy dissipated by the energy dissipation devices or foundation soil during rocking divided by the total seismic input

energy, (2) normalized energy dissipation: defined as energy dissipated by the energy dissipation devices or foundation soil during rocking divided by V·L, where V is the weight of the structure and L is the length of the base of the structure or length of the footing, (3) normalized base shear force: defined as base shear force divided by the weight of the structure, (4) normalized base moment: defined as moment at the base divided by V·L and (5) normalized total settlement: defined as the total settlement of the footing divided by the length of the footing. In addition, maximum cyclic drift and residual drift of the structure (structural model) is compared with the maximum cyclic rotation and permanent rotation of the footing (centrifuge soil-foundation-structure model) for corresponding maximum base acceleration.

5.4.1. Energy Dissipation

Fig. 5.5 compares the energy dissipation, base shear force, and maximum cyclic and residual drift ratio of the structure from the numerical simulations of shaking table experiments (structural energy dissipation) with centrifuge experimental results (foundation soil energy dissipation due to footing rocking). As expected, in both cases, energy dissipation increases as the shaking intensity increases, however this increase in energy dissipation occurs at the expense of increased drift demands in the structure. More than 85% of seismic energy is dissipated by steel braces or SMA base isolation system, whereas SMA braces dissipate about 60% to 80% of the total seismic energy. This structural energy dissipation ratio is in between the energy dissipation ratios in the foundation soil for shear wall structures (85% to 95%) and bridge structures (20% to 60%). Interestingly, the

normalized energy dissipation in both structural devices and foundation soil show similar trend with maximum base acceleration.

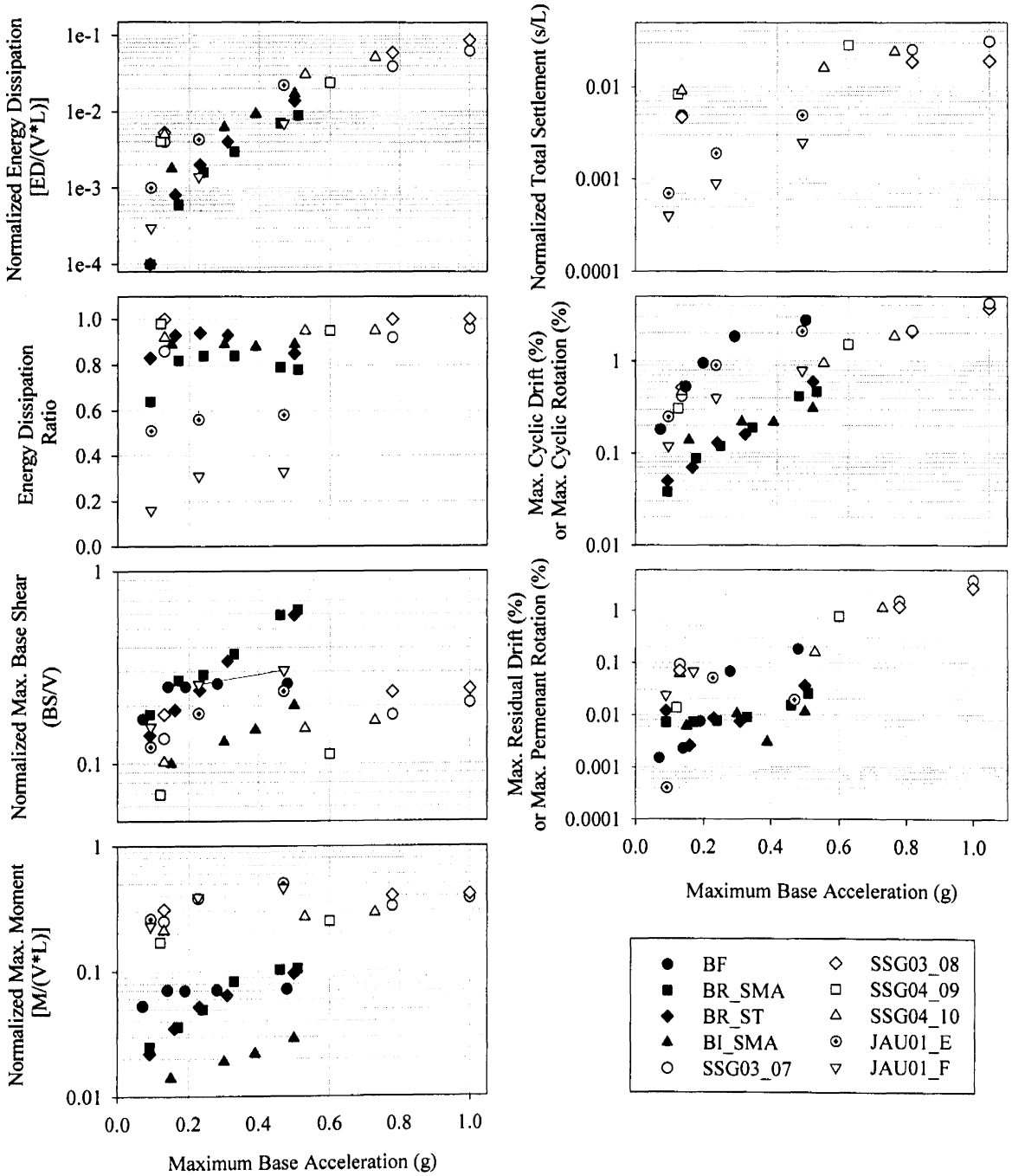

Fig. 5.5. Comparison between effects of structural energy dissipation devices and foundation rocking

5.4.2. Force and Displacement Demands

As can be seen from Fig. 5.5, for the structures with energy dissipating braces, base shear force increases by as much as 150%, whereas for the structure with base-isolation system, base shear force decreases by about 25% to 50%. Normalized base shear forces transmitted to the foundation during centrifuge experiments are smaller than those of the structures with energy dissipating devices (isolation effect of rocking foundations). On the other hand, the normalized base moment in the foundation is bigger than the moment transmitted to the base of the fixed base structure. Maximum cyclic and residual drift of the bare frame structure are comparable to the maximum cyclic and permanent rotation of the foundation during rocking, however maximum cyclic and residual drift of the structure are reduced by about 70% to 80% respectively when energy dissipation devices are used. As explained in the previous chapter, the displacements and rotations of the foundation during rocking, including permanent settlement, decrease as the static factor of safety increases.

CHAPTER 6. SUMMARY AND CONCLUSIONS

Comparison of the effectiveness of different structural energy dissipation devices using numerical simulations and comparison of the effectiveness of foundation energy dissipation (during footing rocking) with that of structural devices using experimental results and numerical simulation results are the two objectives of this thesis work. Numerical models were developed using the sections, elements, material models, and solution algorithms available in OpenSees finite element framework to simulate the seismic behavior of frame structures with and without passive energy dissipation devices. The numerical model was first calibrated using cyclic loading experimental results of energy dissipating devices and then validated using available shaking table experimental results (dynamic base shaking). Several numerical simulations were systematically carried out to study the seismic behavior and energy dissipation characteristics of different energy dissipating devices inserted into the frame structures. Results for energy dissipation, cyclic and residual displacements and drifts, and base shear force and moment on the structure are compared with centrifuge experimental results for energy dissipation in foundation soil through footing rocking and the consequences of rocking behavior.

For the structures with energy dissipating devices, about 70% to 90% of the seismic input energy is dissipated by energy dissipating devices, leading to minimal hysteretic behavior of the regular structural members (beams and columns). As a result of this energy dissipation in the devices, maximum cyclic displacement and drift of the structure are reduced by more than 70% and 80% respectively when compared to the structure without energy dissipating devices. The inclusion of energy dissipating devices also decreases the residual displacement and drift of the structure for shakes with maximum base

accelerations of 0.2 g or bigger. For smaller shakes (less than 0.2 g), the residual displacement and drift are not affected by the inclusion of energy dissipating devices. The inclusion of the energy dissipating braces makes the structure stiffer, resulting in increased base shear forces transmitted to the base of the structure (as much as 150% increase when compared to bare frame structure). The base-isolation system, as expected, decreases the base shear force by about 25% to 50%. Based on the numerical simulation results presented in this paper, it can be concluded that the SMA base-isolation is the most effective energy dissipation system and it is followed by steel brace and SMA brace in that order.

Foundation rocking dissipates about 90% of the total seismic input energy in foundation soil for rigid structure (for footings with FSv = 4 to 10), and for flexible structures, the energy dissipation in foundation soil due to rocking is about 60% (for footings with FSv = 17) to 30% (for footings with FSv = 31). Normalized base shear forces transmitted to the foundation during rocking are smaller than those of the structures with energy dissipating devices because of the isolation effect of rocking foundations. Moreover, the ultimate moment capacity of the foundation did not show any softening behavior, indicating the ductile behavior of the footing-soil system during rocking. Foundation rocking results in permanent settlement and cyclic displacements on the structure, however, the displacements and rotations of the foundation during rocking decrease as the static factor of safety increases.

Results clearly indicate that foundation energy dissipation mechanism is as efficient as structural passive energy dissipation devices. As long as the settlement and displacements are within tolerable limits, foundation energy dissipation mechanism would be a much cheaper alternative as opposed to structural energy dissipation devices. Based on

the centrifuge experimental results, it is apparent that an optimum factor of safety can be selected where moment capacity is reasonably high, considerable energy dissipation in foundation soil, and the resulting deformations are within allowable limiting values. If properly designed, adverse effects of foundation rocking can be minimized, while taking advantage of the favorable features of foundation rocking and hence they can be used as efficient and economical seismic energy dissipation mechanisms in buildings and bridges.

CHAPTER 7. RECOMMENDATIONS FOR FUTURE WORK

Flexible-base bare frame structure with shallow foundations

The reinforced concrete frame numerical model can be attached to shallow foundation (instead of fixed-base) in order to study the effects of flexible soil-foundation system on the seismic performance of this structure as shown in Fig. 7.1. A contact interface model (CIM), available in OpenSees, can be used to simulate the nonlinear cyclic load-displacement behavior and energy dissipation of rocking shallow foundations. Parametric studies can be carried out to systematically study the effect of geometry of structure, dimension of shallow foundations, depth of embedment, soil types, soil strength, and soil stiffness. Energy dissipation in soil due to foundation rocking and the reduced force and displacement demands on the structure can be compared with the adverse effects on the structure, such as, permanent deformations of the foundation. The findings of these analyses could help improve the design of safe and cost-effective structural systems in performance-based earthquake engineering design framework.

Flexible-base frame structures with structural energy dissipation devices and foundation rocking

As a next step, energy dissipation in braces can be included in soil-foundation-structure system to study the combined energy dissipation behavior of soil-foundation-structure systems. The effect of properties and locations of energy dissipation devices can be studied together with different footing dimensions, depth of embedment, soil types, soil strength, and soil stiffness. The energy dissipation in structural elements can be compared

to the combined energy dissipation in both structural elements and foundation soil. Optimum footing design and critical locations of energy dissipation devices can be found.

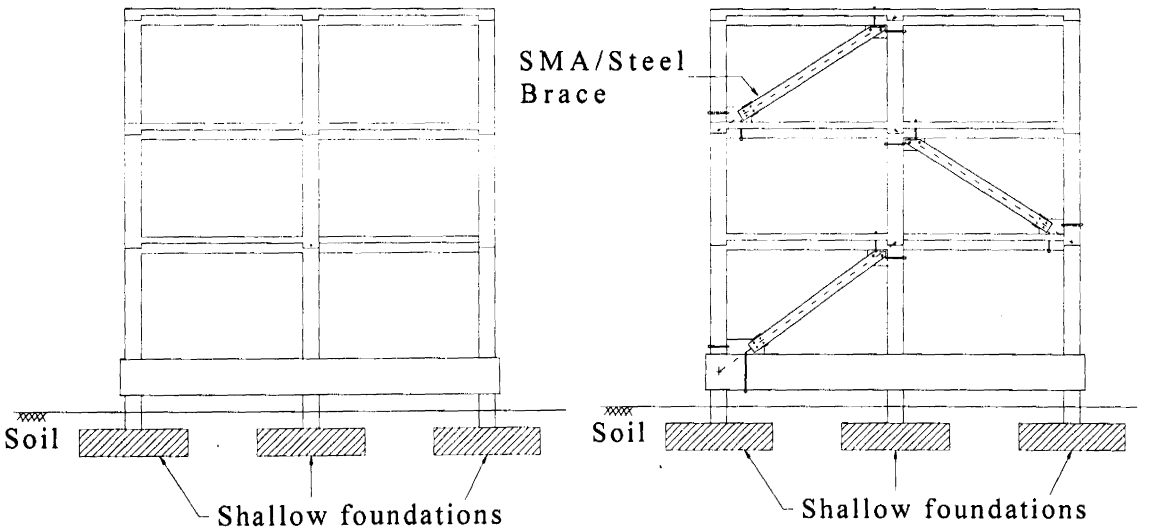

Fig. 7.1. Bare frame structure with shallow foundations and Foundation- Structure system with energy dissipating braces

REFERENCES

Aiken, I. D., Nims, D. K., Whittaker, A. S., Kelly, J. M. (1993), "Testing of passive energy dissipation systems," *Earthquake Spectra*, 9(3)

Allotey, N. and Naggar, M. H. E. (2003), "Analytical moment–rotation curves for rigid foundations based on a Winkler model," *Soil Dynamics and Earthquake Engineering,* 23, 367–381

Allotey, N. and Naggar, M. H. E. (2008), "An investigation into the Winkler modeling of the cyclic response of rigid footings," *Soil Dynamics and Earthquake Engineering,* 28, 44–57

Black, C. J., Makris, N. and Aiken, I. D. (2004), "Component Testing, Seismic Evaluation and Characterization of Buckling-Restrained Braces," *Journal of Structural Engineering*, 130(6), 880-894

Bouc, R. (1971), ''Mode`l mathe´matique d'hysteresis,'' *Acustica,* 24, 16–25

Braga, F., Crew, A., D'Anzi, P., Dolce, M. and Ponzo, F. C. (2002), "Experimental and Numerical Behavior of R/C Building Frames Upgraded with Energy Dissipating Braces," *European Earthquake Engineering*, 16 (1), 27 - 39

Braga, F. and D'Anzi, P. (1994), "Steel Braces with Energy Absorbing Devices: A Design Method to Retrofit Reinforced Concrete Existing Buildings," *Strengthening and repair of structures in Seismic Area (V. Davidovici and D. Benedetti), Ouest Editions Presses Academiques*, Nice, France, 146 – 154

Braga, F., D'Anzi, P., Dolce, M. and Ponzo, F. C. (1996), "Retrofitting of R.C Building by Energy Dissipating Bracing: Earthquake Simulator Tests," *Eleventh World Conference on Earthquake Engineering*, Acapulco, Mexico, Paper No. 806

Chang, K. C. and Lin, Y. Y. (2004), "Seismic response of full-scale structure with added viscoelastic dampers," *Journal of Structural Engineering*, Vol. 130 (4), 600-608

Chang, K. C., Soong, T. T., Oh, S.-T., and Lai, M. L. (1995), "Seismic behavior of steel frames with added viscoelastic dampers," *Journal of Structural Engineering*, Vol. 121 (10), Paper No. 8941

Chopra, A. K. (2006), "Dynamics of Structures: Theory and Applications to Earthquake Engineering," Third Edison, Prentice-Hall: Upper Saddle River, NJ, 2006

Christopoulos, C., Tremblay, R., Kim, H.-J., and Lacerte, M. (2008), "Self-centering energy dissipative bracing system for the seismic resistance of structures: Development and Validation," *Journal of Structural Engineering,* 134, 96-107

Comartin, C.D., Niewiarowski, R.W., Freeman, S.A. and Turner, F.M. [2000] "Seismic retrofit and evaluation of concrete buildings: A practical overview of the ATC 40 document," *Earthquake Spectra* 16, 241–262

Constantinou, C. M., Tsopelas, P., Hammel, W., and Sigaher, A. N. (2001), "Toggle-Brace-Damper seismic energy dissipation systems," *Journal of Structural Engineering*, Vol. 127 (2), Paper No.22317

Cremer, C., Pecker, A. and Davenne, L. (2001), "Cyclic macro-element of soil structure interaction: Material and geometrical nonlinearities," *Inernational Journal for Numerical and Analyical Methods in Geomechanics*, 25, 1257–1284

Croci, G., Bonci, A., and Viskovic, A. (2000), "Use of SMA devices in the basilica of St. Francis of Assisi," *Proceeding of the Shape Memory Alloy Devices for Seismic Protection of Cultural Heritage Structures*, Ispra, Italy.

D'Anzi, P., Crewe, A. J. and Ponzo, F. C. (1996), "Retrofitting of R.C Building by Energy Dissipating Bracing: Earthquake Simulator Tests," *Eleventh World Conference on Earthquake Engineering*, Acapulco, Mexico, Paper No. 1531

Dolce, M. and Cardone, D. (2001), "Mechanical Behavior of SMA Elements for Seismic Applications—Part 1: Martensite and Austenite NiTi Bars Subjected to Torsion," *International Journal of Mechanical Science*, 43(11), 2631–2656

Dolce, M. and Cardone, D. (2003), "Seismic protection of light secondary systems through different base isolation systems," *Journal of Earthquake Engineering*, 7(2), 223–250

Dolce, M. and Cardone, D. (2006), "Theoretical and Experimental studies for the application of shape memory alloys in civil engineering," *Journal of Engineering Materials and Technology*, 128, 302 – 311

Dolce, M., Cardone, D. and Giuseppe, P. (2007a), "Seismic Isolation of Bridges using isolation systems based on flat sliding bearings," *Bull Earthquake Engineering*, 5, 491 – 509

Dolce, M., Cardone, D., Giuseppe, P. and Claudio, V. (2005), "Shaking table test on reinforced concrete frames without and with passive control systems," *Earthquake Engineering and Structural Dynamics*, 34, 1687 – 1717

Dolce, M., Cardone, D. and Marnetto, R. (2000), "Implementation and testing of passive control devices based on shape memory alloys," *Earthquake Engineering and Structural Dynamics*, 29, 945–68

Dolce, M., Cardone, D., Marnetto, R., Nigro, D., Ponzo, F. C., and Santarsiero, G. (2004), "Experimental static and dynamic response of a real R/C frame upgraded with SMA re-centering and dissipating braces," *13th World Conference on Earthquake Engineering*, Vancouver, B.C., Canada, August 1-6, Paper No. 2878.

Dolce, M., Cardone, D. and Ponzo, F. C. (2007b), "Shaking table test on reinforced concrete frames with different isolation systems," *Earthquake Engineering and Structural Dynamics*, 36, 573 – 596

Donatello, C., Dolce, M., Ponzo, F. C. and Coelho, E. (2004), "Experiment Behavior of R/C Frames Retrofitted with Dissipating and Re-Centering Braces," *Journal of Earthquake Engineering*, Vol. 8, No.3, 361-396

Faccioli, E., Paolucci, R. and Vivero, G. (2001), "Investigation of seismic soil-footing interaction by large scale cyclic tests and analytical models," *Proc. of the 4th Int. Conf. on Recent Advances in Geotechnical Earthquake Engineering and Soil Dynamics*, San Diego, California

FEMA 273 (1997), "NEHRP guidelines for the seismic rehabilitation of buildings," Federal Emergency Management Agency, Washington, DC, 1997

FEMA 356 (2000), "Prestandard and Commentary for the Seismic Rehabilitation of Buildings," Federal Emergency Management Agency, Washington, DC

Filippou, F. C., Popov, E. P., and Bertero, V. V. (1983), "Effect of bond deterioration on hysteretic behavior of reinforced concrete joints," Report No. EERC 83-19, Earthquake Engineering Research Center, University of California, Berkeley,

Gajan, S. and Kutter, B. L. (2008a), "Capacity, settlement, and energy dissipation of shallow footings subjected to rocking," *Journal of Geotechnical and Geoenvironmental Engineering,* Vol. 134(8), 1129 – 1141

Gajan, S. and Kutter, B. L. (2008b), "Numerical Simulations of Rocking Behavior of Shallow Footings and Comparisons with Experiments," *Proceedings of the BGA International Conference on Foundations*, Dundee, Scotland, 2008

Gajan, S. and Kutter, B. L. (2009a), "Contact interface model for shallow foundations subjected to combined cyclic loading," *Journal of Geotechnical and Geoenvironmental Engineering, ASCE*, Vol. 135 (3), pp 407-419

Gajan, S. and Kutter, B. L. (2009b), "Effects of Moment-to-Shear Ratio on Combined Cyclic Load-Displacement Behavior of Shallow Foundations from Centrifuge Experiments," *Journal of Geotechnical and Geoenvironmental Engineering, ASCE*, Vol. 135 (8), pp 1044-1055

Gajan, S., Phalen, J. D., Kutter, B. L., Hutchinson, T. C. and Martin, G. (2005), "Centrifuge modeling of load-deformation behavior of rocking shallow foundations," *Journal of Soil Dynamics and Earthquake Engineering,* Vol. 25 (7-10), 773 - 783

Gajan, S., Raychowdhury, P., Hutchinson, T. C., Kutter, B. L., Stewart, J. P. (2010) "Application and Validation of Practical Tools for Nonlinear Soil-Foundation Interaction Analysis," *Earthquake Spectra*, 26(1), 111-129

Gazetas, G. (2006), "Seismic design of foundations and soil-structure interaction," *Proc. 1st European Conference on Earthquake Engineering and Seismology*, Geneva, Switzerland, September, 2006, paper no. K7

Georgiadis, M. and Butterfield, R. (1988), "Displacements of footings on sand under eccentric and inclined Loads," *Canadian Geotechnical Journal*, Vol. 25, 199 – 212

Gottardi, G. and Butterfield, R. (1995), "The displacement of a model rigid surface footing on dense sand under general planer loading," *Soils and Foundations*, 35(3), 71 - 82

Graesser, E. J., and Cozzarelli F. A. (1991), "Shape memory alloys as new material for aseismic isolation," *Journal of Engineering Mechanics*, 117(11), Paper No. 26345.

Gottardi, G., Houlsby, G. T. and Butterfied, R. (1999), "Plastic response of circular footings on sand under general planer loading," *Geotechnique*, 49(4), 453- 469

Hanson, D. R., Aiken, I. D., Nims, D. K., Richter, P. J., and Bachman, R. E. (1993), "State-of-the-art and state-of-the-practice in seismic energy dissipation," *Proceeding of ATC-17-1, seminar on seismic isolation, passive energy dissipation, and active control*; San Francisco, CA.

Harden, C. W, Hutchinson, T. C, Martin, G. R, and Kutter, B. L. (2005), "Numerical modeling of the nonlinear cyclic response of shallow foundations," *Technical Report 2005/04*, Pacific Earthquake Engineering Research Center (PEER)

Houlsby, G. T. and Cassidy, M. J. (2002), "A plasticity model for the behavior of footings on sand under combined loading," *Geotechnique*, 52(2), 117–129

Houlsby, G. T., Cassidy, M. J. and Einav, I. (2005), "A generalized Winkler model for the behavior of shallow foundations," *Geotechnique*, 55(6), 449-460

Housner, G. W., Bergman, L. A., Caughey, T. K., Chassiakos, A. G., Claus, R. O., Masri, S. F., Skelton, R. E.. Soong, T. T., Spencer, B. F. Jr., and Yao, T. P., (1997), "Structural control: past, present, and future," *Journal of Engineering Mechanics,* ASCE, 123(9), 897–971.

Hwang, J. S., Huang, Y. N., Yi, S. L. and Ho, S. Y. (2008), "Design formulations for supplemental viscous dampers to building structures," *Journal of Structural Engineering, ASCE*, 134 (1), 22-31

John, F. Hall (2006), "Problem encountered from the use (or misuse) of Rayleigh damping," *Earthquake Engineering and Structural Dynamics*, 35, 525-545

Kelly, J. M. (1986) "Aseismic base isolation: review and bibliography," *Soil dynamics and earthquake engineering,* 5(4), 202-2016.

Kent, D.C. and Park, R. (1971), "Flexural members with confined concrete," *Journal of the Structural Division, ASCE,* 97(7): 1969–1990.

Keri, L. R. and Jose P. (2008), "Problems with Rayleigh damping in base isolated buildings," *Journal of Structural Engineering, ASCE,* 134 (11), 1780-1784

Lafortune, P., McCormick, J., DesRoches, R. and Terriault, P. (2007), "Testing of superelastic re-centering pre-strained braces for seismic resistant design," *Journal of earthquake engineering,* 11, 383-399

Lu, X., Zhou, Y. and Yan, F. (2008), "Shaking table test and numerical analysis of RC frames with viscous wall dampers," *Journal of Structural Engineering*, 134 (1), 64-76

Martin, G. and Lam, I. P. (2000) "Earthquake Resistant Design of Foundations: Retrofit of Existing Foundations," *Proc. of the GeoEng 2000 Conference*, Melbourne, Australia.

Menegotto, M. and Pinto, E. (1973), "Method of analysis for cyclically loaded reinforced concrete plane frames including changes in geometry and non-elastic behavior of elements under combined normal force and bending," *Proceedings*, IABSE Symposium. Lisbon, Portugal

Mergos, P. E. and Kawashima, K. (2005), "Rocking isolation of a typical bridge pier on spread foundation," *Journal of Earthquake Engineering* 9(Sp. Iss. 2), 395-414.

Monti, G., Spacone, E. and Filippou, F. C. (1993), "Model for anchored reinforcing bars under seismic excitations," Report No. UCB/EERC-93/08, Earthquake Engineering Research Center, University of California, Berkeley, December 1993.

Motahari, S.A., Ghassemieh, M. (2006), "Multi-linear one-dimensional shape memory material model for use in structural engineering applications," *Engineering Structure*, 29, 904-913

Motahari, S.A., Ghassemieh, M. and Abolmaali, S. A. (2007), "Implementation of shape memory alloys dampers for passive control of structures subjected to seismic exitations," *Journal of Constructional Steel Design*, 63, 1570 – 1579

Naeim, F. and Kelly, J. M. (1999), Design of seismic isolated structures, John Wiley & Sons, Inc., New York

Nova, R. and Montrasio, L. (1991), "Settlements of shallow foundations on sand," *Geotechnique*, 41(2), 243–256

OpenSees (2008), Open System for Earthquake Engineering Simulation: OpenSees, Pacific Earthquake Engineering Research Center (PEER), University of California, Berkeley, URL: http://opensees.berkeley.edu.

Orakcal, K., Massone, L. M. and Wallace J. W. (2006), "Analytical Modeling of Reinforced Concrete Walls for Predicting Flexural and Coupled-Shear-Flexural Responses," Pacific Earthquake Engineering Research Center, PEER Report 2006/07, October 2006.

Pall, A. S. and March, C. (1982), "Response of friction damped braced frames," *Journal of the Structural Division*, Vol. 108, No. ST6

Pampanin, S., Christopoulos, C., and Priestley, M. J. N. (2003), "Performance-based seismic response of frame Structures including residual deformations. Part II: multi-degree of freedom systems," *Journal of earthquake engineering,* 7 (1), 119-147

Paolucci, R., Shirato, M. and Yilmaz, M. T. (2007), "Seismic behavior of shallow foundations: shaking table experiments versus numerical modeling," *Earthquake Engineering and Structural Dynamics*, 34(7), 577-595.

Pecker, A. and Pender, M. (2000), "Earthquake resistant design of foundations: New construction," *Proc. of the GeoEng 2000 Conference*, Melbourne, Australia

PEER (2008), Pacific Earthquake Engineering Research Center, http://peer.berkeley.edu/

Raychowdhury, P. and Hutchinson, T. C. (2009), "Performance evaluation of a nonlinear Winkler-based shallow foundation model using centrifuge test results," *Earthquake Engineering and Structural Dynamics,* 38, 679 - 698

Scott, B. D., Park, R., and Priestley, M. J. N. (1982), "Stress-strain behavior of concrete confined by overlapping hoops at low and high strain rates," *Journal of the American Concrete Institute,* 79(1), 13–27

Shen, J., and Akbas, B., (1999), "Seismic Energy Demand in Steel Moment Frames," *Journal of Earthquake Engineering*, 3(4), 519 – 559

Song, G., Ma, N., and Li, H N. (2006), "Application of shape memory alloys in civil structures," *Engineering Structures*, 28, 1266-1274

Soong, T. T. and Spencer, B. F. Jr. (2002), "Supplemental energy dissipation: state-of-the-art and state-of-the-practice," *Engineering Structures*, 24, 243-259.

Skinner, R. I., Kelly, J. M., and Heine, A. J. (1975), "Hysteretic Dampers for Earthquake-Resistant Structures," *Earthquake Engineering and Structural Dynamics*, 3, 287 – 296.

Spacone, E., Filippou, F. C. and Taucer, F. F. (1996), "Fiber beam-column model for non-linear analysis of R/C frames: Part 1. Formulation," *Earthquake Engineering and Structural Dynamics*, 25, 711 – 725.

Symans, M. D., Charney, F. A., Whittaker, A. S., Constantinou, M. C., Kircher, C. A., Johnson, M. W., and McNamara, R. J. (2008), "Energy dissipation systems for seismic applications: Current Practice and recent developments," *Journal of Structural Engineering, ASCE*, 134 (1), 3-21

Taylor, P. W., Bartlett, P. E. and Weissing, P. R. (1981), "Foundation Rocking under Earthquake Loading," *Proc. of the 10th Intl. Conf. on Soil Mechanics and Foundation Engineering*, Vol. 3, 33-322.

Tremblay, R., Lacerte, M., and Christopoulos, C. (2008), "Seismic Response of Multistory Buildings with Self-Centering Energy Dissipative Steel Braces," *Journal of Structural Engineering, ASCE,* 134(1), 108-120

Tsai, K. C., Chen, H. W., Hong, C. P. and Su, Y. F. (1993), "Design of Steel Triangular Plate Energy Absorbers for Seismic-Resistant Construction," *Earthquake Spectra*, 9(3), 505-528

Uang, C. M. and Bertero, V. V. (1990), "Evaluation of Seismic Energy in Structure," *Earthquake Engineering and Structural Dynamics*, 19, 77-90

Ugalde, J. A. (2005), "Rocking Response of Bridges on Shallow Foundation," M.S. Thesis, University of California, Davis

Ugalde, J. A., Kutter, B. L., Jeremic, B., and Gajan, S. (2007), "Centrifuge modeling of rocking behavior of bridges on shallow foundations," *Proc. of the 4th Intl. Conf. on Earthquake Geotechnical Engineering*, Thessaloniki, Greece, Paper No. 1484.

Ugalde, J. A., Kutter, B. L., Jeremic, B., Gajan, S. and Deng, L. (2008), "Centrifuge modeling of rocking of shallow foundations for bridges," *Proc. of the Intl. Conf. on Urban Earthquake Engineering*, Tokyo, Japan

Wen, Y.-K. (1975), "Approximate method for nonlinear random vibration," *Journal of Engineering Mechanics,* 101(4), 389–401

Wen, Y.-K. (1976), "Method for random vibration of hysteretic systems," *Journal of Engineering Mechanics,* 102(2), 249–263

Whittaker, A. S., Bertero, V. V., Thompson, C. L., and Alonso, L. J. (1991), "Seismic Testing of Steel Plate Energy Dissipation Devices," *Earthquake Spectra*, 7(4), 563 – 604

Wilde, K., Gardoni, P., and Fujino, Y. (2000), "Base isolation system with shape memory alloy devices for elevated highway bridges," *Engineering Structures*, 22(3), 222–229

Wong, K. K. F. and Yang, R. (2002), "Earthquake response and energy evaluation of inelastic structures," *Journal of Engineering Mechanics*, 128(3), 308–317

Xia, C. and Hanson, R. D. (1992), "Influence of ADAS Element Parameters on Building Seismic Response," *Journal of Structural Engineering*, 118(7), Paper No. 1762, 1903-1918

Yassin, M. H. M. (1994), "Nonlinear analysis of prestressed concrete structures under monotonic and cyclic loads," *Dissertation*, University of California, Berkeley, California

Zhang, Y., Camilleri, J. A, and Zhu, S. (2008), "Mechanical properties of superelastic Cu-Al-Be wires at cold temperatures for the seismic protection of bridges," *Smart Materials and Structures,* 17, 025008

Zhang, Y. and Zhu, S. (2008), "Seismic response control of building structures with superelastic shape memory alloy wire dampers," *Journal of Engineering Mechanics,* 134(3), 240-251.

APPENDIX: OPENSEES CODES

OpenSEES Code for Bare Frame (BF) Structure

```
# ------------------------------------------------------------------------
# MANSIDE_ BF_Model for test BF_28 -- Build Model
# nonlinearBeamColumn element, inelastic fiber section -- Reinforced Concrete Section
# kg, N, m, Sec
# SET UP ---------------------------------------------------------------------

wipe;
model BasicBuilder -ndm 2 -ndf 3;
source BuildRCrectSection.tcl;      # procedure for defininining RC fiber section

# define structure-geometry paramters ----------------------------------------------------------

set LCol 1.05;              # column length
set LColstory1 1.23;        #1st story Col length
set LColBase 0.275
set LBeam 1.65;  # beam length

# calculate locations of beam/column intersections:

set X1 0.
set X2 [expr $X1 + $LBeam];
set X3 [expr $X2 + $LBeam];
set YB1 0.
set Y1 [expr $YB1 + $LColBase];
set Y2 [expr $Y1 + $LColstory1];
set Y3 [expr $Y2 + $LCol];
set Y4 [expr $Y3 + $LCol];

# define nodal coordinates

node 01 $X1 $YB1
node 02 $X2 $YB1
node 03 $X3 $YB1
node 11 $X1 $Y1
node 12 $X2 $Y1
node 13 $X3 $Y1
node 21 $X1 $Y2
node 22 $X2 $Y2
node 23 $X3 $Y2
node 31 $X1 $Y3
node 32 $X2 $Y3
node 33 $X3 $Y3
node 41 $X1 $Y4
node 42 $X2 $Y4
node 43 $X3 $Y4

# BOUNDARY CONDITIONS

fix 01 1 1 1
fix 02 1 1 1
fix 03 1 1 1
```

```
# Define SECTIONS -------------------------------------------------------

# define section tags:
set ColSecTag 1
set ColBaseSecTag 2
set BeamSecTag 3
set BeamBaseSecTag 4

# Section Properties:
set HCol 0.150;             # Column width
set BCol 0.105
set HBeam 0.150;            # Beam depth -- perpendicular to bending axis
set BBeam 0.105;            # Beam width -- parallel to bending axis
set HColBase 0.150;                 # Base Column width
set BColBase 0.150;
set HBeamBase 0.330;                # Base Beam depth -- perpendicular to bending axis
set BBeamBase 0.165;                # Base Beam width -- parallel to bending axis

# MATERIAL parameters
source LibMaterialsRC.tcl;          # define library of Reinforced-concrete Materials

# FIBER SECTION properties
# Column section geometry:

set cover 0.015;  # rectangular-RC-Column cover
set numBarsTopCol 3;                # number of longitudinal-reinforcement bars on top layer
set numBarsBotCol 3;                # number of longitudinal-reinforcement bars on bottom layer
set barAreaTopCol 0.0000126;        # longitudinal-reinforcement bar area
set barAreaBotCol 0.0000126;        # longitudinal-reinforcement bar area

# Beam section geometry:

set numBarsTopBeam 7;               # number of longitudinal-reinforcement bars on top layer
set numBarsBotBeam 5;               # number of longitudinal-reinforcement bars on bottom layer
set barAreaTopBeam 0.0000126;       # longitudinal-reinforcement bar area
set barAreaBotBeam 0.0000126;       # longitudinal-reinforcement bar area
set nfCoreY 20;             # number of fibers in the core patch in the y direction
set nfCoreZ 20;             # number of fibers in the core patch in the z direction
set nfCoverY 20;            # number of fibers in the cover patches with long sides in the y direction
set nfCoverZ 20;            # number of fibers in the cover patches with long sides in the z direction

# rectangular section with one layer of steel evenly distributed around the perimeter and a confined core.
BuildRCrectSection $ColSecTag $HCol $BCol $cover $cover $IDconcCore  $IDconcCover $IDSteel
$numBarsTopCol $barAreaTopCol $numBarsBotCol $barAreaBotCol $nfCoreY $nfCoreZ $nfCoverY
$nfCoverZ
BuildRCrectSection $BeamSecTag $HBeam $BBeam $cover $cover $IDconcCore  $IDconcCover $IDSteel
$numBarsTopBeam $barAreaTopBeam $numBarsBotBeam $barAreaBotBeam $nfCoreY $nfCoreZ
$nfCoverY $nfCoverZ
BuildRCrectSection $BeamBaseSecTag $HBeamBase $BBeamBase $cover $cover $IDconcCore
$IDconcCover $IDSteel $numBarsTopBeam $barAreaTopBeam $numBarsBotBeam $barAreaBotBeam
$nfCoreY $nfCoreZ $nfCoverY $nfCoverZ

#Elastic Section Properties

set EBase 199.9e+15
set AColBase [expr $HColBase*$BColBase]
```

```
set IzColBase [expr 1./12.*$BColBase*pow($HColBase,3)];

section Elastic $ColBaseSecTag   $EBase $AColBase $IzColBase;       # elastic beam section

puts "section OK"

# define ELEMENTS
# set up geometric transformations of element

set IDTransf 1
geomTransf Linear $IDColTransf  ;

# Define Beam-Column Elements

set np 5; # number of Gauss integration points for nonlinear curvature distribution

# columns

element nonlinearBeamColumn 101 01 11 $np $ColBaseSecTag $IDTransf;      # level 0-1
element nonlinearBeamColumn 102 02 12 $np $ColBaseSecTag $IDTransf
element nonlinearBeamColumn 103 03 13 $np $ColBaseSecTag $IDTransf
element nonlinearBeamColumn 111 11 21 $np $ColSecTag $IDTransf; # level 1-2
element nonlinearBeamColumn 112 12 22 $np $ColSecTag $IDTransf
element nonlinearBeamColumn 113 13 23 $np $ColSecTag $IDTransf
element nonlinearBeamColumn 121 21 31 $np $ColSecTag $IDTransf; # level 2-3
element nonlinearBeamColumn 122 22 32 $np $ColSecTag $IDTransf
element nonlinearBeamColumn 123 23 33 $np $ColSecTag $IDTransf
element nonlinearBeamColumn 131 31 41 $np $ColSecTag $IDTransf; # level 3-4
element nonlinearBeamColumn 132 32 42 $np $ColSecTag $IDTransf
element nonlinearBeamColumn 133 33 43 $np $ColSecTag $IDTransf

# beams

element nonlinearBeamColumn 211 11 12 $np $BeamBaseSecTag $IDTransf;   # level 1
element nonlinearBeamColumn 212 12 13 $np $BeamBaseSecTag $IDTransf;
element nonlinearBeamColumn 221 21 22 $np $BeamSecTag $IDTransf;        # level 2
element nonlinearBeamColumn 222 22 23 $np $BeamSecTag $IDTransf;
element nonlinearBeamColumn 231 31 32 $np $BeamSecTag $IDTransf;                # level 3
element nonlinearBeamColumn 232 32 33 $np $BeamSecTag $IDTransf;
element nonlinearBeamColumn 241 41 42 $np $BeamSecTag $IDTransf;                # level 4
element nonlinearBeamColumn 242 42 43 $np $BeamSecTag $IDTransf;

# Define GRAVITY LOADS, weight and masses
# calculate dead load of frame, assume this to be an internal frame (do LL in a similar manner)
# calculate distributed weight along the beam length

set GammaConcrete 23544;
set Tslab 0.040;
set Lslab 1.30;
set Qslab [expr $GammaConcrete*$Tslab*$Lslab];
set QBeam 8401;          # W-section weight per length
set QdlBeam [expr $Qslab + $QBeam];      # dead load distributed along beam.
set QdlBeamBase 1273
set QdlCol 310.8;          # W-section weight per length
set QdlColBase 370
set WeightCol [expr $QdlCol*$LCol];      # total Column weight
```

```
set WeightBeam [expr $QdlBeam*$LBeam];          # total Beam weight
set WeightBeamBase 2100
set WeightColBase 100
set g 9.81

# assign masses to the nodes that the columns are connected to
# each connection takes the mass of 1/2 of each element framing into it (mass=weight/$g)

mass 11 [expr ($WeightColBase/2 + $WeightCol/2 +$WeightBeamBase/2)/$g] 0. 0.;                    #
level 2
mass 12 [expr ($WeightColBase/2 + $WeightCol/2 +$WeightBeamBase/2 +$WeightBeamBase/2)/$g] 0. 0.;
mass 13 [expr ($WeightColBase/2 + $WeightCol/2 +$WeightBeamBase/2)/$g] 0. 0.;
mass 21 [expr ($WeightCol/2 + $WeightCol/2 +$WeightBeam/2)/$g] 0. 0.;                            # level 2
mass 22 [expr ($WeightCol/2 + $WeightCol/2 +$WeightBeam/2 +$WeightBeam/2)/$g] 0. 0.;
mass 23 [expr ($WeightCol/2 + $WeightCol/2 +$WeightBeam/2)/$g] 0. 0.;
mass 31 [expr ($WeightCol/2 + $WeightCol/2 +$WeightBeam/2)/$g] 0. 0.;                            # level 3
mass 32 [expr ($WeightCol/2 + $WeightCol/2 +$WeightBeam/2 +$WeightBeam/2)/$g] 0. 0.;
mass 33 [expr ($WeightCol/2 + $WeightCol/2 +$WeightBeam/2)/$g] 0. 0.;
mass 41 [expr ($WeightCol/2 +$WeightBeam/2)/$g] 0. 0.;                                           # level 4
mass 42 [expr ($WeightCol/2 +$WeightBeam/2 +$WeightBeam/2)/$g] 0. 0.;
mass 43 [expr ($WeightCol/2 +$WeightBeam/2)/$g] 0. 0.;

# Define RECORDERS ----------------------------------------------------------

recorder Node -file Dnode01.out -node 01 -dof 1 2 3 disp
recorder Node -file Dnode02.out -node 02 -dof 1 2 3 disp
recorder Node -file Dnode03.out -node 03 -dof 1 2 3 disp
recorder Node -file Dnode11.out -node 11 -dof 1 2 3 disp
recorder Node -file Dnode12.out -node 12 -dof 1 2 3 disp
recorder Node -file Dnode13.out -node 13 -dof 1 2 3 disp
recorder Node -file Dnode21.out -time -node 21 -dof 1 2 3 disp
recorder Node -file Dnode22.out -node 22 -dof 1 2 3 disp
recorder Node -file Dnode23.out -node 23 -dof 1 2 3 disp
recorder Node -file Dnode31.out -node 31 -dof 1 2 3 disp
recorder Node -file Dnode32.out -node 32 -dof 1 2 3 disp
recorder Node -file Dnode33.out -node 33 -dof 1 2 3 disp
recorder Node -file Dnode41.out -node 41 -dof 1 2 3 disp
recorder Node -file Dnode42.out -node 42 -dof 1 2 3 disp
recorder Node -file Dnode43.out -node 43 -dof 1 2 3 disp
recorder Node -file RBase01.out -node 01 -dof 1 2 3 reaction;
recorder Node -file RBase02.out -node 02 -dof 1 2 3 reaction
recorder Node -file RBase03.out -node 03 -dof 1 2 3 reaction
recorder Node -file acc01.out -time -node 01 -dof 1 accel
recorder Node -file acc02.out -time -node 02 -dof 1 accel
recorder Node -file acc03.out -time -node 03 -dof 1 accel
recorder Node -file acc11.out -time -node 11 -dof 1 accel
recorder Node -file acc12.out -time -node 12 -dof 1 accel
recorder Node -file acc13.out -time -node 13 -dof 1 accel
recorder Node -file acc21.out -time -node 21 -dof 1 accel
recorder Node -file acc22.out -time -node 22 -dof 1 accel
recorder Node -file acc23.out -time -node 23 -dof 1 accel
recorder Node -file acc31.out -time -node 31 -dof 1 accel
recorder Node -file acc32.out -time -node 32 -dof 1 accel
recorder Node -file acc33.out -time -node 33 -dof 1 accel
recorder Node -file acc41.out -time -node 41 -dof 1 accel
recorder Node -file acc42.out -time -node 42 -dof 1 accel
```

```
recorder Node -file acc43.out -time -node 43 -dof 1 accel

# define GRAVITY -------------------------------------------------------------
# GRAVITY LOADS # define gravity load applied to beams and columns -- eleLoad applies loads in local
coordinate axis

pattern Plain 101 Linear {
  eleLoad -ele 211 212  -type -beamUniform -$QdlBeamBase; ; # beams level 1 (in -y direction)
  eleLoad -ele 221 222  -type -beamUniform -$QdlBeam; ; # beams level 2 (in -y direction)
  eleLoad -ele 231 232  -type -beamUniform -$QdlBeam;
  eleLoad -ele 241 242  -type -beamUniform -$QdlBeam
  eleLoad -ele 101 102 103  -type -beamUniform 0 -$QdlColBase
  eleLoad -ele 111 112 113  -type -beamUniform 0 -$QdlCol; # columns level 1-2 (in -x direction)
  eleLoad -ele 121 122 123  -type -beamUniform 0 -$QdlCol;
  eleLoad -ele 131 132 133  -type -beamUniform 0 -$QdlCol;
}

# Gravity-analysis parameters -- load-controlled static analysis

set Tol 1.0e-8;                    # convergence tolerance for test
variable constraintsTypeGravity Plain;              # default;
constraints $constraintsTypeGravity ;      # how it handles boundary conditions
numberer RCM;                      # renumber dof's to minimize band-width (optimization), if you want to
system BandGeneral ;               # how to store and solve the system of equations in the analysis (large
model: try UmfPack)
test NormDispIncr $Tol 6 ;                 # determine if convergence has been achieved at the end of an
iteration step
algorithm Newton;                          # use Newton's solution algorithm: updates tangent stiffness at
every iteration
set NstepGravity 10;               # apply gravity in 10 steps
set DGravity [expr 1./$NstepGravity];      # first load increment;
integrator LoadControl $DGravity; # determine the next time step for an analysis
analysis Static;                   # define type of analysis static or transient
analyze $NstepGravity;             # apply gravity

# maintain constant gravity loads and reset time to zero

loadConst -time 0.0

#----- Determine Period ------------

set nEigenI 1;              # mode 1
set nEigenK 2;              # mode 2
set nEigenJ 3;              # mode 3
set lambdaN [eigen [expr $nEigenJ]]; # eigenvalue analysis for nEigenJ modes
set lambdaI [lindex $lambdaN [expr $nEigenI-1]];    # eigenvalue mode i
set lambdaK [lindex $lambdaN [expr $nEigenK-1]]; # eigenvalue mode k
set lambdaJ [lindex $lambdaN [expr $nEigenJ-1]];    # eigenvalue mode j
set OmegaI [expr pow($lambdaI,0.5)];
set OmegaK [expr pow($lambdaK,0.5)];
set OmegaJ [expr pow($lambdaJ,0.5)];
set pi [expr 2*asin(1)]
set Tperiod1 [expr 2*$pi /$OmegaI]; # period (sec)
set Tperiod2 [expr 2*$pi /$OmegaK]; # period (sec)
set Tperiod3 [expr 2*$pi /$OmegaJ]; # period (sec)
# define analysis objects for seismic loading
```

```
wipeAnalysis
test NormDispIncr 1e-12 10 1
algorithm Newton
system UmfPack
constraints Plain
numberer RCM
integrator Newmark 0.6 0.32
analysis VariableTransient

# ------------ define & apply damping
# RAYLEIGH damping parameters, Where to put M/K-prop damping, switches
# D=$alphaM*M + $betaKcurr*Kcurrent + $betaKcomm*KlastCommit + $beatKinit*$Kinitial

set xDamp 0.02;  # damping ratio
set MpropSwitch 1.0;
set KcurrSwitch 0.0;
set KcommSwitch 1.0;
set KinitSwitch 0.0;
set nEigenI 1;              # mode 1
set nEigenJ 3;              # mode 3
set lambdaN [eigen [expr $nEigenJ]];                    # eigenvalue analysis for nEigenJ modes
set lambdaI [lindex $lambdaN [expr $nEigenI-1]];    # eigenvalue mode i
set lambdaJ [lindex $lambdaN [expr $nEigenJ-1]];    # eigenvalue mode j
set omegaI [expr pow($lambdaI,0.5)];
set omegaJ [expr pow($lambdaJ,0.5)];
set alphaM [expr $MpropSwitch*$xDamp*(2*$omegaI*$omegaJ)/($omegaI+$omegaJ)];
set betaKcurr [expr $KcurrSwitch*2.*$xDamp/($omegaI+$omegaJ)];
set betaKcomm [expr $KcommSwitch*2.*$xDamp/($omegaI+$omegaJ)];
set betaKinit [expr $KinitSwitch*2.*$xDamp/($omegaI+$omegaJ)];
rayleigh $alphaM $betaKcurr $betaKinit $betaKcomm;

# define ground motion characteristics

set dT 0.002675
set dTmin [expr $dT/10]
set dTmax $dT

# acceleration time history is read from an external file

set Series "Path -filePath shake28g.txt -dt $dT -factor 9.81"

# acceleration is applied at the fixed base node in horizontal direction (1)

pattern UniformExcitation 2 1 -accel $Series
# apply shaking
set steps 12000
set itr 50

for {set i 1} {$i < $steps} {incr i 1} {
test NormDispIncr 1e-12 $itr 0
set ok [analyze 1 $dT $dTmin $dTmax $itr]

        if {$ok != 0} {
        test NormDispIncr 1e-10 $itr 0
        set ok [analyze 1 $dT $dTmin $dTmax $itr]
       }
```

```
        if {$ok != 0} {
        test NormDispIncr 1e-8 $itr 0
        set ok [analyze 1 $dT $dTmin $dTmax $itr]
        }

        if {$ok != 0} {
        test NormDispIncr 1e-6 $itr 0
        set ok [analyze 1 $dT $dTmin $dTmax $itr]
        }
}

# print out final node and element outputs on screen

for {set n 1} {$n <= 3} {incr n 1} {
    print node $n
}
print ele

puts "done"
```

BuildRCrectSection.tcl: Build fiber rectangular RC section

```
# modified from OpenSEES example manual (OpenSEES, 2008)
# Define a procedure which generates a rectangular reinforced concrete section

proc BuildRCrectSection {id HSec BSec coverH coverB coreID coverID steelID numBarsTop barAreaTop
numBarsBot barAreaBot nfCoreY nfCoreZ nfCoverY nfCoverZ} {

set coverY [expr $HSec/2.0];
set coverZ [expr $BSec/2.0];
set coreY [expr $coverY-$coverH];
set coreZ [expr $coverZ-$coverB];

# Define the fiber section

section fiberSec $id {

# Define the core patch

patch quadr $coreID $nfCoreZ $nfCoreY -$coreY $coreZ -$coreY -$coreZ $coreY -$coreZ $coreY $coreZ

# Define the four cover patches

patch quadr $coverID 2 $nfCoverY -$coverY $coverZ -$coreY $coreZ $coreY $coreZ $coverY $coverZ
patch quadr $coverID 2 $nfCoverY -$coreY -$coreZ -$coverY -$coverZ $coverY -$coverZ $coreY -$coreZ
patch quadr $coverID $nfCoverZ 2 -$coverY $coverZ -$coverY -$coverZ -$coreY -$coreZ -$coreY $coreZ
patch quadr $coverID $nfCoverZ 2 $coreY $coreZ $coreY -$coreZ $coverY -$coverZ $coverY $coverZ

# define reinforcing layers
        layer straight $steelID $numBarsTop $barAreaTop  $coreY $coreZ $coreY -$coreZ;      # top layer
reinfocement
        layer straight $steelID $numBarsBot $barAreaBot  -$coreY $coreZ  -$coreY -$coreZ;   # bottom
layer reinforcement

        };      # end of fibersection definition
};              # end of procedure
```

LibMaterialsRC.tcl: define a library of Reinforced-Concrete materials

```
# nominal concrete compressive strength
set fc -34.2e+6;   # CONCRETE Compressive Strength(+Tension, -Compression)
set Ec 22.5e+9;   # Concrete Elastic Modulus
set nu 0.2;
set Gc [expr $Ec/2./[expr 1+$nu]]; # Torsional stiffness Modulus

# confined concrete
set Kfc 1.3;                    # ratio of confined to unconfined concrete strength
set Kres 0.2;                   # ratio of residual/ultimate to maximum stress
set fc1C [expr $Kfc*$fc]; # Confined concrete (mander model), maximum stress
set eps1C [expr 2.*$fc1C/$Ec];    # strain at maximum stress
set fc2C [expr $Kres*$fc1C];            # ultimate stress
set eps2C  [expr 20*$eps1C];            # strain at ultimate stress
set lambda 0.1;                 # ratio between unloading slope at $eps2 and initial slope $Ec
# unconfined concrete
set fc1U  $fc;                  # Unconfined concrete (todeschini parabolic model), maximum stress
set eps1U -0.003;               # strain at maximum strength of unconfined concrete
set fc2U [expr $Kres*$fc1U];            # ultimate stress
set eps2U -0.01;                # strain at ultimate stress
# tensile-strength properties
set ftC [expr -0.14*$fc1C];             # tensile strength +tension
set ftU [expr -0.14*$fc1U];             # tensile strength +tension
set Ets [expr $ftU/0.002];      # tension softening stiffness

# set up library of materials
set IDconcCore 1
set IDconcCover 2
uniaxialMaterial Concrete02 $IDconcCore $fc1C $eps1C $fc2C $eps2C $lambda $ftC $Ets;       # Core
concrete (confined)
uniaxialMaterial Concrete02 $IDconcCover $fc1U $eps1U $fc2U $eps2U $lambda $ftU $Ets;     # Cover
concrete (unconfined)

# Reinforcing Steel parameters
set Fy 560.6e+6;          # Steel yield stress
set Es 199.9e+9;          # modulus of steel
set Bs 0.01;                    # strain-hardening ratio
set R0 18;                      # control the transition from elastic to plastic branches
set cR1 0.925;                  # control the transition from elastic to plastic branches
set cR2 0.15;                   # control the transition from elastic to plastic branches

set IDSteel 3
uniaxialMaterial Steel02 $IDSteel  $Fy $Es $Bs $R0 $cR1 $cR2
```

Additional codes for Steel Braced structures (within BF model codes)

```
# Under Define Section----------------------------------
source StBraces.tcl

set EDB1SecTag 5
set EDB2SecTag 6
set EDB3SecTag 7

#EDBsection
```

```
BuildEDBSection $EDB1SecTag $EDB1MatTag
BuildEDBSection $EDB2SecTag $EDB2MatTag
BuildEDBSection $EDB3SecTag $EDB3MatTag

# Under Define Elements-----------------------------------

#Energr Dissipating Brazes(EDB)

element nonlinearBeamColumn 311 11 22 $np $EDB1SecTag $IDTransf;        # level 1-2
element nonlinearBeamColumn 322 23 32 $np $EDB2SecTag $IDTransf;        # level 2-3
element nonlinearBeamColumn 331 31 42 $np $EDB3SecTag $IDTransf;        # level 3-4

# Under Define Recorders ------------------------

recorder Element -file ele311sec1F.out -ele 311 section 1 force
recorder Element -file ele311sec1D.out -ele 311 section 1 deformation
recorder Element -file ele322sec1F.out -ele 322 section 1 force
recorder Element -file ele322sec1D.out -ele 322 section 1 deformation
recorder Element -file ele331sec1F.out -ele 331 section 1 force
recorder Element -file ele331sec1D.out -ele 331 section 1 deformation
```

STBraces.tcl: define steel02 materials

```
# all units are in N, m, second
# NonlinearBeamColumn ELEMENT

set EDB1MatTag  4
set EDB2MatTag  5
set EDB3MatTag  6

set S1fy [expr 5.55*pow(10,6)]
set S2fy [expr 3.7*pow(10,6)]
set S3fy [expr 2.96*pow(10,6)]

set S1Es 56.73e+9;
set S2Es 55.70e+9;
set S3Es 56.1e+9;

set S1b 0.085
set S2b 0.053
set S3b 0.0125

set BR0 40;                          # control the transition from elastic to plastic branches
set BcR1 0.925;                      # control the transition from elastic to plastic branches
set BcR2 0.55;

uniaxialMaterial Steel02  $EDB1MatTag  $S1fy  $S1Es  $S1b $BR0 $BcR1 $BcR2;
uniaxialMaterial Steel02  $EDB2MatTag  $S2fy  $S2Es  $S2b $BR0 $BcR1 $BcR2;
uniaxialMaterial Steel02  $EDB3MatTag  $S3fy  $S3Es  $S3b $BR0 $BcR1 $BcR2;
```

BuildEDBSection.tcl: Build fiber Circular section

```
proc BuildEDBSection {EDBSecTag EDBmatTag} {
# all units are in N, m, second
```

```
# Define Section----------
# EDB section

set colIJ 10;
set colJK 10;
set sRad 29.316e-3;

section Fiber $EDBSecTag {

        patch circ $EDBmatTag $colIJ   $colJK   0.0 0.0 0.0 $sRad 0.0 360.0;
}

}
```

Additional codes for SMA Braced structures (within BF model codes)

```
# Under Define Section----------
source SmaBraces.tcl
set SMA1SecTag 5
set SMA2SecTag 6
set SMA3SecTag 7

#SMA Brace section

BuildSMASection  $SMA1SecTag  $SC1MatTag $St1matTag
BuildSMASection  $SMA2SecTag  $SC2MatTag $St2matTag
BuildSMASection  $SMA3SecTag  $SC3MatTag $St3matTag

# Under Define Elements----------

#Energr Dissipating Brazes(EDB)

element nonlinearBeamColumn 311 11 22 $np $SMA1SecTag $IDTransf     #-level 1-2
element nonlinearBeamColumn 322 23 32 $np $SMA2SecTag $IDTransf     #  level 2-3
element nonlinearBeamColumn 331 31 42 $np $SMA3SecTag $IDTransf     #  level 3-4

# Under Define Recorders ----------
recorder Element -file ele311sec1F.out -ele 311 section 1 force
recorder Element -file ele311sec1D.out -ele 311 section 1 deformation
recorder Element -file ele322sec1F.out -ele 322 section 1 force
recorder Element -file ele322sec1D.out -ele 322 section 1 deformation
recorder Element -file ele331sec1F.out -ele 331 section 1 force
recorder Element -file ele331sec1D.out -ele 331 section 1 deformation
```

SmaBraces.tcl: define self centering and steel02 materials

```
# all units are in N, m, second
# NonlinearBeamColumn ELEMENT
#SelfCentering
set SC1MatTag 4
set SC2MatTag 5
set SC3MatTag 6

set S1k1 280.0e+9
set S1k2 16.0e+9
set S1sigAct 45.0e+6
```

```
set S1beta .67

set S2k1 380.0e+9
set S2k2 9.0e+9
set S2sigAct 28.2e+6
set S2beta .78

set S3k1 160.19e+9
set S3k2 4.25e+9
set S3sigAct 10.55e+6
set S3beta .385

uniaxialMaterial SelfCentering  $SC1MatTag  $S1k1  $S1k2  $S1sigAct $S1beta
uniaxialMaterial SelfCentering  $SC2MatTag  $S2k1  $S2k2  $S2sigAct $S2beta
uniaxialMaterial SelfCentering  $SC3MatTag  $S3k1  $S3k2  $S3sigAct $S3beta

#Steel
set St1matTag 7
set St2matTag 8
set St3matTag 9

set S1fy [expr 21.59*pow(10,6)]
set S2fy [expr 15.0*pow(10,6)]
set S3fy [expr 7.273*pow(10,6)]

set Es 15.59e+9;
set b 0.015
set R0 40;                              # control the transition from elastic to plastic branches
set cR1 0.925;                  # control the transition from elastic to plastic branches
set cR2 0.15;

uniaxialMaterial Steel02  $St1matTag  $S1fy  $Es  $b $R0 $cR1 $cR2;
uniaxialMaterial Steel02  $St2matTag  $S2fy  $Es  $b $R0 $cR1 $cR2;
uniaxialMaterial Steel02  $St3matTag  $S3fy  $Es  $b $R0 $cR1 $cR2;
```

BuildSMASection.tcl: Build fiber Circular section

```
# Define a procedure which generates a circular SMA section

proc BuildSMASection {BrSecTag SCmatTag STmatTag} {
# all units are in N, m, second
# NonlinearBeamColumn ELEMENT

# Define Section----------------------------------

set colIJ 10;
set colJK 10;
set intRad 13.231e-3;
set outRad 18.712e-3;

section Fiber $BrSecTag {

# EDB Section(upper, left, right, bottom)

        patch circ $SCmatTag $colIJ  $colJK  0.0 0.0 $intRad $outRad 0.0 360.0;
        patch circ $STmatTag $colIJ  $colJK  0.0 0.0 0.0 $intRad 0.0 360.0;
```

```
}

}
```

OpenSEES Code for Frame with Base Isolation (BI) Structure

Note: BuildRCrectSection.tcl and LibMaterialsRC.tcl are similar as BF model codes

```
# ------------------------------------------------------------------------------
# MANSIDE_ BI_Model for test BI_SMA_30 -- Build Model
# nonlinearBeamColumn element, inelastic fiber section -- Reinforced Concrete Section
# kg, N, m, Sec
#last modified on Apr 2009
# SET UP ---------------------------------------------------------------------
wipe;
model BasicBuilder -ndm 2 -ndf 3;
source BuildRCrectSection.tcl;      # procedure for defininig RC fiber section

# define GEOMETRY -----------------------------------------------------------
# define structure-geometry paramters
set LCol 1.05;              # column length
set LColstory1 1.23;        #1st story Col length
set LColBase 0.275
set LBeam 1.65;  # beam length

# calculate locations of beam/column intersections:
set X1 0.
set X2 [expr $X1 + $LBeam];
set X3 [expr $X2 + $LBeam];
set YB1 0.
set Y1 [expr $YB1 + $LColBase];
set Y2 [expr $Y1 + $LColstory1];
set Y3 [expr $Y2 + $LCol];
set Y4 [expr $Y3 + $LCol];

# define nodal coordinates
node 02 $X2 $YB1
node 91 $X1 $YB1
node 92 $X2 $YB1
node 93 $X3 $YB1
node 11 $X1 $Y1
node 12 $X2 $Y1
node 13 $X3 $Y1
node 21 $X1 $Y2
node 22 $X2 $Y2
node 23 $X3 $Y2
node 31 $X1 $Y3
node 32 $X2 $Y3
node 33 $X3 $Y3
node 41 $X1 $Y4
node 42 $X2 $Y4
node 43 $X3 $Y4

# BOUNDARY CONDITIONS
fix 02 1 1 1
fix 91 0 1 1
```

```
fix 92 0 1 1
fix 93 0 1 1

# Define SECTIONS -------------------------------------------------------------
# define section tags:
set ColSecTag 1
set ColBaseSecTag 2
set BeamSecTag 3
set BeamBaseSecTag 4

# Section Properties:
set HCol 0.150;
set BCol 0.105
set HBeam 0.150;
set BBeam 0.105;
set HColBase 0.150;
set BColBase 0.150;
set HBeamBase 0.330;
set BBeamBase 0.165;

# MATERIAL parameters
source LibMaterialsRC.tcl;          # define library of Reinforced-concrete Materials

# FIBER SECTION properties
 # Column section geometry:
set cover 0.015;
set numBarsTopCol 3;
set numBarsBotCol 3;
set barAreaTopCol 0.0000126;
set barAreaBotCol 0.0000126;

# Beam section geometry:
set numBarsTopBeam 7;
set numBarsBotBeam 5;
set barAreaTopBeam 0.0000126;
set barAreaBotBeam 0.0000126;
set nfCoreY 20;
set nfCoreZ 20;
set nfCoverY 20;
set nfCoverZ 20;

# rectangular section with one layer of steel evenly distributed around the perimeter and a confined core.

BuildRCrectSection $ColSecTag $HCol $BCol $cover $cover $IDconcCore  $IDconcCover $IDSteel
$numBarsTopCol $barAreaTopCol $numBarsBotCol $barAreaBotCol $nfCoreY $nfCoreZ $nfCoverY
$nfCoverZ

BuildRCrectSection $BeamSecTag $HBeam $BBeam $cover $cover $IDconcCore  $IDconcCover $IDSteel
$numBarsTopBeam $barAreaTopBeam $numBarsBotBeam $barAreaBotBeam $nfCoreY $nfCoreZ
$nfCoverY $nfCoverZ

BuildRCrectSection $BeamBaseSecTag $HBeamBase $BBeamBase $cover $cover $IDconcCore
$IDconcCover $IDSteel $numBarsTopBeam $barAreaTopBeam $numBarsBotBeam $barAreaBotBeam
$nfCoreY $nfCoreZ $nfCoverY $nfCoverZ

#Elastic Section Properties
```

```
set EBase 199.9e+9
set AColBase [expr $HColBase*$BColBase]
set IzColBase [expr 1./12.*$BColBase*pow($HColBase,3)];

section Elastic $ColBaseSecTag  $EBase $AColBase $IzColBase;      # elastic beam section

# IS MATERIAL parameters
source SMA1IS.tcl

# define ELEMENTS
# set up geometric transformations of element
set IDTransf 1;
geomTransf Linear $IDTransf

# Define Beam-Column Elements
set np 5; # number of Gauss integration points

#Isolation Systems
element zeroLength  992  02  92 -mat 4 5 6 -dir 1 1 1

# Base columns
element nonlinearBeamColumn 101 91 11 $np $ColBaseSecTag $IDTransf;              # level 0-1
element nonlinearBeamColumn 102 92 12 $np $ColBaseSecTag $IDTransf
element nonlinearBeamColumn 103 93 13 $np $ColBaseSecTag $IDTransf

# columns
element nonlinearBeamColumn 111 11 21 $np $ColSecTag $IDTransf;          # level 1-2
element nonlinearBeamColumn 112 12 22 $np $ColSecTag $IDTransf
element nonlinearBeamColumn 113 13 23 $np $ColSecTag $IDTransf
element nonlinearBeamColumn 121 21 31 $np $ColSecTag $IDTransf;          # level 2-3
element nonlinearBeamColumn 122 22 32 $np $ColSecTag $IDTransf
element nonlinearBeamColumn 123 23 33 $np $ColSecTag $IDTransf
element nonlinearBeamColumn 131 31 41 $np $ColSecTag $IDTransf;          # level 3-4
element nonlinearBeamColumn 132 32 42 $np $ColSecTag $IDTransf
element nonlinearBeamColumn 133 33 43 $np $ColSecTag $IDTransf

# beams
element nonlinearBeamColumn 211 11 12 $np $BeamBaseSecTag $IDTransf;  # level 1
element nonlinearBeamColumn 212 12 13 $np $BeamBaseSecTag $IDTransf;
element nonlinearBeamColumn 221 21 22 $np $BeamSecTag $IDTransf;              # level 2
element nonlinearBeamColumn 222 22 23 $np $BeamSecTag $IDTransf;
element nonlinearBeamColumn 231 31 32 $np $BeamSecTag $IDTransf;              # level 3
element nonlinearBeamColumn 232 32 33 $np $BeamSecTag $IDTransf;
element nonlinearBeamColumn 241 41 42 $np $BeamSecTag $IDTransf;              # level 4
element nonlinearBeamColumn 242 42 43 $np $BeamSecTag $IDTransf;

# Define GRAVITY LOADS, weight and masses

# calculate dead load of frame, assume this to be an internal frame (do LL in a similar manner)
# calculate distributed weight along the beam length
set GammaConcrete 23544;
set Tslab 0.040;
set Lslab 1.30;
set Qslab [expr $GammaConcrete*$Tslab*$Lslab];
set QBeam 8401;          # W-section weight per length
set QdlBeam [expr $Qslab + $QBeam];      # dead load distributed along beam.
```

```
set QdlBeamBase 1273
set QdlCol 310.8;            # W-section weight per length
set QdlColBase 370
set WeightCol [expr $QdlCol*$LCol];        # total Column weight
set WeightBeam [expr $QdlBeam*$LBeam];            # total Beam weight
set WeightBeamBase 2100
set WeightColBase 100
set g 9.81

# assign masses to the nodes that the columns are connected to
# each connection takes the mass of 1/2 of each element framing into it (mass=weight/$g)

mass 11 [expr ($WeightColBase/2 + $WeightCol/2 +$WeightBeamBase/2)/$g] 0. 0.
mass 12 [expr ($WeightColBase/2 + $WeightCol/2 +$WeightBeamBase/2 +$WeightBeamBase/2)/$g] 0. 0.;
mass 13 [expr ($WeightColBase/2 + $WeightCol/2 +$WeightBeamBase/2)/$g] 0. 0.;
mass 21 [expr ($WeightCol/2 + $WeightCol/2 +$WeightBeam/2)/$g] 0. 0.;
mass 22 [expr ($WeightCol/2 + $WeightCol/2 +$WeightBeam/2 +$WeightBeam/2)/$g] 0. 0.;
mass 23 [expr ($WeightCol/2 + $WeightCol/2 +$WeightBeam/2)/$g] 0. 0.;
mass 31 [expr ($WeightCol/2 + $WeightCol/2 +$WeightBeam/2)/$g] 0. 0.;
mass 32 [expr ($WeightCol/2 + $WeightCol/2 +$WeightBeam/2 +$WeightBeam/2)/$g] 0. 0.;
mass 33 [expr ($WeightCol/2 + $WeightCol/2 +$WeightBeam/2)/$g] 0. 0.;
mass 41 [expr ($WeightCol/2 +$WeightBeam/2)/$g] 0. 0.;
mass 42 [expr ($WeightCol/2 +$WeightBeam/2 +$WeightBeam/2)/$g] 0. 0.;
mass 43 [expr ($WeightCol/2 +$WeightBeam/2)/$g] 0. 0.;

# Define RECORDERS ----------------------------------------------------------
recorder Node -file Dnode91.out -node 91 -dof 1 2 3 disp
recorder Node -file Dnode92.out -node 92 -dof 1 2 3 disp
recorder Node -file Dnode93.out -node 93 -dof 1 2 3 disp
recorder Node -file Dnode11.out -node 11 -dof 1 2 3 disp
recorder Node -file Dnode12.out -node 12 -dof 1 2 3 disp
recorder Node -file Dnode13.out -node 13 -dof 1 2 3 disp
recorder Node -file Dnode21.out -node 21 -dof 1 2 3 disp
recorder Node -file Dnode22.out -node 22 -dof 1 2 3 disp
recorder Node -file Dnode23.out -node 23 -dof 1 2 3 disp
recorder Node -file Dnode31.out -node 31 -dof 1 2 3 disp
recorder Node -file Dnode32.out -node 32 -dof 1 2 3 disp
recorder Node -file Dnode33.out -node 33 -dof 1 2 3 disp
recorder Node -file Dnode41.out -node 41 -dof 1 2 3 disp
recorder Node -file Dnode42.out -node 42 -dof 1 2 3 disp
recorder Node -file Dnode43.out -node 43 -dof 1 2 3 disp
recorder Element -file Fele101.out -ele 101 globalForce;
recorder Element -file Fele102.out -ele 102 globalForce
recorder Element -file Fele103.out -ele 103 globalForce
recorder Node -file acc91.out -time -node 91 -dof 1 accel
recorder Node -file acc92.out -time -node 92 -dof 1 accel
recorder Node -file acc93.out -time -node 93 -dof 1 accel
recorder Node -file acc11.out -time -node 11 -dof 1 accel
recorder Node -file acc12.out -time -node 12 -dof 1 accel
recorder Node -file acc13.out -time -node 13 -dof 1 accel
recorder Node -file acc21.out -time -node 21 -dof 1 accel
recorder Node -file acc22.out -time -node 22 -dof 1 accel
recorder Node -file acc23.out -time -node 23 -dof 1 accel
recorder Node -file acc31.out -time -node 31 -dof 1 accel
recorder Node -file acc32.out -time -node 32 -dof 1 accel
recorder Node -file acc33.out -time -node 33 -dof 1 accel
```

```
recorder Node -file acc41.out -time -node 41 -dof 1 accel
recorder Node -file acc42.out -time -node 42 -dof 1 accel
recorder Node -file acc43.out -time -node 43 -dof 1 accel

# define GRAVITY -------------------------------------------------------------
# GRAVITY LOADS

pattern Plain 1 Linear {
  eleLoad -ele 211 212  -type -beamUniform -$QdlBeamBase;
  eleLoad -ele 221 222  -type -beamUniform -$QdlBeam;
  eleLoad -ele 231 232  -type -beamUniform -$QdlBeam;
  eleLoad -ele 241 242   -type -beamUniform -$QdlBeam
  eleLoad -ele 101 102 103  -type -beamUniform 0 -$QdlColBase
  eleLoad -ele 111 112 113  -type -beamUniform 0 -$QdlCol;
  eleLoad -ele 121 122 123  -type -beamUniform 0 -$QdlCol;
  eleLoad -ele 131 132 133  -type -beamUniform 0 -$QdlCol;
}

# Gravity-analysis parameters -- load-controlled static analysis
set Tol 1.0e-8;
variable constraintsTypeGravity Plain;
constraints $constraintsTypeGravity ;
numberer RCM;
system BandGeneral ;
test NormDispIncr $Tol 6 ;
algorithm Newton;
set NstepGravity 10;
set DGravity [expr 1./$NstepGravity];
integrator LoadControl $DGravity;
analysis Static;
analyze $NstepGravity;

#-- maintain constant gravity loads and reset time to zero
loadConst -time 0.0

# define analysis objects for seismic loading
wipeAnalysis
test NormDispIncr 1e-12 10 0
algorithm Newton
system UmfPack
constraints Plain
numberer RCM
integrator Newmark 0.6 0.32
analysis VariableTransient

# define ground motion characteristics
set dT 0.002675
set dTmin [expr $dT/10]
set dTmax $dT

# acceleration time history is read from an external file
set Series "Path -filePath shake30g.txt -dt $dT -factor 9.81"

# acceleration is applied at the fixed base node in horizontal direction (1)
pattern UniformExcitation 2 1 -accel $Series
```

```
# apply shaking
set steps 12000
set itr 50

for {set i 1} {$i < $steps} {incr i 1} {
test NormDispIncr 1e-12 $itr 0
set ok [analyze 1 $dT $dTmin $dTmax $itr]

        if {$ok != 0} {
        test NormDispIncr 1e-10 $itr 0
        set ok [analyze 1 $dT $dTmin $dTmax $itr]
       }

       if {$ok != 0} {
       test NormDispIncr 1e-8 $itr 0
       set ok [analyze 1 $dT $dTmin $dTmax $itr]
       }

       if {$ok != 0} {
       test NormDispIncr 1e-6 $itr 0
       set ok [analyze 1 $dT $dTmin $dTmax $itr]
       }
}

# print out final node and element outputs on screen

for {set n 1} {$n <= 3} {incr n 1} {
    print node $n
}
print ele
puts "done"
```

SMA1IS.tcl: define Self-Centering, Steel02, and ElasticPP materials

```
#SelfCentering
set k1 2.0e+6
set k2 0.152e+6
set sigAct 5.4e+3
set beta .2

uniaxialMaterial SelfCentering  4  $k1  $k2  $sigAct $beta

#Steel
set Esi 0.84e+6;                        #load/deformation
set fyi 1.75e+3;                  # yeilding load
set bi 0.010
set R0i 40;                             # control the transition from elastic to plastic branches
set cR1i 0.925;                   # control the transition from elastic to plastic branches
set cR2i 0.15;

uniaxialMaterial Steel02  5  $fyi  $Esi  $bi $R0i $cR1i $cR2i

set Ef 3.5e+7
set epsyP 0.50e-4

uniaxialMaterial ElasticPP 6 $Ef $epsyP
```